BUCKLING OF T-SECTION TRANSITION RINGBEAMS IN ELEVATED STEEL SILOS AND TANKS

CHAN FONG

M. PHIL

THE HONG KONG
POLYTECHNIC UNIVERSITY

1998

Abstract of thesis entitled "Buckling of T-Section Transition Ringbeams in Elevated Steel Silos and Tanks" submitted by Chan Fong for the degree of Master of Philosophy at the Hong Kong Polytechnic University in November, 1998

Elevated steel silos for the storage of bulk solids or elevated steel tanks for liquid storage commonly consist of a cylindrical vessel above a conical hopper (or end closure) supported on a skirt or a number of columns. The point of intersection between the cylindrical vessel and the conical hopper is often referred to as the transition. The transition junction formed by the intersecting shell segments is subject to a large circumferential compressive force which arises from the radial component of the meridional tension in the hopper. A ring is generally provided at the junction to resist this compressive force. As this ring is a main structural member rather than a relatively light stiffener used on a flexible shell wall, it is referred to as a ringbeam in this thesis. This transition ringbeam may be a simple annular plate, but in many cases a stiffened annular plate in the form of a T or angle section is preferred due to their higher out-of-plane bending stiffness. Under the large circumferential compressive force, the ringbeam may fail by buckling. In-plane buckling involving flexure only is generally prevented by the adjacent shells, so out-of-plane buckling failure is usually the critical buckling mode. The out-of-plane buckling mode consists of an overall rotation of the ringbeam cross-section around the point of attachment (the inner edge of the ringbeam) with associated distortion of the cross-section.

A review of the existing literature reveals that the elastic and plastic out-of-plane buckling strengths of annular plate transition ringbeams have been studied extensively, and design rules have been proposed. Much less has been done on T-section transition ringbeams. Previous studies on T-section ringbeams have been concentrated on the flexural-torsional buckling strength, treating the ringbeam cross-section as rigid during buckling. This however overestimates the buckling strength, particularly for ringbeams with a heavy rotational restraint from the shell walls. Furthermore, the effect of material yielding on the buckling strength has received limited attention. This thesis thus presents the results of a major study to correct current deficiency in our knowledge on the buckling behaviour and strength of T-section transition ringbeams. The comprehensive theoretical/numerical investigation presented here has been carried out with the aid of an advanced finite element program NEPAS, which can perform linear or non-linear bifurcation buckling analysis of elastic or elastic-plastic branched axisymmetric shells.

The work consists of four parts. The first part is concerned with the development of an elastic buckling strength approximation for inner edge clamped T-section ringbeams. This is achieved through a careful examination of extensive numerical results and by making use of the existing solution of Bulson for edge stiffened plates under axial compression. Part two of the work deals with the elastic buckling strength of inner edge simply supported ringbeams. An existing closed form solution for this case is substantially simplified without sacrificing its accuracy. The third part is aimed at developing an elastic buckling strength approximation for T-section ringbeams with an elastic rotational restraint from the adjacent shell walls. This buckling strength is

formulated through an interpolation of the buckling strengths of the two limiting cases investigated in the first two parts, following the approach adopted for annular plate ringbeams by Jumikis and Rotter. Their interpolation function for annular plate ringbeams is found to be satisfactory also for T-section ringbeams. Finally, the effect of plasticity on buckling strength is investigated, leading to the development of a design proposal for the buckling strength of steel T-section ringbeams in elevated silos and tanks. Application of the design method is illustrated through an example.

Declaration

I hereby declare that this thesis entitled "Buckling of T-Section Transition Ringbeams in Elevated Steel Silo and Tanks" has not been, either in whole or in part, previously submitted to any other institution for a degree or other qualification, and the work presented in this thesis is the original contribution of the author except where due reference is made in the text.

_____

(Chan Fong)

Acknowledgements

This project was supported by The Hong Kong Polytechnic University and the Civil and Structural Engineering Department. I am grateful for this support. The author would like to thank Dr. J. G. Teng , the chief supervisor, for his approach, guidance and encouragement from the beginning till the completion of the whole project. Thanks also go to Professor S.L. Chan, the co-supervisor, for his support, Mrs. Anson for her linguistic assistance and Mr. Y.F. Lou, Mr. T. Hong, Mr. Y. Zhao and Miss J.H. Wang for their helpful discussions and friendship. Final thanks go to Mr Ho of the computer lab for his help with the printing work of this thesis and all friends who have supported me during the whole period.

Finally, special thanks go to my parents, my sister and brother who made my education possible. To them I dedicate this thesis.

Table of Contents

page

Figure List

Notation

The following symbols are used in this thesis:

A_e = elastic effective section area
A_p = plastic effective section area
A_{ps} = contribution of shell segments to plastic effective section area
A_r = ringbeam cross sectional area
A_{rp} = cross-sectional area of annular plate of T-section ringbeam
A_{rs} = cross-sectional area of stiffener of T-section ringbeam
a = defined by Eq. 4-15
B = width of annular plate ringbeam
B_p = width of annular plate of T-section ringbeam
B_s = height of stiffener of T-section ringbeam
B_{se} = equivalent stiffener height of T-section ringbeam
c, c_s, c_c = coefficients defined by Eqs 3-2 and 3-3
c_1,c_2,c_3= coefficients defined by Eqs 4-5, 4-6 and 4-7
E = elastic modulus
F = circumferential compressive force at junction
F_e = elastic buckling strength in terms of circumferential compressive force F
F_p = plastic collapse strength in terms of circumferential compressive force F
F_f = ultimate failure strength in terms of circumferential compressive force F
$f(k, B_s/B_p, \lambda)$ = reduction factor on plastic collapse strength due to instability effects (Eq. 6-12)
G = shear modulus
H = cylinder height
I_s = second moment of area of the stiffener of T-section ringbeam
I_x = second moment of area of the ringbeam about the radial axis
I_y = second moment of area of the ringbeam about the vertical axis
i = ith shell segment
J = torsional constant
K = coefficient defined by Eq. 4-14
K_{min} = coefficient defined by Eq. 3-10
k = dimensionless ringbeam size parameter, defined by Eq. 6-10
L_b = linear elastic bending half-wavelength of shell segment
l_p = plastic effective length
l_e = elastic effective length
N_{ϕ} = meridional tension at hopper top
n = circumferential buckling wave number
n_{cr} = critical circumferential buckling wave number
p = normal pressure
p_{c1}, p_{c2}, p_{h1}, p_{h2} = defined in Fig. 5-2
p_e = elastic buckling pressures for simplified structural models of Fig. 5-3
p_f = ultimate failure pressures for simplified structural models of Fig. 5-3
p_p = plastic buckling pressures for simplified structural models of Fig. 5-3

q	=	radial inward load per unit circumference
R	=	radius of cylinder
r_o^2	=	defined by Eq. 4-4
T	=	thickness of annular plate ringbeam
T_s	=	thickness of stiffener of T-section ringbeam
T_p	=	thickness of annular plate of T-section ringbeam
t_c	=	cylinder wall thickness
t_h	=	hopper wall thickness
t_s	=	skirt wall thickness
x_c	=	distance between the centroid of the T-section cross-section and its inner edge
α	=	hopper apex half angle
β	=	annular plate width-to-radius ratio
ϕ	=	plate length to width ratio
γ_p	=	modification factor for plastic effective length
γ_e	=	modification factor for elastic effective length
η_s, η_c	=	interpolation parameters (Eqs 3-5 and 3-6)
φ	=	α for hopper and =0 for cylinder and skirt
λ	=	dimensionless slenderness parameter, $\sqrt{F_p/F_e}$
μ	=	wall fictional coefficient
ν	=	Poisson's ratio
ρ	=	coefficient defined by Eq. 3-10
$\sigma_{\theta cr}$	=	maximum circumferential compressive stress in annular plate of T-section ringbeam at buckling
$\sigma_{\theta crE1}$, $\sigma_{\theta crE2}$, $\sigma_{\theta crE3}$, $\sigma_{\theta crE4}$	=	defined by Eqs 5-11, 5-12, 5-13, 5-14
σ_y	=	yield stress
ζ	=	equivalent thickness ratio

CHAPTER 1 INTRODUCTION

1.1 Steel Silos

Steel silos are widely used for short and long term storage of large quantities of bulk solids in many industries including mining, chemical, electric power generation, agriculture and food processing. As industrial storage demands have risen, the number and size of steel silos have been growing rapidly in recent years. The unit storage capacity of elevated silos has reached 10,000 tonnes, while that of ground-supported steel silos is even bigger. As the size has risen, many design aspects have ceased to be governed by nominal dimensions and are instead controlled by strength considerations. Traditional design techniques for steel silos are over-simplistic and have led to many steel silo failures. In addition to the loss of the structure, failure of a silo often causes greater economic losses through disruption of industrial processes. For example, large chemical plants or power stations are stopped as a result. Silos probably have the highest failure rate among all engineered structures. There are currently no codes for the structural design of steel silos, although a European code is under development (CEN, 1997). More research on the structural design of steel silos is clearly needed.

Steel silos may be ground-supported or elevated . Typical elevated steel silos consist of a cylindrical shell and a conical hopper (Fig. 1-1). They may be supported by a long skirt which extends to the ground (Fig. 1-2a), or by a number of evenly-spaced columns (Fig. 1-2b, 1-2c, 1-2d). The columns may be terminated below the transition junction (Fig. 1-2b, Fig. 1-3), extended to the eaves (Fig. 1-2c), or terminated part way up the cylinder (Fig. 1-2d). The point of intersection between the cylinder and the

hopper is commonly referred to as the transition, and the cylinder/hopper/skirt/ring junction the transition junction. Even in column-supported silos, a skirt is often included by extending the cylinder beyond the transition. The ring provided at the transition (Fig. 1-3) serves two functions: to redistribute the column forces by acting as a bow girder, and to resist the large circumferential compression from the meridional tension in the hopper. This ring is a main structural member (in contrast to relatively light ring stiffeners on shell walls), and is referred to as a ringbeam throughout the thesis. The structural form of an elevated liquid storage tank is similar to that of a steel silo, so the work presented in this thesis is also directly applicable to the design of elevated liquid storage tanks.

The advantage of an elevated steel silo over a ground-supported one lies in its ability to discharge the stored bulk solid by gravity flow. Different flow patterns may occur depending on the silo geometry, wall roughness, properties of the stored material and other factors. Mass flow is likely to develop in silos with a steep hopper and a smooth wall surface (Fig 1-4a), while funnel flow (Fig 1-4b) including pipe flow (Fig. 1-4c) is more likely in silos with a shallow hopper and a rough wall surface.

Most large steel silos are of circular planform, as they are structurally more efficient than rectangular silos. Steel silos generally have thin walls, with the radius-to-diameter ratio between 200 and 3000. They are complex branched thin shell structures.

1.2 Transition Junctions

The transition junction is formed by a number of intersecting shell segments including the cylinder, the hopper and often also the skirt. A ringbeam is often placed outside the transition to strengthen the junction which is subject to a large circumferential compressive force due to bulk solid loading as explained next. Some typical geometries of transition junctions are shown in Fig. 1-5. The ringbeam may be an annular plate, but an annular plate is weak in torsion and is thus susceptible to failure by out-of-plane buckling. A common way to increase the out-of-plane stiffness of an annular plate ringbeam is to attach a vertical stiffener to the outer edge of the annular plate, resulting in a T-section ringbeam (Fig. 1-3).

1.3 Circumferential Compression at Transition Junction

Loads on the silo walls due to the stored bulk solid are of a complex form, and depend on whether the stored solid is at rest or moving and many other factors. Design codes exist (eg AS 3774) for the prediction of bulk solid pressures on silo walls.

The stored bulk solid in the hopper exerts a non-uniform internal pressure and a related downward frictional drag on the hopper wall. These pressures lead to a meridional tension in the cone which generally reaches its maximum at the transition. The vertical component of the meridional tension acting at the transition is transferred to a vertical support directly or through the skirt, while the radial component needs to be resisted by the transition junction itself. Consequently, a large circumferential compressive force develops at the transition junction. The buckling behaviour and

strength of the T-section ringbeam subject to this compressive force is the concern of this thesis.

1.4 Failure Modes at Transition Junctions

1.4.1 General

If the structure is supported by a skirt on the ground, a deep stiff skirt on columns, or many evenly spaced columns (typically more than 12), the stress distributions in the ringbeams are effectively axisymmetric. Under such an axisymmetric loading condition, the junction can fail by elastic or plastic buckling of the transition ringbeam or by plastic collapse of the junction (Teng and Rotter, 1992). Buckling failure of the ringbeam generally involves rotational deformations about the attached point, whilst plastic collapse of the junction involves large radial inward deformations. For a structure supported on only a few columns, buckling of the ringbeam is again possible (Teng and Rotter, 1989a), with plastic collapse being another possible mode, although little is currently known about discretely supported ringbeams. This thesis is concerned only with silos which are axisymmetrically stressed.

1.4.2 In-Plane Buckling of Transition Ringbeams

In general, the buckling mode of the ringbeam involves simultaneously in-plane flexure, out-of-plane flexure and torsion. However, for ringbeams with an axis of symmetry lying in the plane of the ringbeam, in-plane and out-of-plane buckling become uncoupled. The in-plane buckling mode of an isolated and unrestrained ring involves two complete waves (Fig. 1-6).

For a ringbeam at a silo transition junction, due to the restraint provided by the shell walls, this simple in-plane buckling mode cannot occur, if in-plane buckling is possible at all. Existing research (Jumikis and Rotter, 1983) suggests, for a ringbeam positioned at the transition junction of a steel silo, in-plane buckling deformations are generally prevented by the membrane stiffness of the cone. Therefore, out-of-plane buckling is generally the critical buckling mode.

1.4.3 Out-of-Plane Buckling of Transition Ringbeams

Out-of-plane buckling failure usually involves twisting deformations of the ringbeam about the point of attachment (Fig 1-7), and the buckling deformations assume many waves around the circumference. When the ringbeam is slender, it may fail by elastic buckling, with plastic buckling becoming critical when it is stockier.

1.4.4 Plastic Collapse of Transition Junctions

The ringbeam may fail by axisymmetric plastic collapse rather than buckling if it is sufficiently stocky (i.e. the out-of-plane stiffness is sufficiently high). The collapse mechanism requires the formation of a plastic hinge circle at the point of intersection and a plastic hinge circle in each shell segment at a suitable distance from the point of intersection (Fig 1-8). As the shell segments are more explicitly involved in this mode of failure, it is generally viewed and referred to as a junction collapse mode rather than a ringbeam collapse mode.

1.4.5 Local Buckling of Transition Ringbeams

T-section transition ringbeams with slender plate/shell elements may fail in a local buckling mode as shown in Fig. 1-9. Local buckling should be avoided by properly proportioning the plate/shell elements in practical design as little is known about this mode at present.

1.5 Review of Topics Covered in This Thesis

This thesis presents a comprehensive theoretical study on the buckling behaviour and strength of T-section transition ringbeams with particular emphasis on the development of a simple design procedure.

To arrive at a simple method for assessing the elastic buckling strength of T-section transition ringbeams, strength approximations are first established in Chapter 3 and Chapter 4 for inner edge fully clamped and inner edge simply supported ringbeams respectively. The buckling strength of T-section ringbeams with restraints typical of those in a real silo is then formulated in Chapter 5 by a suitable interpolation of the buckling strengths of these two idealised cases. This is followed by the development of a design approximation for the plastic buckling strength of T-section transition ringbeams in Chapter 6. A numerical example is also included in Chapter 6 to demonstrate the application of the developed design method.

The approach adopted to develop the simple design approximations combines thorough numerical investigations into the structural behaviour with full exploitation of existing solutions and methods. The final design proposal developed, the first ever

rigorous design proposal for this problem, is rational, simple and accurate. It can be used directly in the practical design of steel silos, tanks and pressure vessels and is suitable for future inclusion into their design codes. With suitable modifications, the developed method may also be applied in designing any other structures (e.g. offshore tubular members and tubular towers incorporating a conical shell section and ring-stiffened cylinders) where a ring is placed at a shell intersection or on a shell wall to resist a circumferential compressive force.

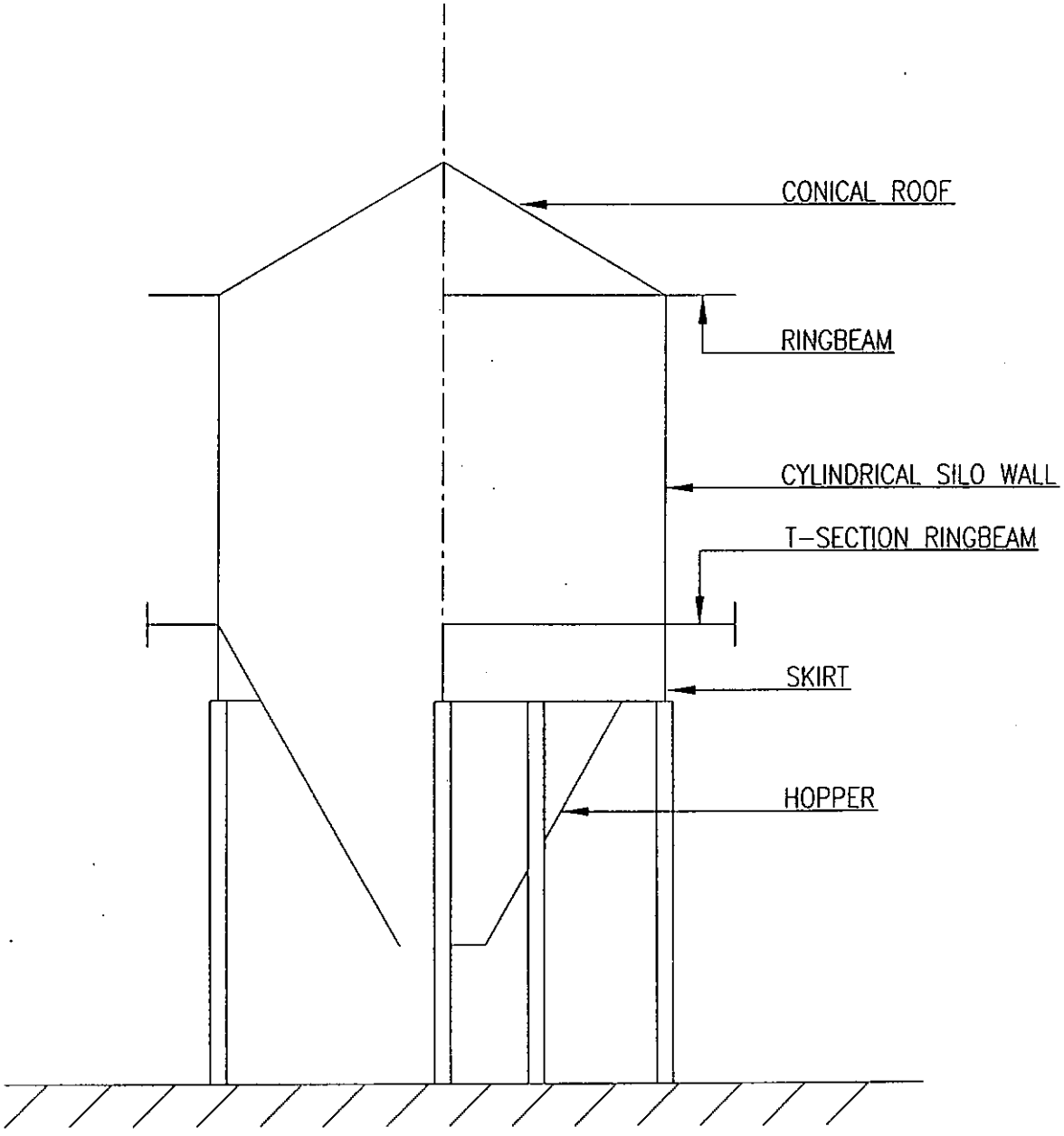

Fig. 1-1 Typical Form of Elevated Steel Silo with a T-Section Ringbeam

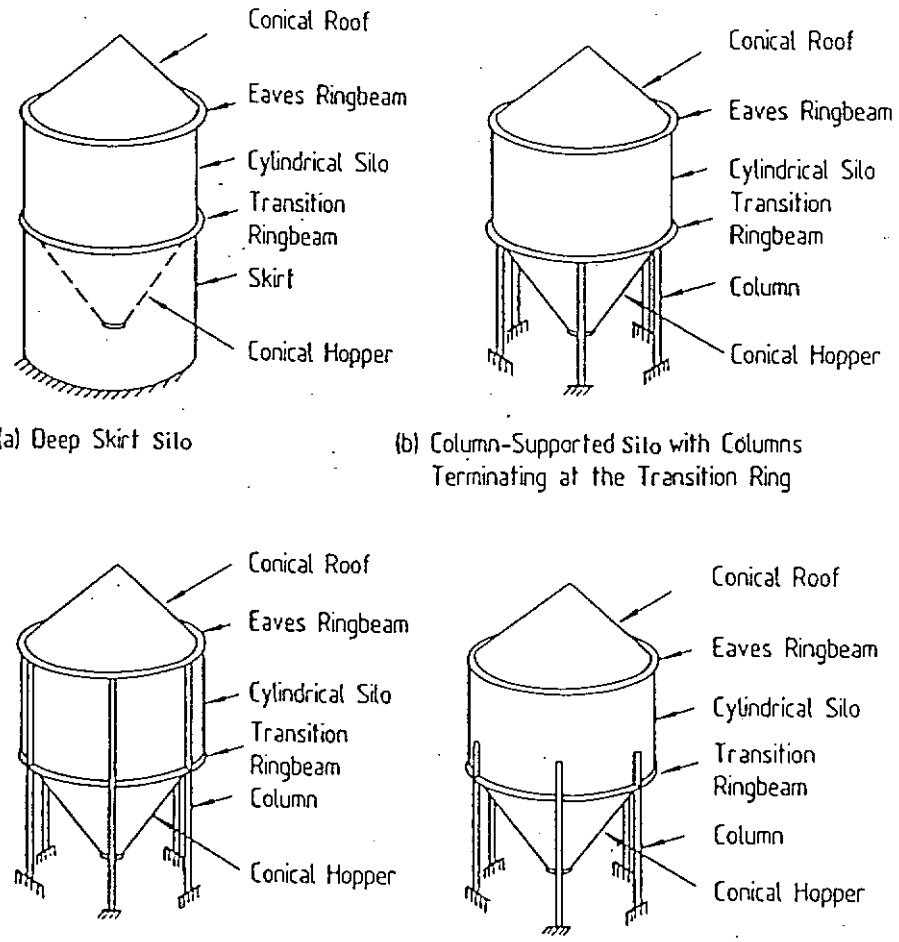

(After Teng & Rotter, 1992)

Fig. 1-2 Alternative Elevated Silo Support Arrangements

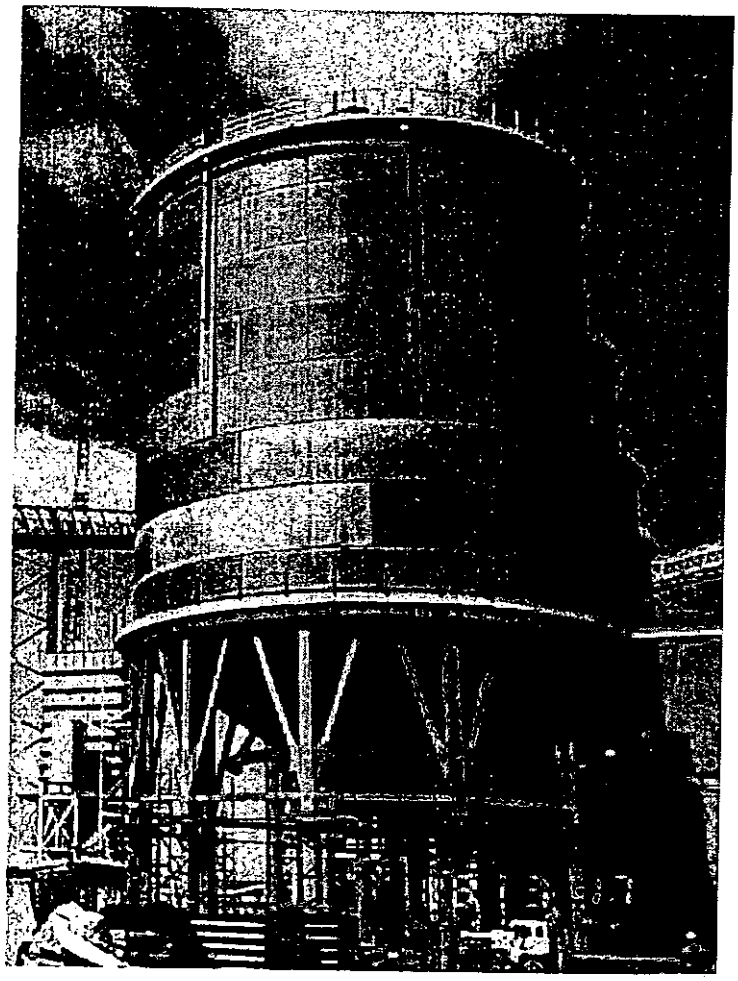

Fig. 1-3 A Large Elevated Steel Silo with a T-Section Ringbeam

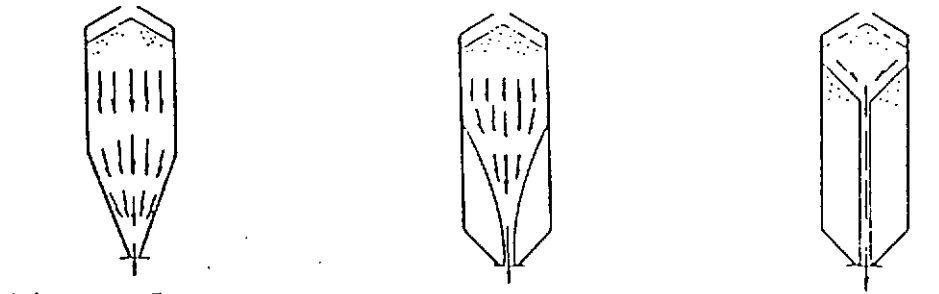

(After AS3774-1990)

Fig. 1-4 Flow Types

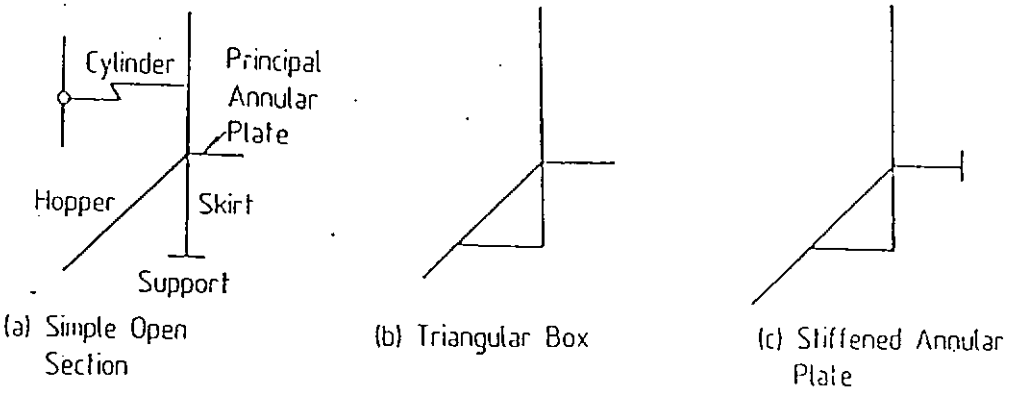

(After Rotter, 1985)

Fig. 1-5 Some Typical Ringbeam Geometries

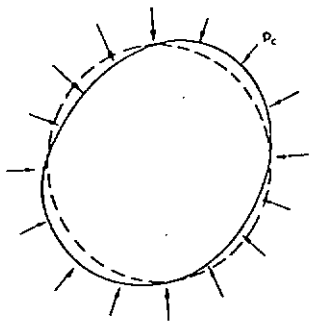

(After Trahair, et al, 1983)

Fig. 1-6 In-Plane Buckling of a ring

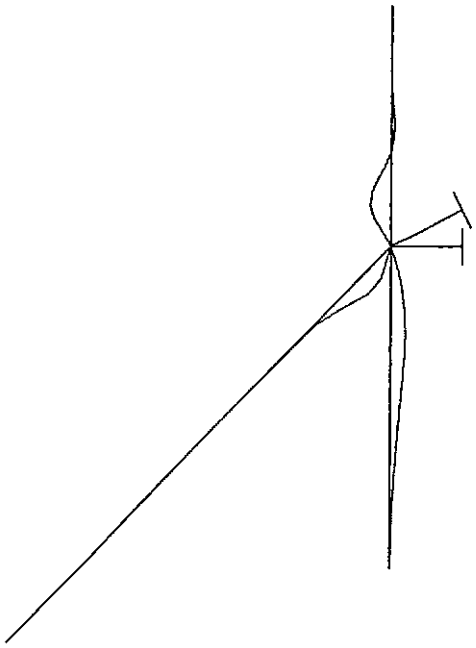

Fig. 1-7 Out-of-Plane Buckling of a T-Section Transition Ringbeam

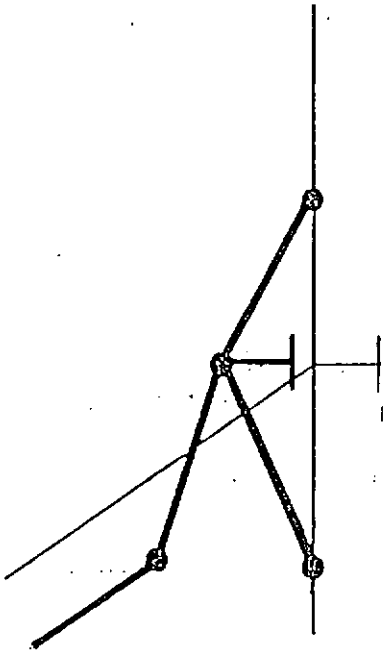

(Modified from Rotter, 1987)

Fig. 1-8 Plastic Collapse Mechanism of Transition Junction

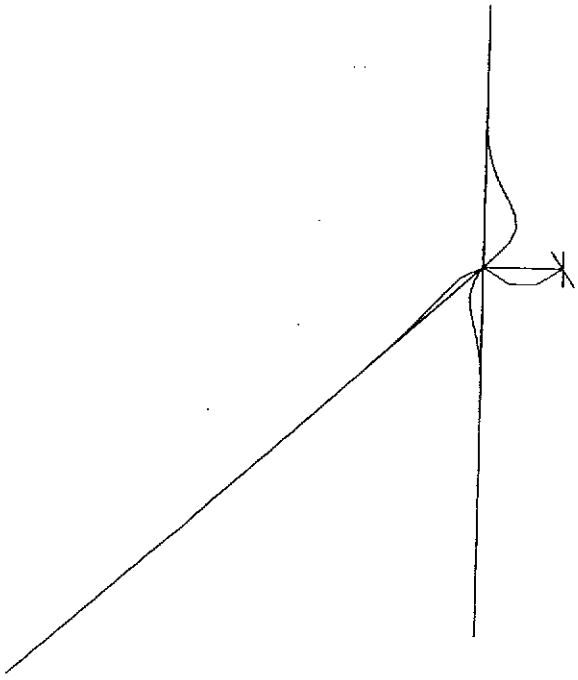

Fig. 1-9 Local Buckling of a T-Section Transition Ringbeam

CHAPTER 2 LITERATURE REVIEW

2.1 Introduction

This Chapter aims to provide a review of existing work relevant to the buckling and collapse of transition ringbeams in steel silos under axisymmetric loading and support conditions, with particular attention to transition junctions with a T-section ringbeam.

The chapter starts with a discussion of the classical theories for the in-plane and out-of-plane buckling of isolated rings and points out their deficiencies for applications to the buckling analysis of transition ringbeams in steel silos. This is followed by a review of recent attempts in extending these theories to include realistic restraint and loading characteristics of transition ringbeams and of the alternative approach using finite element shell buckling analysis for the development of design approximations for annular plate ringbeams.

Elastic buckling occurs for slender rings, while for stocky rings plastic buckling or plastic collapse are likely to control the strength. Existing work on the plastic buckling and collapse of transition junctions/ringbeams is thus discussed. The inadequacy of existing information for designing transition junctions with a T-section ringbeam is next noted. Finally, the NPEAS program employed to obtain buckling and collapse loads of transition ringbeams in this thesis is briefly described.

2.2 In-Plane Buckling of Isolated Rings

The critical load for the in-plane buckling of a ring is known to be a function of the behaviour of the external load applied to the ring (e.g. Smith and Simitses, 1969). The following three load cases are usually considered for the in-plane buckling of rings: (a) the load remains parallel to its initial direction during buckling; (b) the load remains normal to the ring surface; and (c) the load remains directed to the initial centre of curvature.

Bresse (1866) derived the first solution to the in-plane buckling problem of rings for Load Case (b) mentioned above. This solution was later described in Timoshenko and Gere (1961). Boresi (1955) developed a refined analysis for Load Cases (a) and (c) which is applicable to annular plate rings, with the thin ring problem as a limiting case. Wasserman (1961) presented results for all three cases as a by-product of a vibration analysis. Wempner and Kesti (1962) also derived a solution for Load Case (c). All these solutions are in agreement with each other. Later, Smith and Simitses (1969) presented a systematic study which considered all three cases and the effect of transverse shear deformation. Other in-plane buckling problems which have been investigated include buckling of a ring resting on an elastic foundation (Cheney, 1963a; Brush and Almroth, 1975) and rings with residual stresses (Anand and Griffith, 1973).

It has been found previously that in-plane buckling is unlikely for a transition ringbeam as it is strongly resisted by the membrane stiffness of the cone (Jumikis and Rotter, 1983).

2.3 Out-of-Plane Buckling of Isolated Rings and Transition Ringbeams

There have been a number of studies on the out-of-plane buckling of rings. Timoshenko and Gere (1961) described a solution for the out-of-plane buckling of a ring with a narrow rectangular cross-section. Since then, a number of different theories have been developed including Goldberg and Bogdanoff (1962), Cheney (1963b), Wah (1967), Yoo (1982), Trahair and Papangelis (1987), Teng and Rotter (1987). Teng and Rotter (1987) presented a simple and accurate theory for the out-of-plane buckling of unrestrained mono-symmetric rings. They also presented a comprehensive evaluation of the existing theories.

The solutions reviewed above are not applicable to the ringbeam at a silo transition junction as they do not include the two important features of a transition ringbeam. Firstly, the circumferential compressive force in the ringbeam is derived from the conical hopper, so the radial inward load is applied at the inner edge of the ringbeam. The second characteristic is that the adjacent structural elements provide a rigid restraint against out-of-plane translations and a rotational restraint at the inner edge of the ringbeam. To overcome these limitations of the existing theories, Teng and Rotter (1988) presented a thin-walled member theory for the out-of-plane buckling of monosymmetric ringbeams considering the two features, but the effect of cross-section distortion was not considered. This theory was later extended to ringbeams of general open sections by Teng and Lucas (1994). This closed-form solution considers both a rigid transitional restraint and an elastic rotational restraint provided by the shell wall to the ringbeam during buckling. T-section ringbeams were treated as a

special case in Teng and Rotter (1988) where a simplified solution was derived for inner edge simply-supported T-section ringbeams. As the assumption of a rigid ringbeam cross-section was used, the theories of Teng and Rotter (1988) and Teng and Lucas (1994) significantly overestimate the buckling strength of ringbeams with a heavy elastic rotational restraint from the adjacent shell walls compared with a finite element shell buckling analysis (Teng and Babagallo, 1995) including cross-section distortion, although its accuracy is high for ringbeams with a weak inner edge rotational restraint, including the case of a simply-supported inner edge which provides no rotational restraint. The effect of cross-section distortion is to reduce the buckling load, and the phenomenon has been extensively studied for straight members (Bradford, 1992; 1996).

Jumikis and Rotter (1983) adopted an alternative approach in developing their design approximation for annular plate transition ringbeams. They used a finite element shell buckling analysis program to study annular plate ringbeams attached to a silo transition junction. As both the ringbeam and the adjacent shell walls were modelled as axisymmetric shells, the assumption of a rigid cross-section was not made. To establish a simple design approximation, they first established the buckling strengths of two limiting cases: inner edge clamped annular plates and inner edge simply-supported annular plates. The buckling strength of a transition annular plate ringbeam was then formulated through an appropriate interpolation of the buckling strengths of these two cases. Their approximate design equations were later modified and further verified over a very wide range of geometry by Sharma et al (1987). Rotter and Jumikis (1985) also carried out a finite element study on the elastic buckling of T-section ringbeams at silo transition junctions, but with the elastic rotational restraints

ignored and established a rather complex approximate equation based on their numerical results.

2.4 Plastic Collapse of Transition Ringbeams

Ringbeams of a stocky cross-section may be expected to fail by plastic collapse of the cylinder/cone/skirt/ringbeam junction instead of buckling. The plastic collapse behaviour and strength of these transition junctions were first studied by Rotter (1985, 1987) and later by Teng and Rotter (1991a; 1991b). Rotter first described the collapse mechanism which requires two plastic hinge circles to develop within each shell segment adjacent to the transition: one at the transition and the other within the shell segment. He also produced a simple equation to predict the collapse strength of junctions of uniform thickness. Teng and Rotter (1991a; 1991b) conducted a comprehensive study into the plastic collapse behaviour and strength of these junctions and developed an improved form of Rotter's (1987) design equation for application to transition junctions of non-uniform thickness.

All the existing studies on plastic collapse strength are explicitly concerned only with junctions with an annular plate ringbeam. Nevertheless, the design equation of Teng and Rotter (1991a; 1991b) should also be valid for transition junctions with a T-section ringbeam provided the extra area of the vertical stiffener is properly accounted for.

2.5 Plastic Out-of-Plane Buckling of Transition Ringbeams

Ringbeams of intermediate slenderness are expected to fail by plastic buckling, a form of failure involving interaction between buckling and yielding. Plastic out-of-plane buckling of annular plate ringbeams was examined briefly by Rotter (1987), Greiner (1991), and Teng and Rotter (1991c), who also briefly considered plastic buckling of T-section ringbeams at the transition junction of steel silos. Teng (1997) presented a comprehensive investigation into the plastic out-of-plane buckling strength of annular plate ringbeams at steel silo transition junctions, leading to the first ever rational design approximation. The design approximation is based on the more conservative predictions of the deformation theory of plasticity (Teng and Rotter, 1989b). It was found that the characteristics of interaction between yielding and buckling is controlled by a single parameter, termed the dimensionless ringbeam size parameter. As long as this key parameter is given, a single function is sufficient to relate the plastic buckling strength to the elastic buckling strength and plastic collapse strength. Based on the numerical results and the existing design equations for plastic collapse and elastic buckling, respectively, a lower bound design approximation was proposed for practical use. The application of the proposed design method was illustrated using an example (Teng, 1997).

The study by Teng and Rotter (1991c) is the only existing study which has examined the plastic buckling of T-section transition ringbeam. This study is limited in scope and produced no simple design approximation.

2.6 Existing Design Guidance on Transition Ringbeams

There is yet no code of practice for the structural design of steel silos in any country, though a few design guides are available (Ketchum, 1909; Lambert, 1968; Wozniak, 1979; Trahair et al, 1983; Gaylord and Gaylord, 1984) and a European code (CEN, 1997) is being developed. An examination of these design guides reveals that the more recent design guides (Trahair et al., 1983; Gaylord and Gaylord, 1984) have paid more attention to design against buckling and collapse in steel silo structures, but insufficient information has left many problems in uncertainty.

In-plane buckling is generally the only buckling mode recognised in design guides (Wonziak, 1979; Gaylord and Gaylord, 1984) except for Trahair et al. (1983) which adopted Jumikis and Rotter (1983) design equations for assessing the elastic buckling strength of annular plate ringbeams. For T-section ringbeams, Trahair et al. (1983) also includes a rule for predicting the elastic buckling strength based on Cheney's (1963) work. As Cheney's (1963) has been shown by Teng and Rotter (1988) to be restricted to centroidal loading, this rule gives erroneous results even for lightly restrained ringbeams which do not suffer from cross-section distortion. A rough procedure is also found in Trahair et al. (1983) to account for interaction between yielding and buckling, but there is no rigorous theoretical basis for this procedure.

2.7 Buckling and Collapse Analysis of Axisymmetric Shells Using Program NEPAS

The buckling and collapse studies presented in this thesis were conducted using the NEPAS program (program for geometrically Non-linear Elastic-Plastic Analysis for

Stability) (Teng and Rotter, 1989b). A variety of analysis may be performed using NEPAS on a given structure.

Linear elastic buckling analysis can be carried out if the structure is assumed to be linear elastic and the effect of geometric changes due to the prebuckling axisymmetric deformations is ignored. The finite element results presented in Chapters 3 and 4 were obtained using the linear elastic buckling analysis option of the NEPAS program. Most of the finite element results presented in Chapters 5 are also linear elastic buckling loads.

If the effect of geometrical changes due to prebuckling axisymmetric deformations is included in the analysis, the buckling loads obtained are referred to as the nonlinear elastic buckling loads.

Plastic buckling loads are obtained from structures which suffer yielding before buckling. Geometrically linear plastic buckling analyses are carried out when the effect of prebuckling deformations are unimportant and ignored. Most of the plastic buckling loads presented in Chapter 6 were obtained using a geometrically linear plastic buckling analysis. If the effect of prebuckling deflections is taken into account, the most complicated type of bifurcation buckling analysis is required, in which both geometrical non-linearity and material plasticity are considered. Only a small number of transition ringbeams were analysed this way, with the results given in Chapter 6.

The finite element analysis, being based on a thin shell theory, does not suffer from the limitations of the thin-walled member theory used by Teng and Rotter (1989) and Teng and Lucas (1994) for out-of-plane buckling of rings. That is, all possible

buckling modes including flexural-torsional, distortional and local buckling modes, are considered in the finite element model. The buckling strength of the ring is given in terms of the circumferential compressive stress at the inner edge of the ringbeam.

All results were obtained with an elastic modulus E of 2 x 10^5 MPa and a Poisson's ratio of 0.3. The results are presented in such a way that they are independent of the elastic modulus and vary little with Poisson's ratio, so they can also be used for other isotropic materials such as aluminium which has a similar Poisson's ratio. The plastic behaviour of the material of the transition junction is assumed to be elastic perfectly-plastic, and the material may have different yield stresses.

2.8 Conclusions

This Chapter has provided a review on existing work relevant to the buckling and collapse of transition ringbeams in steel silos under axisymmetric loading and support conditions, with particular attention to transition junctions with a T-section ringbeam. Despite many studies, existing information is still insufficient to establish a simple stability design procedure for transition junctions with a T-section ringbeam.

It is clear from the review that, to develop a simple method for assessing the elastic buckling strength of T-section transition ringbeams, the thin-walled member theory cannot be solely relied on as cross-section distortion cannot be properly accounted for. The approach adopted by Jumikis and Rotter (1983) for annular plate ringbeams is more promising. To account for the effect of plasticity on buckling strength, a study similar to that by Teng (1997) is required.

CHAPTER 3 ELASTIC BUCKLING OF T-SECTION RINGBEAMS CLAMPED AT INNER EDGE

3.1 Introduction

From the review presented in Chapter 2, it is clear that the approach adopted by Jumikis and Rotter (1983) to develop a simple design approximation for the elastic buckling strength of annular plate transition ringbeams should be followed here to develop a similar approximation for T-section transition ringbeams.

It is therefore appropriate to briefly describe their approach so that the work of this chapter and Chapter 4 is set in its proper context. They modelled both the ringbeam and the adjacent shell walls using an axisymmetric shell element, so the assumption of a rigid ringbeam cross-section was not made. To establish a simple design approximation, they first established the buckling strengths of two limiting cases: inner edge clamped annular plates and inner edge simply-supported annular plates. The elastic buckling strength of an annular plate ringbeam of width B and thickness T is given as:

$$\sigma_{\theta r} = cE\left(\frac{T}{B}\right)^2 \tag{3-1}$$

where $\sigma_{\theta r}$ refers to the maximum circumferential compressive stress which occurs at the inner edge of the ringbeam and E is the elastic modulus. For an annular plate ringbeam with a simply supported inner edge, the coefficient c is given by

$$c = c_s = 0.385 + 0.452\sqrt{\frac{B}{R}} \tag{3-2}$$

whereas if the inner edge is fully clamped

$$c = c_c = 1.154 + 0.56\frac{B}{R} \tag{3-3}$$

in which R is the radius of the ringbeam inner edge (i.e. radius of the cylindrical section of the silo). In general, the value of c lies between the two above values because the silo wall provides some degree of flexural restraint against buckling. The value of c may then be found through the following interpolation:

$$c = \frac{\eta_s c_s + \eta_c c_c}{\eta_s + \eta_c} \tag{3-4}$$

with

$$\eta_s = 0.43 + \frac{(R/B)^2}{4000} \tag{3-5}$$

$$\eta_c = \frac{1}{2}\left[\left(\frac{t_c}{T}\right)^{2.5} + \left(\frac{t_h}{T}\right)^{2.5} + \left(\frac{t_s}{T}\right)^{2.5}\right] \tag{3-6}$$

where t_c, t_h and t_s are the wall thickness of the cylindrical body, the hopper and the skirt respectively.

For a similar approach to be established for a T-section transition ringbeam, a simple approximation needs to be found for each of the two limiting cases: T-section ringbeams with a simply-supported inner edge and T-section ringbeams with a clamped inner edge. The buckling strength of inner edge simply-supported T-section ringbeams will be dealt with in Chapter 4. This chapter presents an investigation into the buckling behaviour of T-section ringbeams with a clamped inner edge, leading to

the establishment of a simple buckling strength approximation. This approximation will form the basis for the development of an approximate design equation for the elastic buckling strength of ringbeams with a semi-rigid rotational restraint from adjacent shell walls.

3.2 Buckling Analysis and Modelling

The finite element buckling loads presented here were obtained using the linear elastic buckling option of the NEPAS program (Teng and Rotter, 1989b), which can perform linear or non-linear bifurcation buckling analysis of branched axisymmetric shells. The finite element analysis, being based on a thin shell theory, does not suffer from the limitations of the thin-walled member theory. That is , all possible buckling modes including flexural-torsional, distortional and local buckling modes, are considered in the finite element model.

The T-section ringbeam has an annular plate of B_p x T_p and a stiffener of B_s x T_s (Fig. 3-1). An inward radial load is applied at the ringbeam inner edge. The inner edge is allowed to move radially in the prebuckling analysis so that the applied radial load leads to circumferential compression in the ringbeam. During buckling, the inner edge is fully clamped. The circumferential compressive stress varies slightly over the ringbeam cross-section with the maximum value at the inner edge. The buckling strength of the ringbeam is characterised using the circumferential compressive stress at the inner edge of the ringbeam following Jumikis and Rotter (1983).

3.3 Buckling Modes

Depending on the geometric proportions of the cross-section, the ringbeam may fail by either distortional buckling or local buckling (Fig. 3-1). This is illustrated by examining the buckling modes of uniform thickness T-sections ($T_p = T_s = T$) with $B_p/R = 0.05$, $B_p/T = 30$ and two different values of B_s/B_p. A critical buckling mode is identified when a minimum buckling load is found as the number of circumferential buckling waves is varied (Fig. 3-2). For both sections, two minima are found: one corresponding to the distortional buckling mode and the other corresponding to the local buckling mode. The distortional buckling mode involves the translational movement of the plate/stiffener junction, with the outer stiffener experiencing both an out-of-plane translation and a rotation (Fig. 3-1). In the local buckling mode, there exists no translational movement at the plate/stiffener junction and the stiffener goes through a rotation about the plate/stiffener junction. The controlling buckling mode is the one which gives the lower buckling strength. For the section with $B_s/B_p = 0.5$, distortional buckling is the controlling buckling mode. On the other hand, the section with a more slender stiffener ($B_s/B_p = 1$) is controlled by local buckling. This is not difficult to understand: as the stiffener becomes higher and thus more slender, the local buckling strength of the stiffener drops while the distortional buckling strength increases as a result of a larger out-of-plane bending resistance. Thus, for a given thickness ratio between the annular plate and the stiffener, local buckling is expected to control the strength once the value of B_s/B_p exceeds a certain limit.

In conventional structural steel design, it is often recommended that the member section be properly proportioned so that local buckling can be avoided. The same philosophy is recommended here. To be able to apply this philosophy, it is necessary to establish appropriate limits on the geometric proportions to ensure that distortional buckling is the controlling mode. To this end, a large number of buckling analyses were carried out, determining both the local buckling strengths and the distortional buckling strengths to identify the controlling mode. The relevant geometric parameters include B_p/R, B_s/B_p, B_p/T_p, and T_s/T_p. Results were obtained for T_s/T_p = 0.5, 1.0 and 2 and B_p/R = 0.01, 0.05 and 0.1. For design application, the chart in Fig. 3-3 based on the results for B_p/R = 0.01 is proposed for use, since the geometric range for ringbeams with B_p/R = 0.01 failing by distortional buckling is more restrictive than those for the other two higher values of B_p/R. Although only three values of T_s/T_p are explicitly covered in Fig. 3-3, a linear interpolation may be used for a T_s/T_p value between 0.5 and 2 but not coinciding with one of these three values. The range of T_s/T_p values covered (between 0.5 and 2) is not too restrictive as in practice the thickness of the annular plate and the stiffener are very often the same or similar. The curve for T_s/T_p of 2 can also be used for higher T_s/T_p values as a conservative measure. The use of this chart in design can thus ensure that the ringbeam geometry selected will be controlled by distortional buckling. A method for estimating the distortional buckling strength is now sought. Distortional buckling has been examined for straight member in many studies (Bradford, 1992 and Bradford, 1996) which may be consulted for more information on the phenomenon of distortional buckling in structural members.

It should be noted that the geometric limits of Fig. 3-3 are based solely on elastic buckling stresses. Some adjustments to these limits may be necessary when yielding, residual stresses and initial geometric imperfections are considered, although such adjustments are beyond the scope of the present study.

3.4 Effect of Ringbeam Radius on Buckling Strength

Figure 3-4 shows the variation of buckling strength with the ringbeam width-to-radius ratio B_p/R for uniform thickness ($T_p = T_s$) ringbeams of four different B_p/T ratios and a B_s/B_p ratio of 0.5. As the ringbeam inner edge radius R reduces (B_p/R increases), the elastic buckling strength may increase or decrease, but the variation overall is quite small. This parameter is thus only weakly influential. This situation contrasts with that of a inner edge simply-supported T-section ringbeam, for which the elastic buckling stress depends strongly on B_p/R.

3.5 Bulson's Solution for Edge-Stiffened Rectangular Plates

If the effect of radius is small, the buckling stress of a ringbeam with a large radius may be used to approximate the buckling strength of ringbeams with smaller radii. Further, the buckling stress of an inner edge clamped ringbeam with a very large radius is similar to that of a longitudinally compressed long rectangular plate of width B_p and thickness T_p with an edge stiffener of width B_s and thickness T_s clamped along the un-stiffened edge. Bulson (1970) presented both accurate and approximate solutions for a rectangular plate with an edge stiffener clamped along the un-stiffened edge and simply supported along top and bottom edges. His approximate closed-form

solution is based on the energy method and the assumption of a single sine half wave in the longitudinal direction for the buckled shape. In the present notation, this solution is given by

$$\sigma_{cr}\left(1+\frac{9A_{rs}}{2A_{rp}}\right)=\frac{\pi^2 E}{12(1-\nu^2)}\left(\frac{T_P}{B_P}\right)^2\left(\frac{1}{\phi^2}+0.14\phi^2+0.67\right)+\frac{9\pi^2 EI_S}{2\phi^2 B_P{}^3 T_P} \qquad (3\text{-}7)$$

The above equation can be modified to give more accurate results by replacing the first term on the right hand side with a more accurate approximation (Bulson, 1970):

$$\sigma_{cr}\left(1+\frac{9A_{rs}}{2A_{rp}}\right)=\frac{\pi^2 E}{12(1-\nu^2)}\left(\frac{T_P}{B_P}\right)^2\left(\frac{1}{\phi^2}+0.14\phi^2+0.5\right)+\frac{9\pi^2 EI_S}{2\phi^2 B_P{}^3 T_P} \qquad (3\text{-}8)$$

where A_{rs} and A_{rp} are the cross-sectional areas of the plate and the stiffener respectively, and EI_s is the out-of-plane bending stiffness of the stiffener. To find the buckling stress of a long rectangular plate, the above equation needs to be minimised with regard to the plate aspect ratio ϕ (= length/width) as a long plate can buckle at the lowest possible stress by forming many waves with each half wave corresponding to a plate with simply-supported top and bottom edges. With this minimisation, the buckling stress can be expressed as

$$\frac{\sigma_{cr}}{E}=K_{\min}\frac{\pi^2}{12(1-\nu^2)}\left(\frac{T}{B_p}\right)^2 \qquad (3\text{-}9)$$

where the coefficient K_{min} is given by

$$K_{\min}=\frac{1}{\phi^2{}_{\min}}\left[1+4.5(1-\nu^2)\left(\frac{B_S}{B_p}\right)\left(\frac{B_S}{T_p}\right)^2\left(\frac{T_S}{T_p}\right)\right]+0.14\phi_{\min}{}^2+0.5 \qquad (3\text{-}10)$$

and
$$\phi^2{}_{\min} = \sqrt{\frac{1+4.5\left(1-\nu^2\right)\left(\frac{B_S}{B_p}\right)\left(\frac{B_S}{T_p}\right)^2\left(\frac{T_S}{T_p}\right)}{0.14}} \tag{3-11}$$

Substitution of Eq. 3-11 into Eq. 3-10 leads to

$$K_{\min} = \frac{\sqrt{0.56\left[1+4.5\left(1-\nu^2\right)\left(\frac{B_S}{B_p}\right)\left(\frac{B_S}{T_p}\right)^2\left(\frac{T_S}{T_p}\right)\right]}+0.5}{1+4.5\left(\frac{B_S}{B_p}\right)\left(\frac{T_S}{T_p}\right)} \tag{3-12}$$

If the edge stiffener has the same thickness as the plate ($T_s = T_p = T$), K_{min} is then given by

$$K_{\min} = \frac{\sqrt{0.56[1+4.5(1-\nu^2)\left(\frac{B_S}{B_p}\right)\left(\frac{B_S}{T}\right)^2]}+0.5}{1+4.5\left(\frac{B_S}{B_p}\right)} \tag{3-13}$$

The accuracy of these equations in predicting the buckling strength of T-section ringbeams will be examined next through comparisons with finite element results.

3.6 Accuracy of Bulson's Solution and Modification

3.6.1 Uniform Thickness Ringbeams

As a first step, uniform thickness T-section ringbeams ($T_s = T_p = T$) are considered. The dimensionless geometric parameters controlling the buckling strength of these ringbeams are: B_p/R, B_p/T, B_s/B_p. The above solution from Bulson (1970) is compared with finite element results for a wide range of geometry and comparisons for three *Bp/R* values (0.01, 0.05 and 0.1) are shown in Fig. 3-5. For thin ringbeams with B_p/R

= 0.01 (Fig. 3-5a), Bulson's solution approximates the finite element results well when B_s/B_p is below 0.6, but becomes unconservative when B_s/B_p = 0.8 and 1.0. For B_p/R = 0.05 and 0.1 (Fig. 3-5b and Fig. 3-5c), Bulson's solution is quite accurate up to B_s/B_p = 0.4. As high values of B_s/B_p probably correspond to sections which are controlled by local buckling and are thus outside the range of section geometries of interest here, a better assessment of Bulson's equation is to compare its predictions with finite element results for sections controlled by distortional buckling according to Fig. 3-3. This is done in Fig. 3-6 for ringbeams with B_p/T = 10, 15, 20, 25, 30, 35, 40, 45, 50, B_p/R = 0.01, 0.025, 0.05, 0.075, 0.1, which are expected to cover a range wider than is used in practice when buckling failure needs to be considered. To achieve a better approximation, the factor of 4.5 in the denominator of Eqs 3-12 and 3-13 is replaced by 5.0, so K_{min} is now given by

$$K_{\min} = \frac{\sqrt{0.56\left[1 + 4.5\left(1-\nu^2\right)\left(\frac{B_S}{B_p}\right)\left(\frac{B_S}{T_p}\right)^2\left(\frac{T_S}{T_p}\right)\right]} + 0.5}{1 + 5\left(\frac{B_S}{B_p}\right)\left(\frac{T_S}{T_p}\right)} \qquad (3\text{-}14)$$

This modified equation for K_{min} together with Eq. 3-9, refer to as Approximation C-I hereafter, provides reasonably close predictions of the finite element results. The ratio between the finite element results and Approximation C-I is within 0.9 and 1.25. Figure 3-6 shows that Approximation C-I becomes unconservative for relatively high B_s/B_p values (Fig. 3-6a) coupled with lower values of B_p/T (Fig. 3-6b), but the number of cases affected is small.

3.6.2 Non-Uniform Thickness Ringbeams

Bulson's equation (Eq. 3-7 or 3-8) shows that the edge stiffener contributes to the buckling resistance mainly through the out-of-plane bending stiffness of the stiffener EI_s (The torsional stiffness of the stiffener is ignored in Bulson's approximate solution). According to Eq. 3-8, for a given cross-section with a fixed annular plate geometry, if the moment of inertia I_S of the stiffener is kept unchanged, the buckling stress multiplied by $(1 + 4.5\ A_s/A_p)$ is independent of the B_s/T_s ratio. Figure 3-7 shows a comparison between Approximation C-I (Eqs 3-9 and 3-14) and finite element results for T-section ringbeams with a constant I_s. The geometry of the annular plate is fixed, but the values of B_s and T_s are changed to arrive at different B_s/T_s ratios while maintaining a constant I_s. This comparison shows that Approximation C-I predicts the influence of a non-uniform thickness closely (Fig. 3-7). Approximation C-I becomes more conservative as B_s/T_s reduces and this is believed to be due to its omission of the torsional stiffness of the stiffener which becomes more significant as the stiffener becomes stockier.

3.7 An Alternative Approximation

3.7.1 Uniform Thickness Ringbeams

Approximation C-I is still a relatively long expression, so it was decided to investigate the possibility of an alternative approximation. By trial and error, it was found that for the range of uniform thickness ringbeams covered here, the elastic buckling stress may be expressed as:

$$\frac{\sigma_{dcr}}{E} = \rho\left(\frac{T}{B_p}\right)^{1.1} \tag{3-15}$$

Equation 3-15 is referred to as Approximation C-II. Figure 3-8 shows that for uniform thickness ringbeams, ρ varies only slightly with B_p/T and depends mainly on B_s/B_p. Values of ρ for five different B_p/R ratios (= 0.01, 0.025, 0.05, 0.075 and 0.1) are shown in Fig. 3-8 and this re-confirms that the effect of B_p/R is small. The effect of B_p/R is further examined in Fig. 3-9 where the variation of ρ (taken as the lowest value of ρ among the B_p/T values examined in Fig. 3-8) with B_s/B_p is plotted for different values of B_p/R ratios. The finite element results shown in Figs 3-8 and 3-9 include only those for sections whose strengths are controlled by distortional buckling. A simple approximation for ρ is to ignore its weak dependence on both B_p/T and B_p/R, so the following expression may be used for all geometries

$$\rho = 0.016 + 0.5\left(\frac{B_s}{B_p}\right) - 0.25\left(\frac{B_s}{B_p}\right)^2 \tag{3-16}$$

Eq. 3-16 implies that if the stiffner height B_s exceeds the annular plate width B_p, the buckling stress will start to decrease. Approximation C-II (Eqs 3-15 and 3-16) is compared with the finite element results for three B_p/R values (0.01, 0.05 and 0.1) and for B_s/B_p of 0.2, 0.4, 0.6, 0.8 and 1.0 in Fig. 3-10. For thin ringbeams with B_p/R = 0.01 (Fig. 3-10a), Approximation C-II is seen to be close or conservative for all B_s/B_p values examined. For ringbeams with B_p/R of 0.05 and 0.1, this is the case for B_s/B_p up to 0.6 (Fig. 3-10b) and 0.4 (Fig. 3-10c), respectively. Approximation C-II becomes more conservative as B_p/T reduces.

The accuracy of Approximation C-II (Eqs 3-15 and 3-16) is assessed in Fig. 3-11 for those sections which are controlled by distortional buckling. For B_p/T values not smaller than 15, the finite element results are well predicted by Approximation C-II and the ratios between the predictions from the finite element analysis and Approximation C-II are between 0.97 and 1.21 (Fig. 3-11a). Approximation C-II is quite conservative for stocky ringbeams (small B_p/T ratios) (Fig. 3-11a) with a short stiffener (Fig. 3-11b).

Approximation C-II has a simpler form than Approximation C-I, but has comparable accuracy. Further, it gives conservative or close predictions for all cases examined. Its significant conservativeness for stocky ringbeams is not a major flaw, at least for steel ringbeams, as the effect of out-of-plane instability has only a small bearing on the ultimate strength of such ringbeams whose strengths are likely to be dominated by plastic collapse (see Chapter 6).

3.7.2 Non-Uniform Thickness Ringbeams

It is possible to extend Approximation C-II to non-uniform thickness ringbeams, based on the conclusion from Bulson's Solution that for a given cross-section with a fixed annular plate geometry, if the moment of inertia I_s of the stiffener is kept unchanged, the buckling stress multiplied by $(1 + 4.5\ A_s/A_p)$ is constant. For a given T-section ringbeam of dimensions B_p, T_p, B_s and T_s, a corresponding equivalent uniform thickness section with the same I_s can be found. This equivalent T-section will have dimensions B_p and B_{se} and a uniform thickness equal to T_p. Here, the

equivalent stiffener height B_{se} needs to take a value to achieve the same I_s as the original section, so

$$B_{se} = B_s \sqrt[3]{\frac{T_s}{T_p}} \tag{3-17}$$

The buckling stresses of the original section σ_{cr} and that of the equivalent uniform thickness section $\sigma_{uniform}$ are related through (using the modified factor 5 instead of 4.5):

$$\sigma_{cr}[1 + 5(\frac{B_s}{B_p})(\frac{T_s}{T_p})] = \sigma_{uniform}[1 + 5(\frac{B_{se}}{B_p})] \tag{3-18}$$

Therefore,

$$\frac{\sigma_{cr}}{E} = \frac{1 + 5\left(\frac{B_s}{B_p}\right)\left(\frac{T_s}{T_p}\right)}{1 + 5\left(\frac{B_s}{B_p}\right)\sqrt[3]{\frac{T_s}{T_p}}}\left[0.016 + 0.549\frac{B_s}{B_p}\sqrt[3]{\frac{T_s}{T_p}} - 0.357\left(\frac{B_s}{B_p}\sqrt[3]{\frac{T_s}{T_p}}\right)^2\right]\left(\frac{T_p}{B_p}\right)^{1.1} \tag{3-19}$$

The accuracy of the above equation is checked in Fig. 3-12 and is found to be satisfactory.

3.8 Conclusion

This chapter has presented a study on the elastic buckling strength of T-section ringbeams clamped at inner edge. Such ringbeams can fail by either local buckling or distortional buckling. In practical design, local buckling should be avoided by proportioning the section properly following the limits set by the design chart proposed here. The distortional buckling strength of clamped T-section ringbeams has been shown to vary only slightly with radius and can be approximated by the

existing solution of Bulson (1970) for an edge-stiffened rectangular plate clamped along the un-stiffened edge with a simple modification (Approximation C-I). An alternative approximation (Approximation C-II) for inner edge clamped T-section ringbeams has also been proposed. Approximation C-II is particularly simple for the commonly used uniform thickness T-section ringbeams and may be used in place of Approximation C-I to keep the design calculations to a minimum.

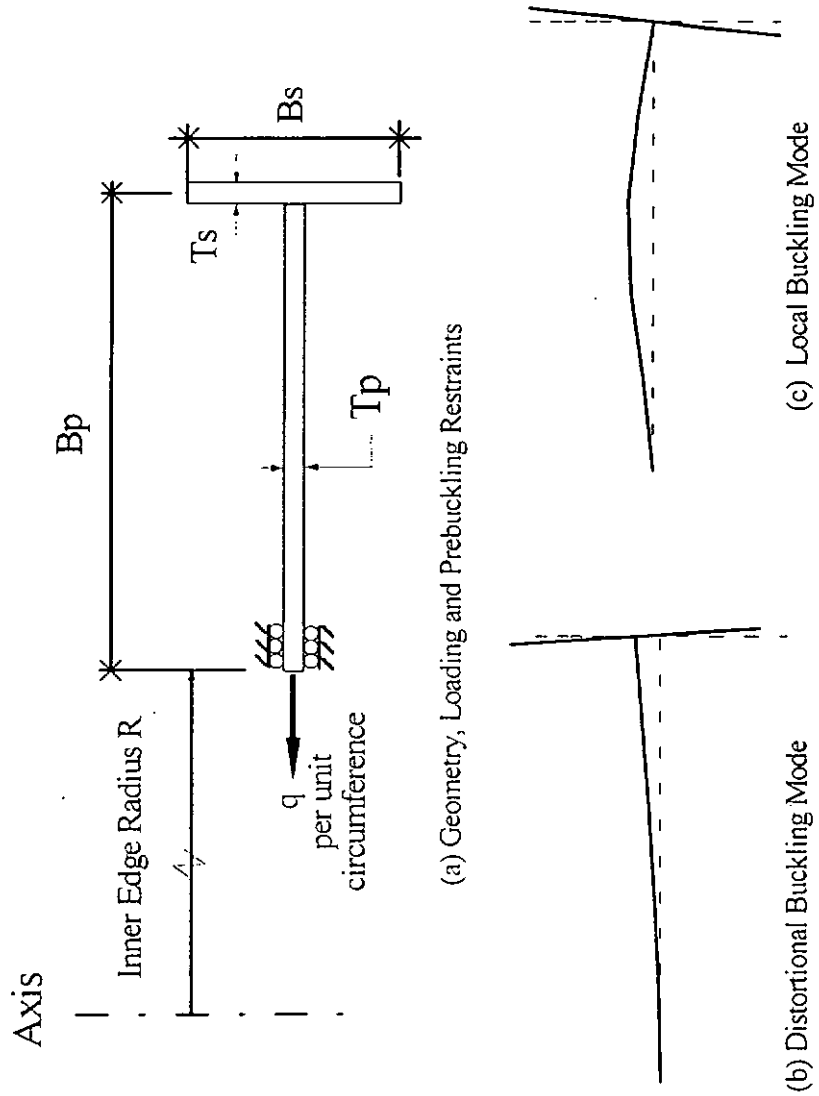

Fig. 3-1. Geometry and Buckling Modes of Clamped T-Section Ringbeams

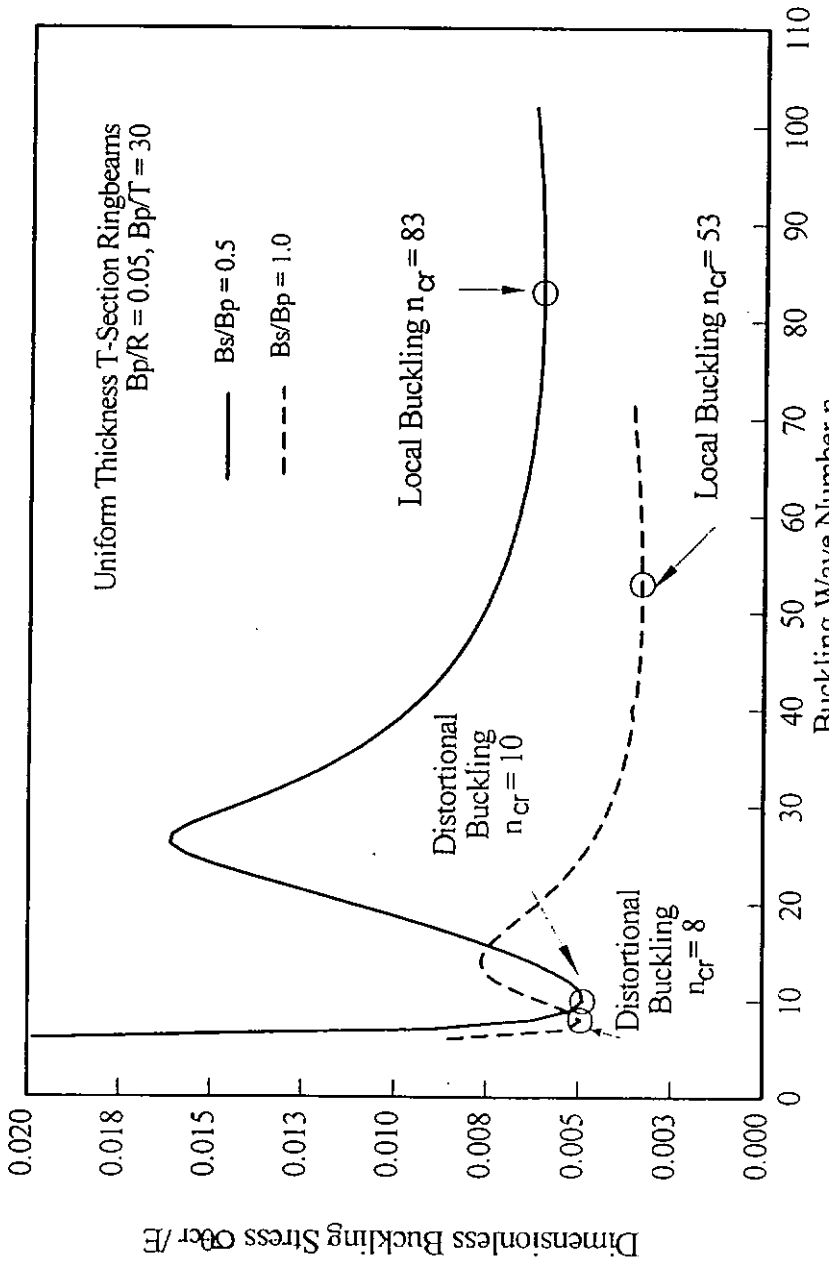

Fig. 3-2 Variation of Buckling Strength with Circumferential Buckling Wave Number

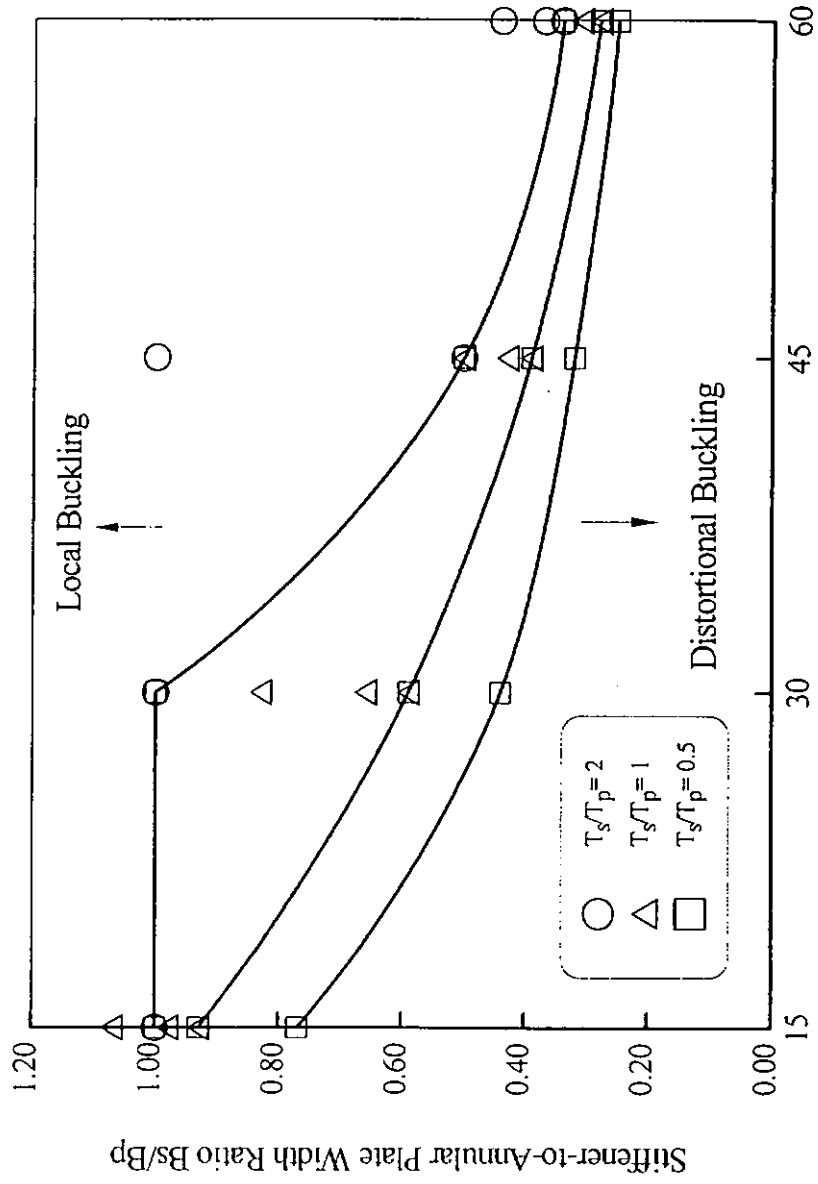

Fig. 3-3 Geometric Limits for Distortional Buckling

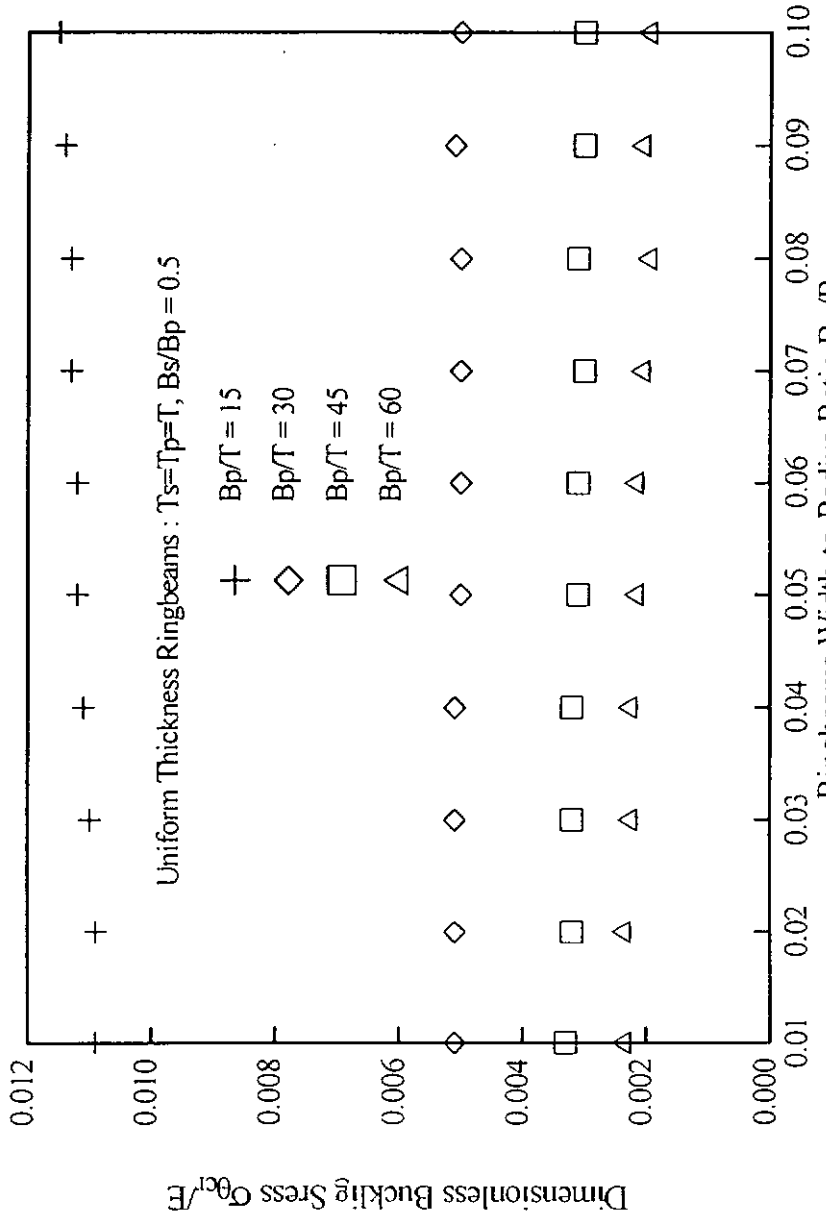

Fig. 3-4 Effect of Ringbeam Width-to-Radius Ratio on Distortional Buckling Strength

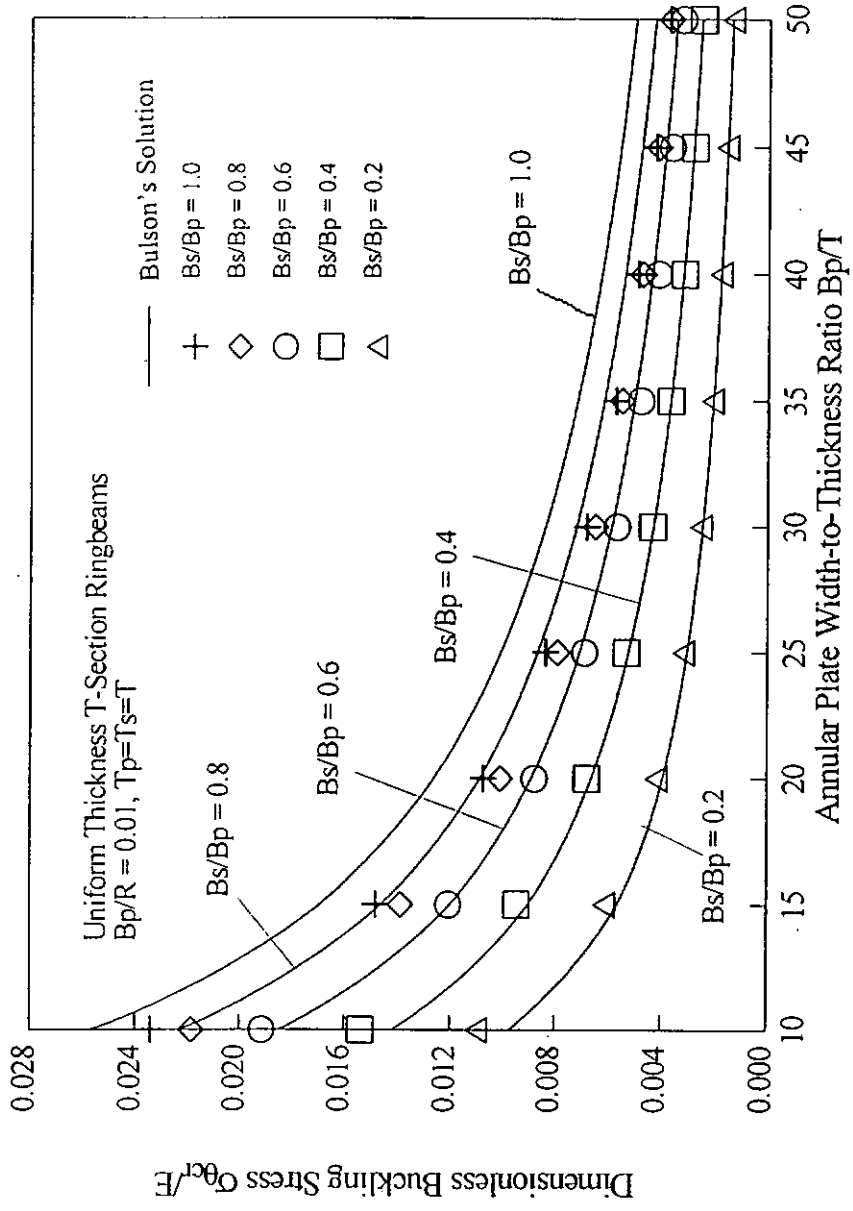

(a) Bp/R = 0.01

Fig. 3-5 Comparison between Bulson's Solution and Finite Element Analysis for Uniform Thickness Ringbeams

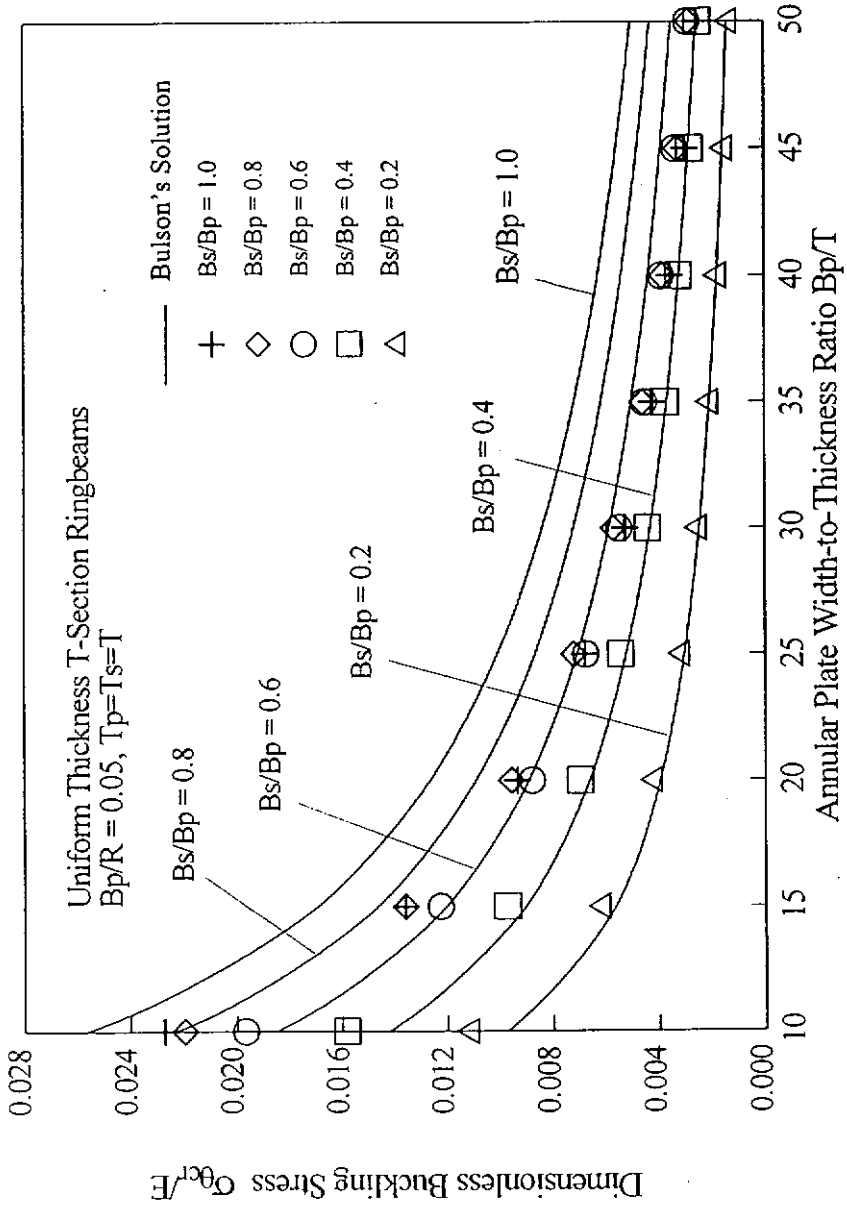

(b) Bp/R = 0.05

Fig. 3-5 Comparison between Bulson's Solution and Finite Element Analysis for Uniform Thickness Ringbeams

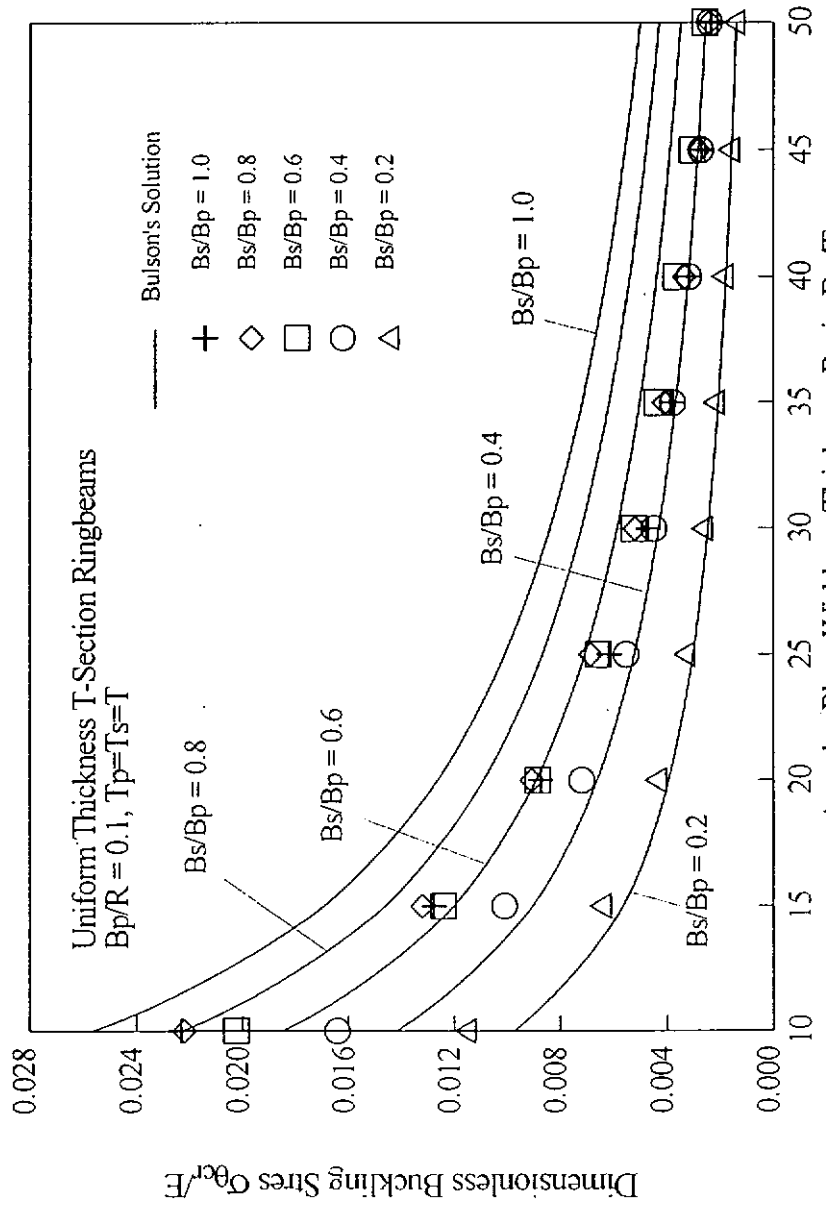

(c) Bp/R = 0.1

Fig. 3-5 Comparison between Bulson's Solution and Finite Element Analysis for Uniform Thickness Ringbeams

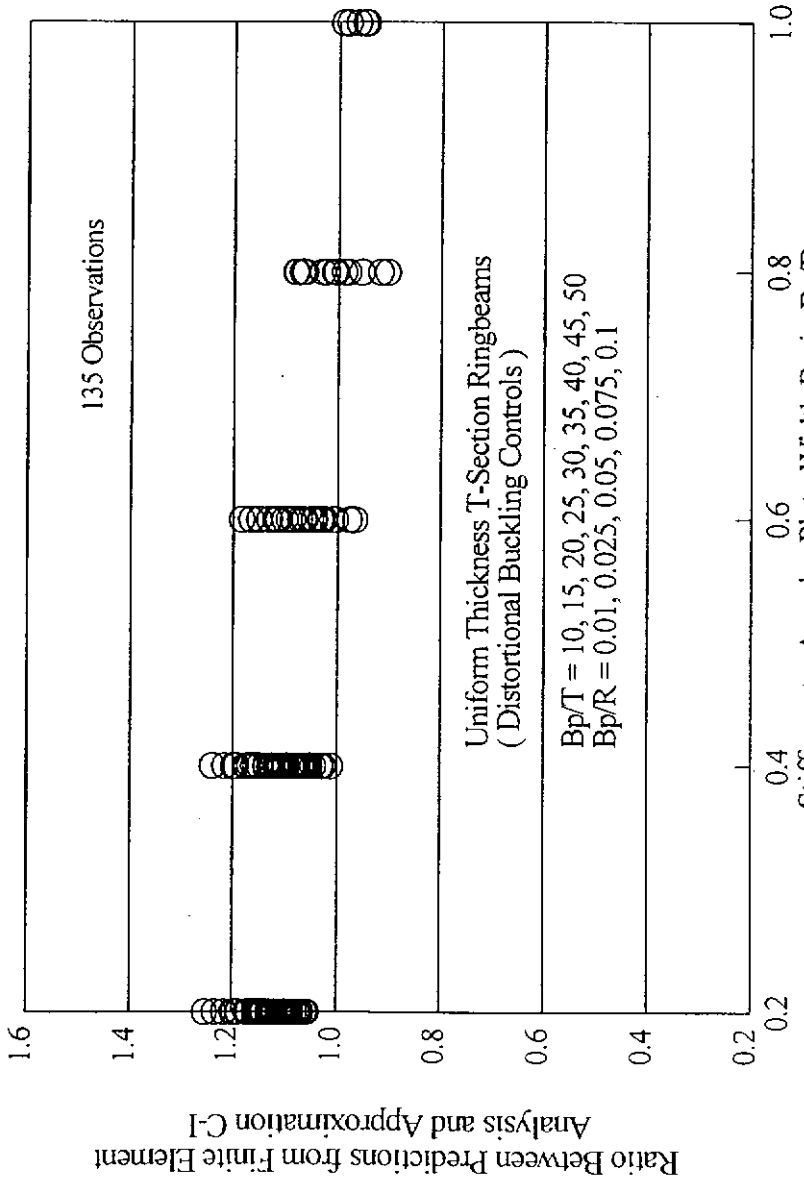

(a)

Fig. 3-6 Accuracy of Approximation C-I for Uniform Thickness Ringbeams

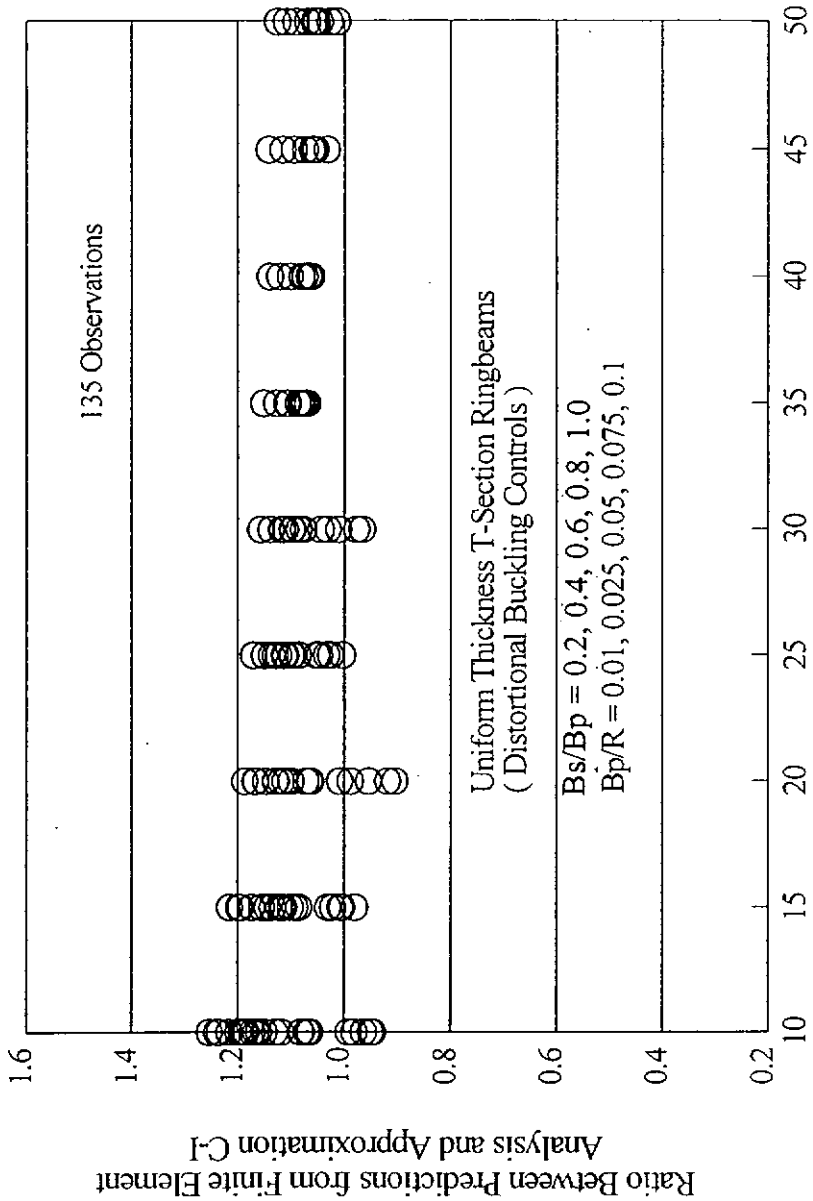

(b)

Fig. 3-6 Accuracy of Approximation C-I for Uniform Thickness Ringbeams

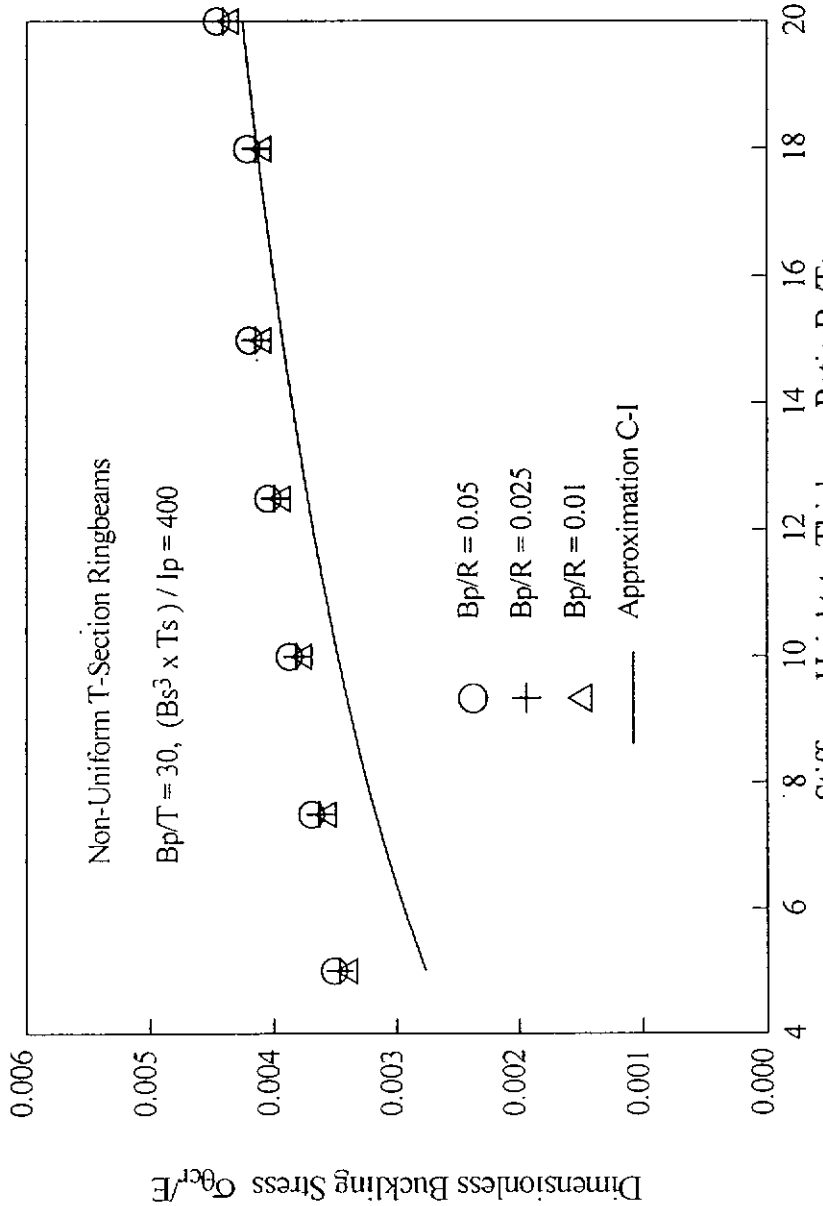

Fig. 3-7 Comparison between Approximation C-I and Finite Element Analysis for Non-Uniform Thickness Ringbeams

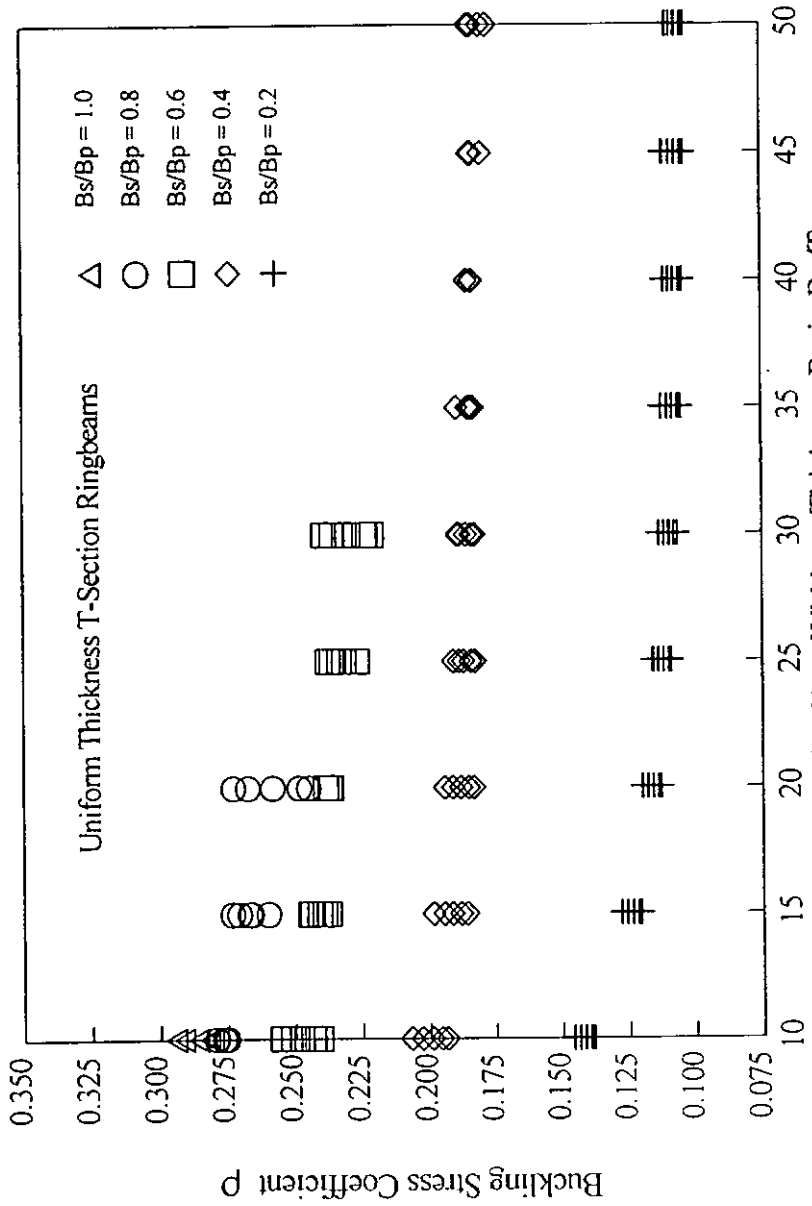

Fig. 3-8 Variation of Buckling Stress Coefficient with Annular Plate Width-to-Thickness Ratio

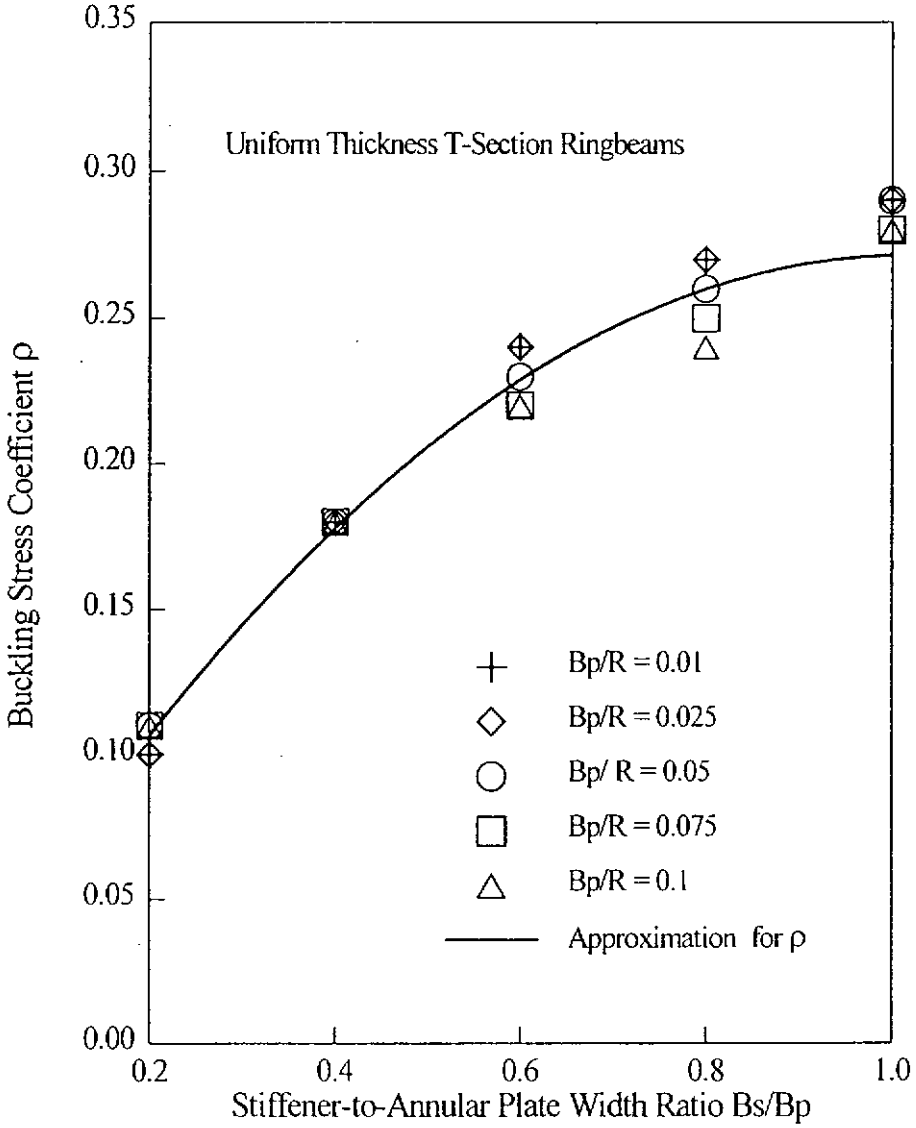

Fig. 3-9 Variation of Buckling Stress Coefficient with Stiffener-to-Annular Plate Width Ratio

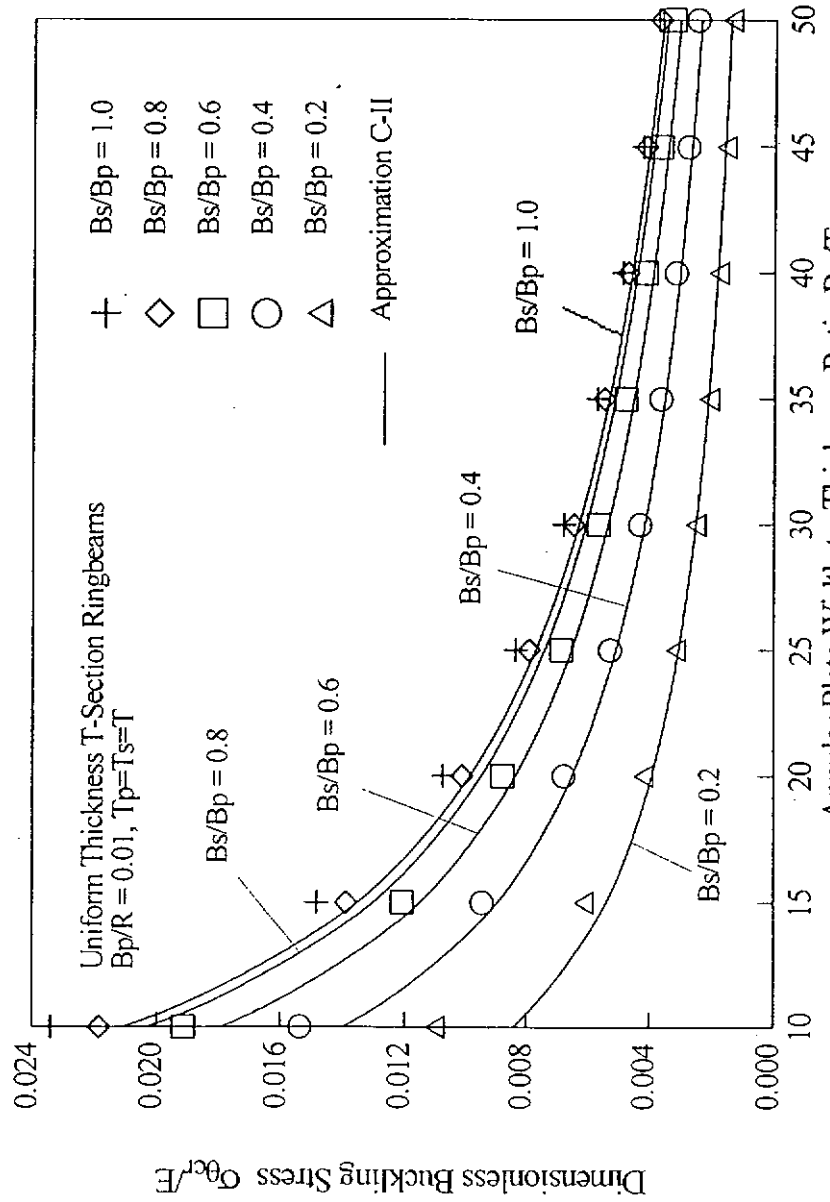

(a) Bp/R = 0.01

Fig. 3-10 Comparison between Approximation C-II and Finite Element Analysis for Uniform Thickness Ringbeams

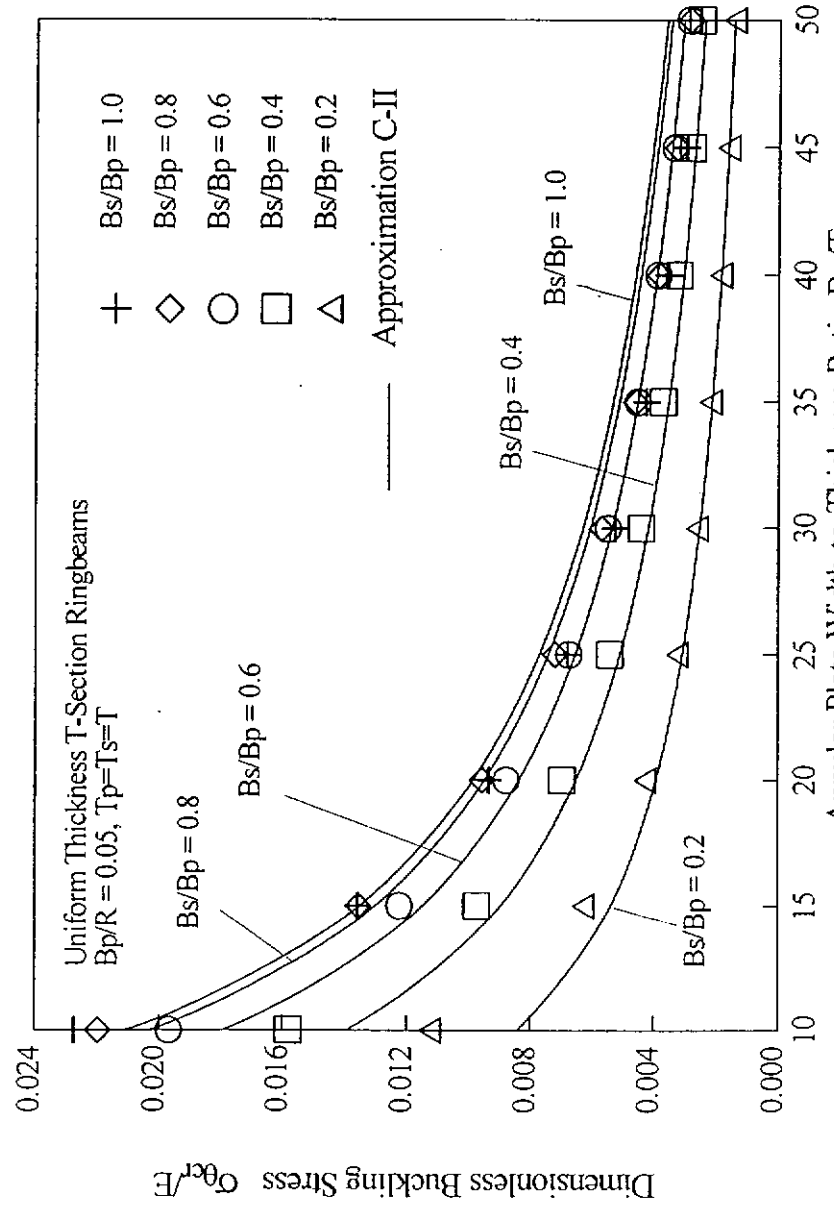

(b) Bp/R = 0.05

Fig. 3-10 Comparison between Approximation C-II and Finite Element Analysis for Uniform Thickness Ringbeams

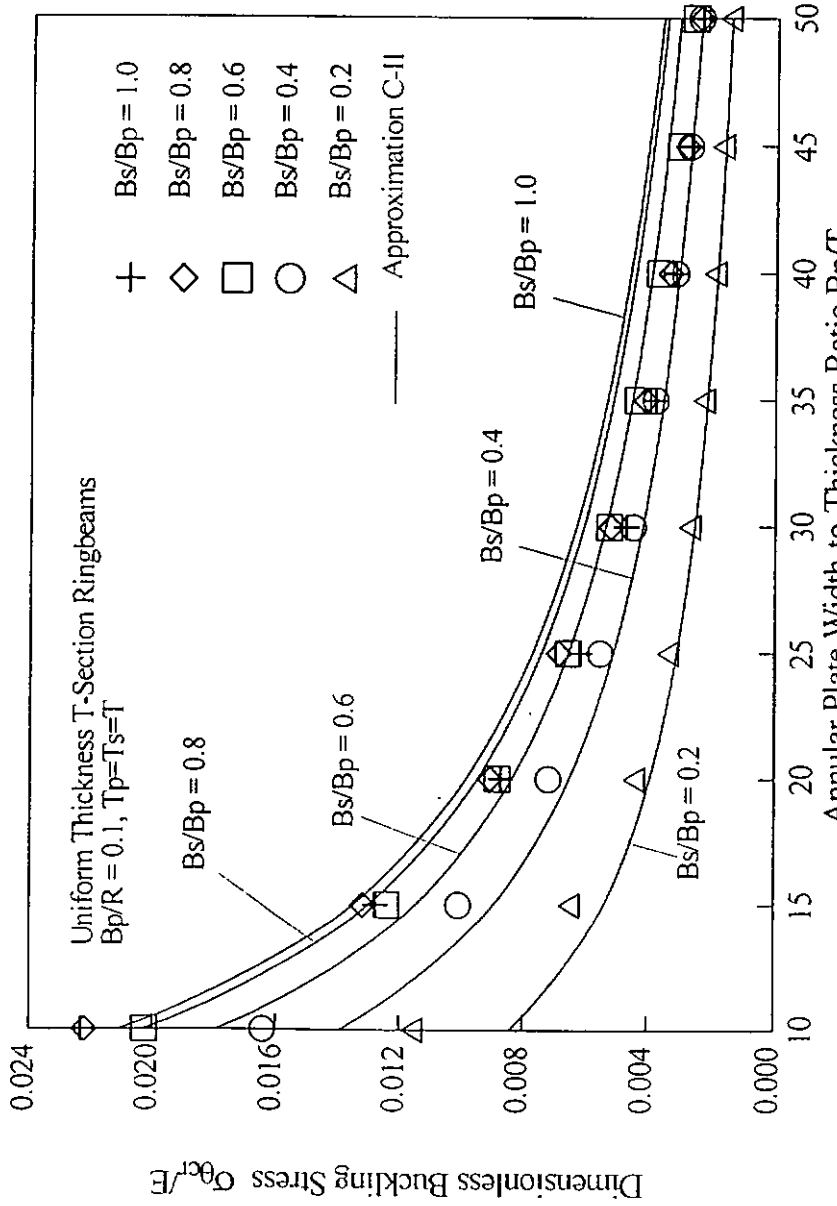

(c) Bp/R = 0.1

Fig. 3-10 Comparison between Approximation C-II and Finite Element Analysis for Uniform Thickness Ringbeams

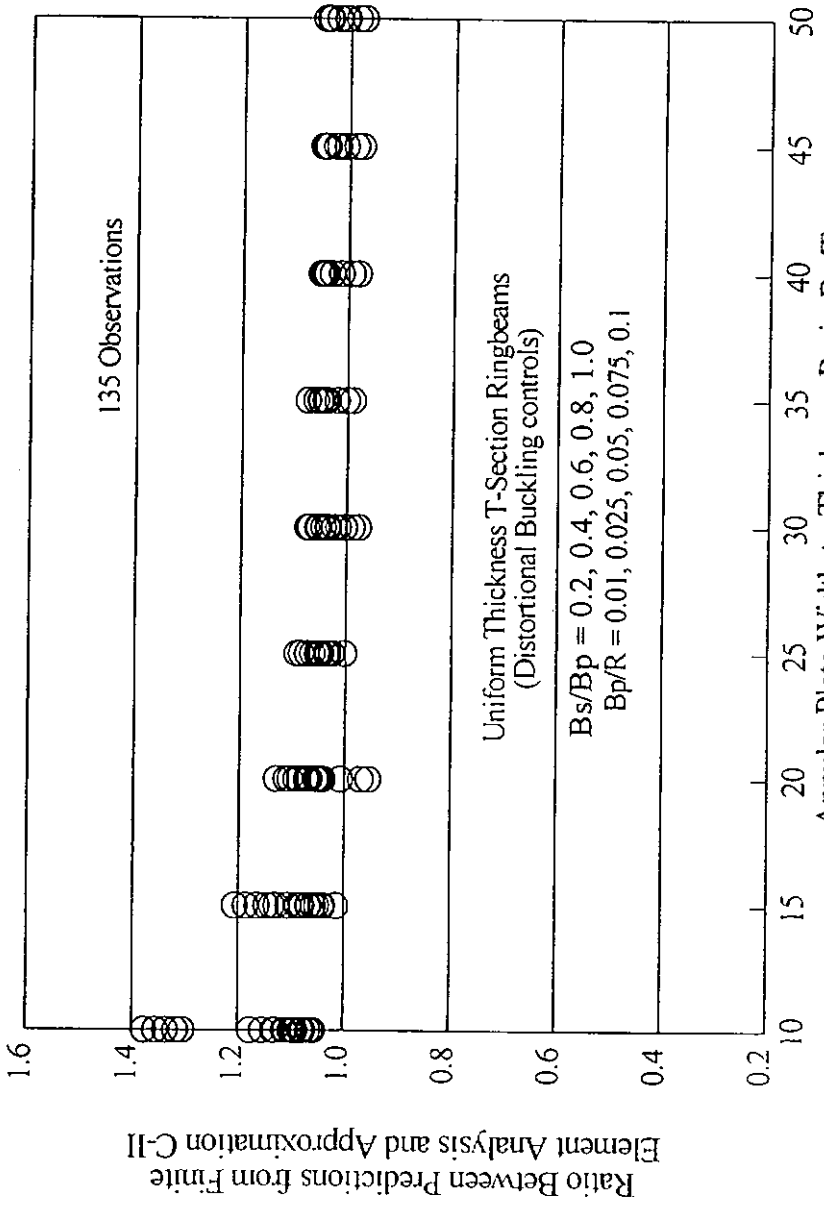

(a)

Fig. 3-11 Accuracy of Approximation C-II for Uniform Thickness Ringbeams

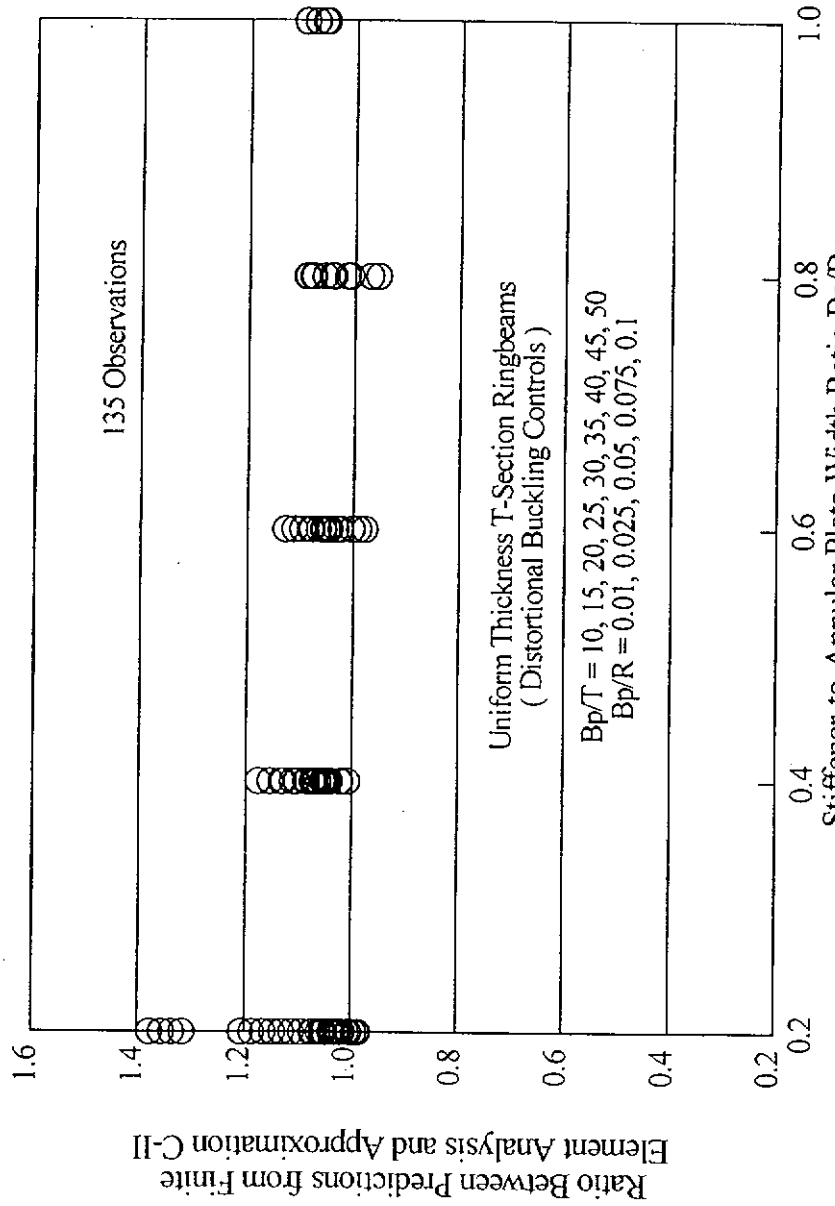

(b)

Fig. 3-11 Accuracy of Approximation C-II for Uniform Thickness Ringbeams

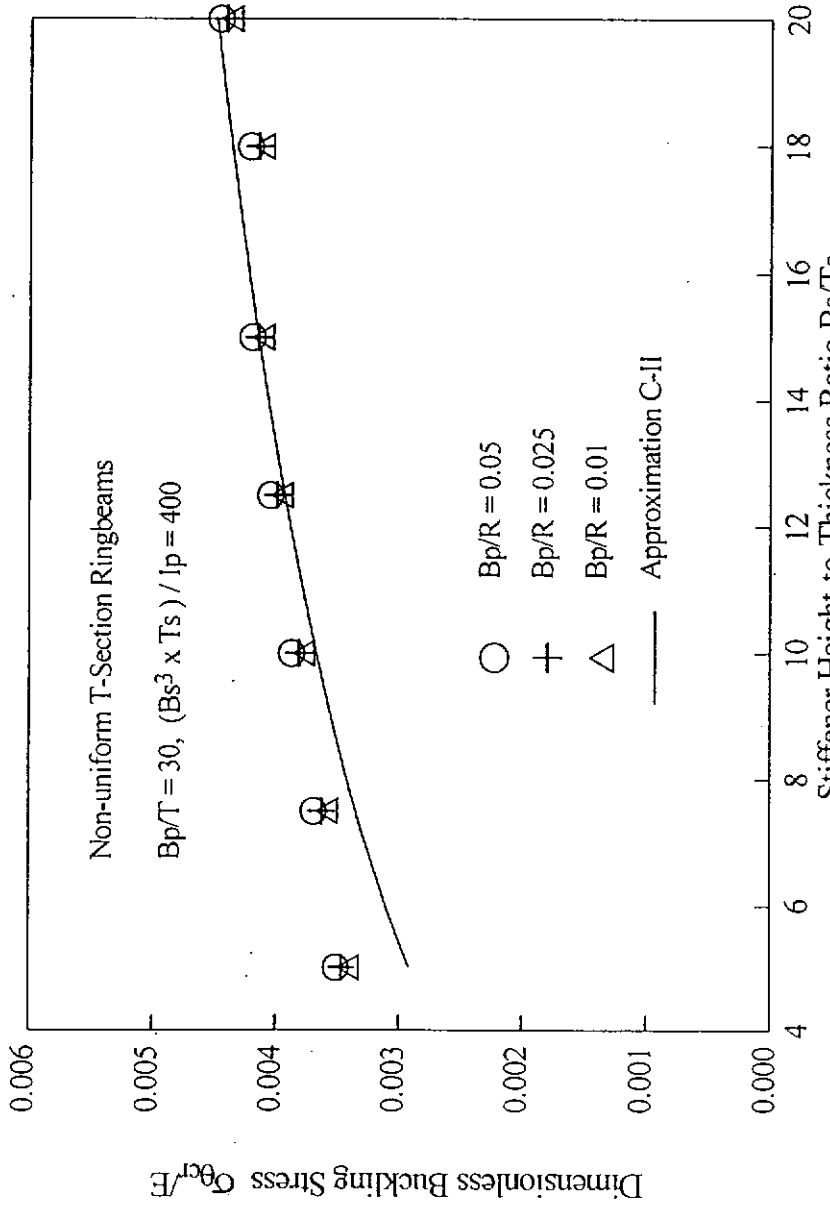

Fig. 3-12 Comparison between Approximation C-II and Finite Element Analysis for Non-Uniform Thickness Ringbeams

CHAPTER 4 ELASTIC BUCKLING OF T-SECTION RINGBEAMS SIMPLY-SUPPORTED AT INNER EDGE

4.1 Introduction

It has previously been mentioned that to establish a simple elastic buckling approximation for T-section transition ringbeams following the approach pioneered by Jumikis and Rotter (1983), it is necessary to first establish simple approximations for the elastic buckling strengths of the two limiting cases: inner edge simply supported T-section ringbeams and inner edge clamped T-section ringbeams.

The buckling strength of inner edge clamped T-section ringbeams has been studied and a simple design approximation has been established in Chapter 3. This chapter is therefore concerned with the elastic buckling strength of T-section ringbeams simply-supported at inner edge. The buckling strength of simply-supported T-section ringbeams can be predicted by the solution of Teng and Rotter (1988). A strength approximation for this case was also developed by Rotter and Jumikis (1985) based on a finite element parametric study. Their approximation is however complex, empirical and limited to very thin ringbeams ($Bp/R < 0.015$), so Teng and Rotter's solution is the preferred option. In this chapter, the accuracy of Teng and Rotter's solution and Rotter and Jumikis's approximation are first assessed for a wide range of geometries through comparisons with a finite element shell buckling analysis,

followed by the development of two new simple and accurate approximations for T-section ringbeams with a simply-supported inner edge.

4.2 Teng and Rotter's Solution

The original solution of Teng and Rotter (1988) is for the out-of-plane buckling of mono-symmetric open section rings loaded at any point in the plane of symmetry, which is also the plane of the ring. When specialised for a T-section ringbeam simply-supported at inner edge, the solution predicts that the circumferential compressive stress, which is assumed to be uniform over the cross-section, is given by

$$\sigma_{\theta cr} = \frac{EI_x\left(1-\frac{B_p}{R+x_c}n^2\right)^2 + GJn^2\left(1-\frac{B_p}{R+x_c}\right)^2}{(I_x + I_y + A_r x_c^2)n^2 - A_r R x_c} \tag{4-1}$$

where B_p is the width of the annular plate (also be referred to as the ringbeam width); A_r is the ringbeam cross-sectional area; I_x and I_y are the second moments of area about the radial and vertical axes of the section, respectively; G is the shear modulus; J is the torsional constant; x_c is the distance between the centroid of the cross-section and its inner edge; and n is the number of waves that the ringbeam buckles into. A trial and error procedure needs to be applied to Eq. 4-1 to find the critical number of buckling waves n_{cr} which gives the minimum buckling stress, and this minimum buckling stress is the critical buckling stress $\sigma_{\theta cr}$. However, if n is viewed as a continuous variable instead of discrete integers, then minimisation of the buckling stress with regard to the number of buckling waves leads to

$$\sigma_{\theta cr} = \frac{EI_X}{A_r r_o^2}\left[\frac{\beta(1-c_3)^2 + c_1 c_3(1-\beta)^2}{c_3 - c_2}\right] \tag{4-2}$$

where

$$\beta = B_p / (R + x_c) \tag{4-3}$$

$$A_r r_o^2 = I_x + I_y + A_r x_c^2 \tag{4-4}$$

$$c_1 = \frac{GJ}{EI_x} \tag{4-5}$$

$$c_2 = \frac{Bx_c}{r_o^2} \tag{4-6}$$

$$c_3 = c_2\left[1 + \sqrt{\left(1 - \frac{1}{c_2}\right)^2 + \frac{c_1}{\beta c_2}(1-\beta)^2}\right] \tag{4-7}$$

The above solution is rather tedious, so Teng and Rotter (1988) attempted to simplify the solution by noting that for thin ringbeams for which β is small, it may be assumed that

$$\frac{c_1(1-\beta)^2}{c_2\beta} \approx \frac{c_1}{c_2\beta} \tag{4-8}$$

and that

$$\left(1 - \frac{1}{c_2}\right)^2 \approx 0 \tag{4-9}$$

for sections which satisfy the following condition:

$$\frac{A_s}{A_p} > 0.3 \text{ and } \frac{B_s}{B_p} < 1.5 \tag{4-10}$$

With these approximations (Eqs 4-8 and 4-9),

$$c_3 = c_2 + \sqrt{\frac{c_1 c_2}{\beta}} \tag{4-11}$$

and the buckling stress can be expressed as

$$\sigma_{\theta_{cr}} = \frac{EI_X\sqrt{\beta}}{A_r r_o^2}\left[\frac{\beta(1-c_3)^2 + c_1c_3(1-\beta)^2}{\sqrt{c_1c_2}}\right] \tag{4-12}$$

If Eq. 4-12 is used to predict the buckling stress, the result is a curve that touches the bottom of each cusp of the precise original solution. Equation 4-12 is thus a satisfactory simplified version. However, Eq. 4-12 is not always conservative when applied to design ringbeams which may experience cross-section distortion during buckling (Teng and Rotter, 1988). An assessment of the accuracy of Eq. 4-12 for a wide range of ringbeam geometry is thus needed.

4.3 Buckling Analysis and Modelling

To assess the accuracy of Eq. 4-12, a large number of finite element buckling analyses were carried out. As the effect of prebuckling deformations is small for this problem, the finite element buckling loads presented here were obtained using the linear elastic buckling option of the NEPAS program (Teng and Rotter, 1989b).

An inward radial load is applied at the ringbeam inner edge (Fig. 4-1). The inner edge is allowed to move radially in prebuckling analysis and to have only out-of-plane rotation during buckling analysis. The circumferential compressive stress varies slightly over the ringbeam cross-section with the maximum value at the inner edge. The buckling strength of the ringbeam is characterised using the circumferential compressive stress at the inner edge of the ringbeam following Jumikis and Rotter(1983). This differs from the uniform circumferential compressive stress Eq. 4-1 or Eq. 4-12 represents, but this difference is generally small. Furthermore, as Eq. 4-12 is expected in design to be compared with the maximum circumferential

compressive stress in the ringbeam (Trahair, N.S., *et., al.*, 1983) which can be determined by the simple hand method of Rotter (Rotter, 1985), the comparisons between the predictions of Eq. 4-1 and Eq. 4-12 and those of finite element analysis as carried out in this chapter are appropriate. The material properties are the same as those used in Chapter 3, with an elastic modulus E of 2 x 10^5 MPa and a Poisson's ratio of 0.3.

4.4. Accuracy of Teng and Rotter's Simplified Solution

Figure 4-2 shows comparisons between finite element results and the predictions of Teng and Rotter's original and simplified solutions. The results presented in Fig. 4-2 are for uniform thickness T-sections ($T_s = T_p = T$) with B_P/T = 30 and 50 and B_S/B_P=0.4, 0.5, 0.6 respectively. These show that a very close agreement between Teng and Rotter's solutions and the finite element results is observed for all the cases with $B_P/R < 0.05$. For thicker ringbeams (ringbeams with larger B_p/R values), the finite element results may be either overestimated or underestimated by Teng and Rotter's solutions. In particular, Teng and Rotter's solutions become rather unconservative for ringbeams with a slender web ($B_p/T = 50$) and a relatively wide stiffener ($B_s/B_p = 0.6$) due to cross-section distortion.

Figure 4-3 shows the ratios of finite element results to Teng and Rotter's simplified solution for 315 ringbeams, covering a wide range of geometries. This figure shows that Teng and Rotter's simplified solution is rather inaccurate. The unconservative predictions are for ringbeam geometries which suffer cross-section distortion during buckling.

As the present solution for a simply-supported ringbeam will eventually be used together with the approximation for the distortional buckling strength of inner edge clamped ringbeams, the design approximation for simply-supported ringbeams needs to be conservative and accurate only for ringbeams within the limits set by Fig. 3-3. By removing the results for those ringbeams outside the geometric limits of Fig. 3-3, Fig. 4-4 is then obtained. Figure 4-4 demonstrates that Teng and Rotter's (1988) simplified solution provides close and conservative predictions of the finite element results. It is thus a satisfactory design approximation in terms of accuracy. The form of Eq. 4-12 is a little complex, considering that it constitutes roughly only one-third of the process of assessing the elastic buckling stress of a ringbeam. Simpler forms are thus desirable.

4.5 Accuracy of Rotter and Jumikis' Approximation

Rotter and Jumikis' empirical fit (1985) to finite element results is given by

$$\sigma_{\theta cr} = \frac{GJ}{A_r r_o^2} + K\sqrt{\frac{B}{R}} \tag{4-13}$$

where

$$K = 1.0x10^{-5}\left[23.7 + 0.852\left(\frac{B_s}{T_s}\right) + 9870\frac{\frac{B_s}{T_s}}{\left(\frac{B}{T}\right)^2} + 30.5a + \frac{15600a}{\left(\frac{B}{T}\right)} - 215\frac{\left(\frac{B_s}{T_s}\right)^3 a}{\left(\frac{B}{T}\right)^3}\right] \tag{4-14}$$

and

$$a = \frac{B_s T_s}{B_p T_p} \tag{4-15}$$

This equation was developed based on finite element results for B_p/R values less than 0.015, which is a rather limited range in comparison with practical ringbeam geometries. Figure 4-5 shows that Eq. 4-13 is, in fact, inaccurate and unconservative even for low values of B_p/R (e.g. at B_p/R = 0.01) for some geometries. Overall, it overestimates the buckling strengths of many ringbeam geometries and is unsatisfactory as a design proposal for a practical range of ringbeam geometries. Again, the results in Fig. 4-5 are for sections satisfying the limits of Fig. 3-3 only. The same limits will be observed in assessing the accuracy of the new approximations to be developed later.

4.6 New Approximations

Equation 4-12, though relatively simple compared to the original solution (Eq. 4-2), is still quite complex. Some bolder but rational simplifications are thus called for. The simplifications in Eqs 4-8 and 4-9 may be extended to the assumptions that

$$c_2 \approx 1 \tag{4-16}$$

$$(1-\beta)^2 \approx 1 \tag{4-17}$$

By implementing these two assumptions, c_3 reduces to

$$c_3 = 1 + \sqrt{\frac{c_1}{\beta}} \tag{4-18}$$

and the buckling stress is given by

$$\sigma_{\theta cr} = \frac{EI_x}{A_r r_o^2}\left[c_1 + 2\sqrt{c_1}\sqrt{\beta}\right] = \frac{GJ}{A_r r_o^2} + \frac{2\sqrt{GJEI_x}}{A_r r_o^2}\sqrt{\frac{B}{R+x_c}} \tag{4-19}$$

Like Rotter and Jumikis' approximation (1985), the first term in Eq. 4-19 represents the buckling stress of a long straight column with an enforced centre of rotation at the ringbeam inner edge, while the second term represents the strength gain due to the ringbeam curvature. It shows that the buckling stress is a linear function of $\sqrt{B/(R+x_c)}$. The difference between R and $R + x_c$ is small and may be ignored, so Eq. 4-19 becomes

$$\sigma_{\theta cr} = \frac{GJ}{A_r r_o^2} + \frac{2\sqrt{GJEI_x}}{A_r r_o^2}\sqrt{\frac{B}{R}} \tag{4-20}$$

Equation 4-20 is then of the same form as that of Rotter and Jumikis (1985), but with a much simpler and more rational expression for the coefficient K of Eq. 4-13. A comparison of Eq. 4-20 with finite element results shows that it is rather conservative for relatively thick ringbeams, so it is necessary to replace the factor 2 by 2.3 in the second term of Eq. 4-20 for a better agreement between the two sets of results. This leads to the following equation, which is referred to as Approximation S-I hereafter:

$$\sigma_{\theta cr} = \frac{GJ}{A_r r_o^2} + \frac{2.3\sqrt{GJEI_x}}{A_r r_o^2}\sqrt{\frac{B}{R}} \tag{4-21}$$

Figure 4-6 shows the ratios between the finite element results and Eq. 4-21 which are between 0.97 and 1.5 for the 225 ringbeams checked here, with the vast majority of them in the range of 1 to 1.3. Equation 4-21 is simple and satisfactory for use in design if this degree of conservativeness can be tolerated.

An alternative modification to Eq. 4-19 leads to the following equation which provides a better approximation: $\sigma_{\theta cr} = \frac{EI_x}{A_r r_o^2}[c_1 + 0.2\beta + 2\sqrt{c_1}\sqrt{\beta}]$ (4-22)

Equation 4-22 is referred to as Approximation S-II. The accuracy of Approximation S-II in predicting the finite element results is demonstrated in Fig. 4-7. Except for four ringbeams out of the 225 ringbeams checked, the ratios between finite element results and Approximation S-II are between 1 and 1.3.

Figure 4-8 illustrates how Teng and Rotter's simplified solution and the new approximations perform for a particular ringbeam cross-section as the ringbeam width-to-radius ratio B_p/R increases. All three predictions become more conservative as the ringbeam becomes thicker. The predictions of the two new approximations are quite similar for this case.

All the above comparisons are for uniform thickness ringbeams, so some comparisons for non-uniform thickness ringbeams are given in Fig. 4-9. The ringbeam cross-sections have $B_p/T_p = 30$, and $B_s/B_p = 0.2$, 0.4 and 0.6, with the thickness ratio T_s/T_p varying from 0.5 to 2.0. The two new approximations provide similar predictions and the effect of non-uniform thickness is seen to be well described by these approximations. It should be noted that the range of thickness variation considered here is not too restrictive as the annular plate and the stiffener normally have similar thicknesses. This is also the range considered in the chart of Fig. 3-3.

4.7 Conclusions

This chapter has been concerned with the establishment of a simple approximate method for predicting the elastic buckling strength of T-section ringbeams with a simply-supported inner edge. The earliest design proposal for this problem made by

Rotter and Jumikis (1985) is complex, empirical and inaccurate, whilst the solution developed by Teng and Rotter (1988) is complex but accurate within the geometric limits set in Chapter 3 to avoid local buckling. By introducing further simplifications and simple modifications into Teng and Rotter's simplified solution (1988), two simple new approximations, Approximations S-I and S-II, have been derived. Approximation S-I is of the simplest form, but is slightly less accurate than Approximation S-II which is slightly more complex. The two new approximations have an accuracy comparable to that of Teng and Rotter's simplified solution and are much simpler in form. Both new approximations give conservative predictions in the vast majority of cases, and are satisfactory as design proposals.

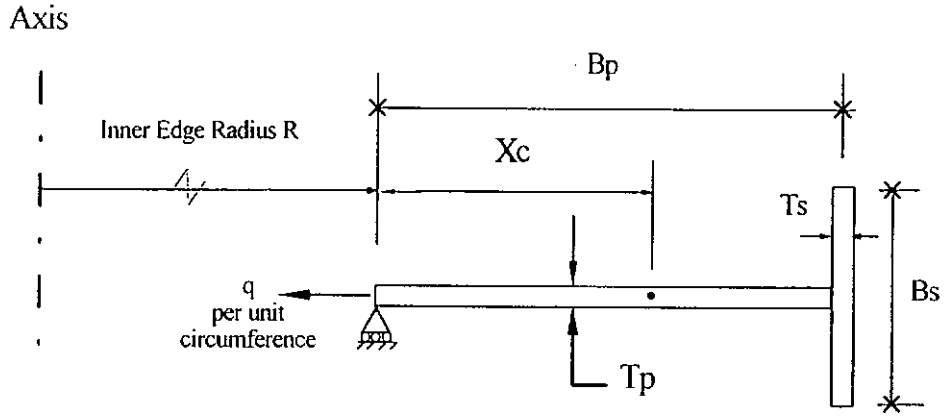

(a) Geometry, Loading and Prebuckling Restraints

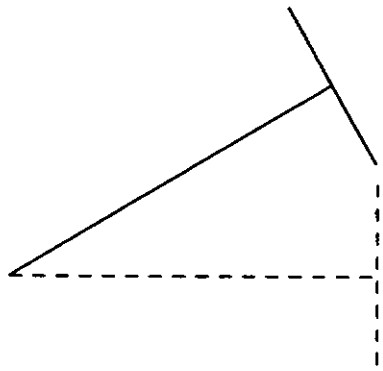

(b) Out-of-Plane Buckling Mode

Fig. 4-1 Geometry and Buckling Mode of Simply-Supported T-Section Ringbeams

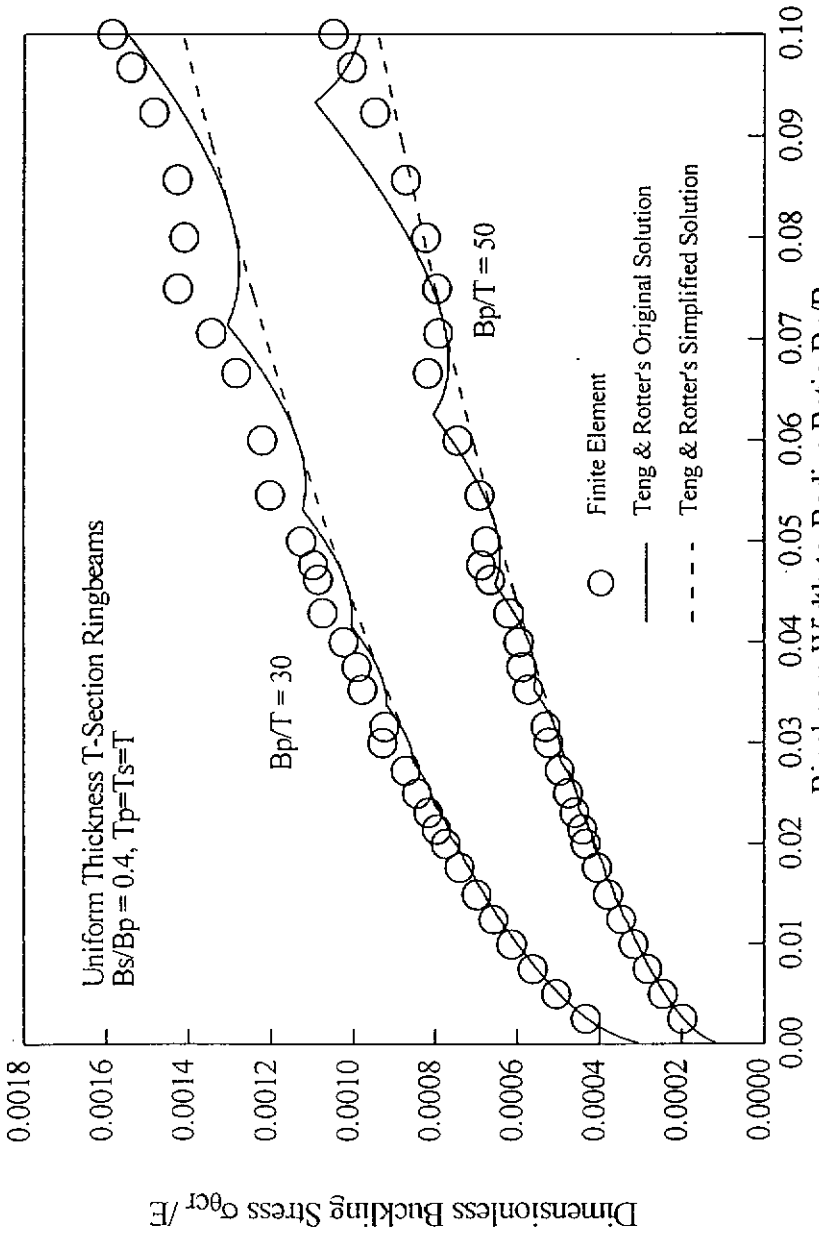

(a) Bs/Bp = 0.4

Fig. 4-2 Comparison between Teng and Rotter's Solutions and Finite Element Analysis

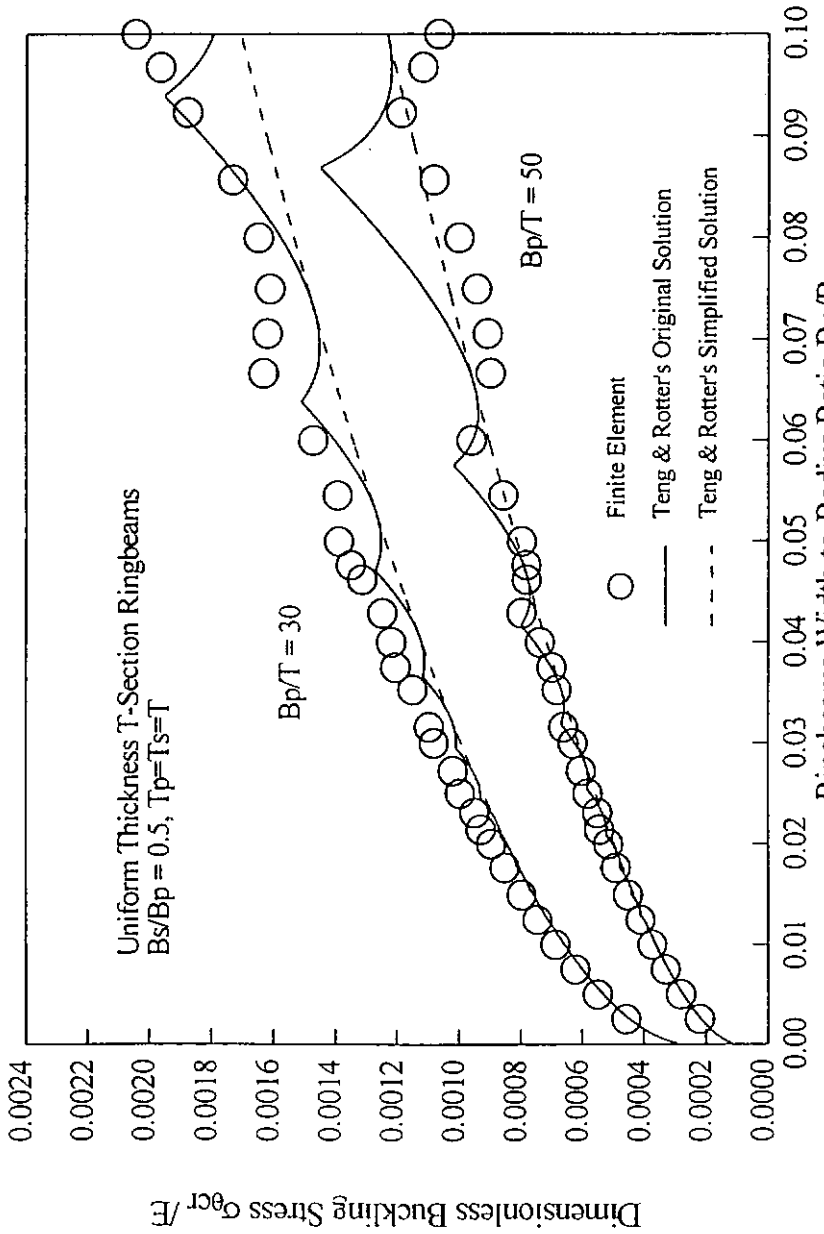

(b) Bs/Bp = 0.5

Fig. 4-2 Comparison between Teng and Rotter's Solutions and Finite Element Analysis

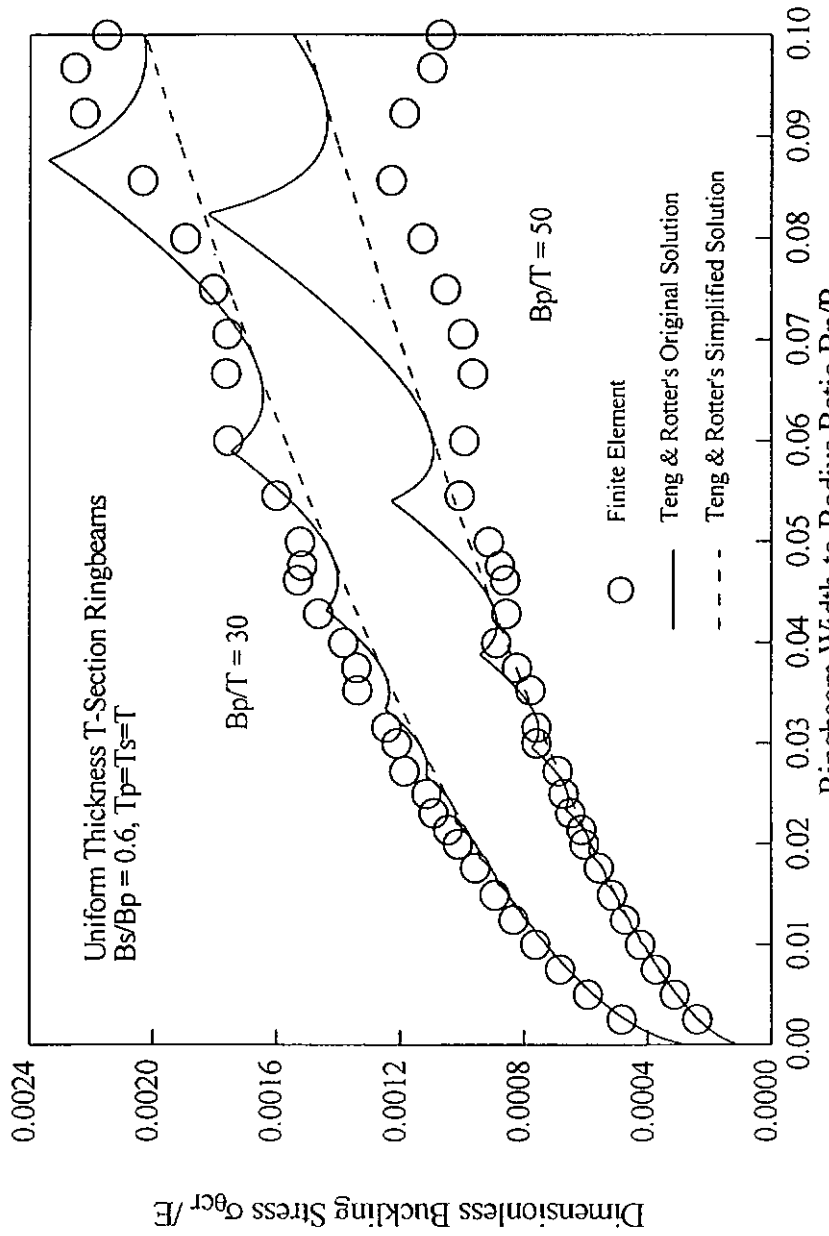

(c) Bs/Bp = 0.6

Fig. 4-2 Comparison between Teng and Rotter's Solutions and Finite Element Analysis

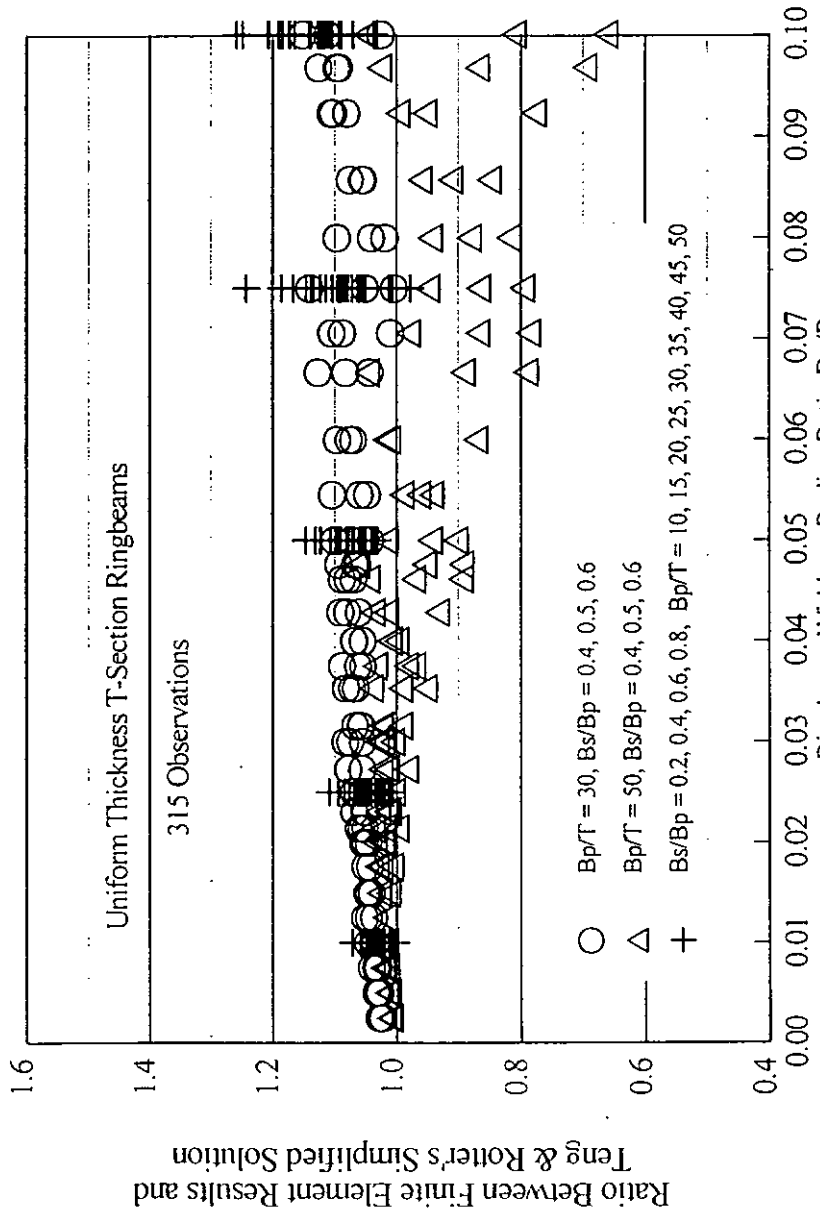

Fig. 4-3 Accuracy of Teng and Rotter's Simplified Solution

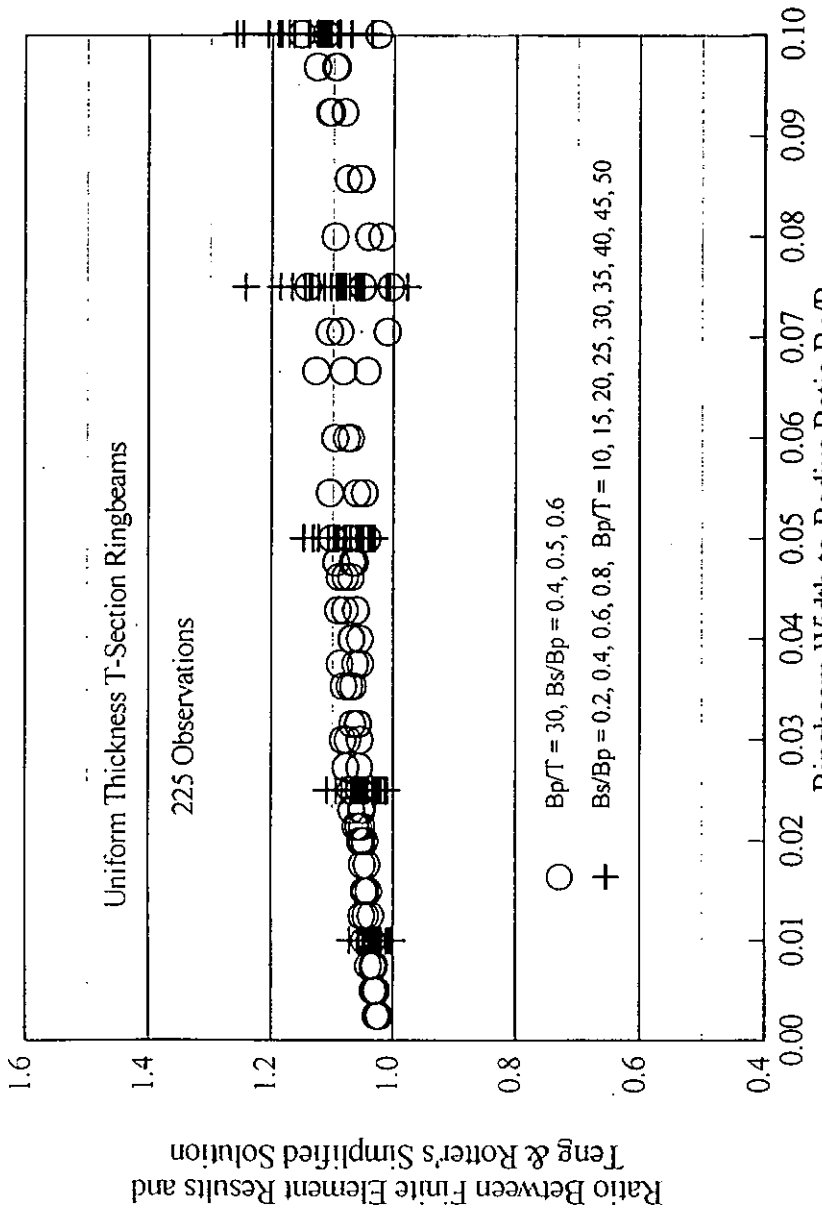

Fig. 4-4 Accuracy of Teng and Rotter's Simplified Solution for Sections Limited by Fig. 3-3

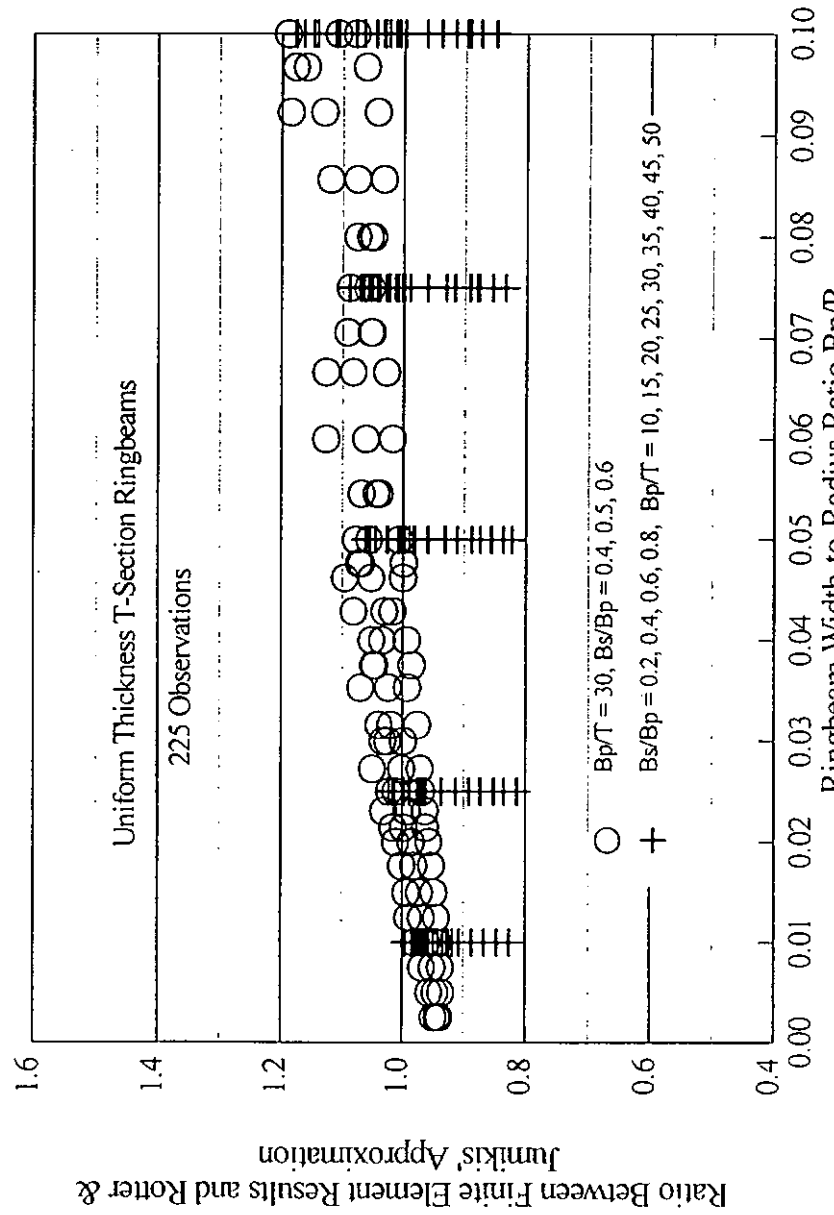

Fig. 4-5 Accuracy of Rotter and Jumikis' Approximation

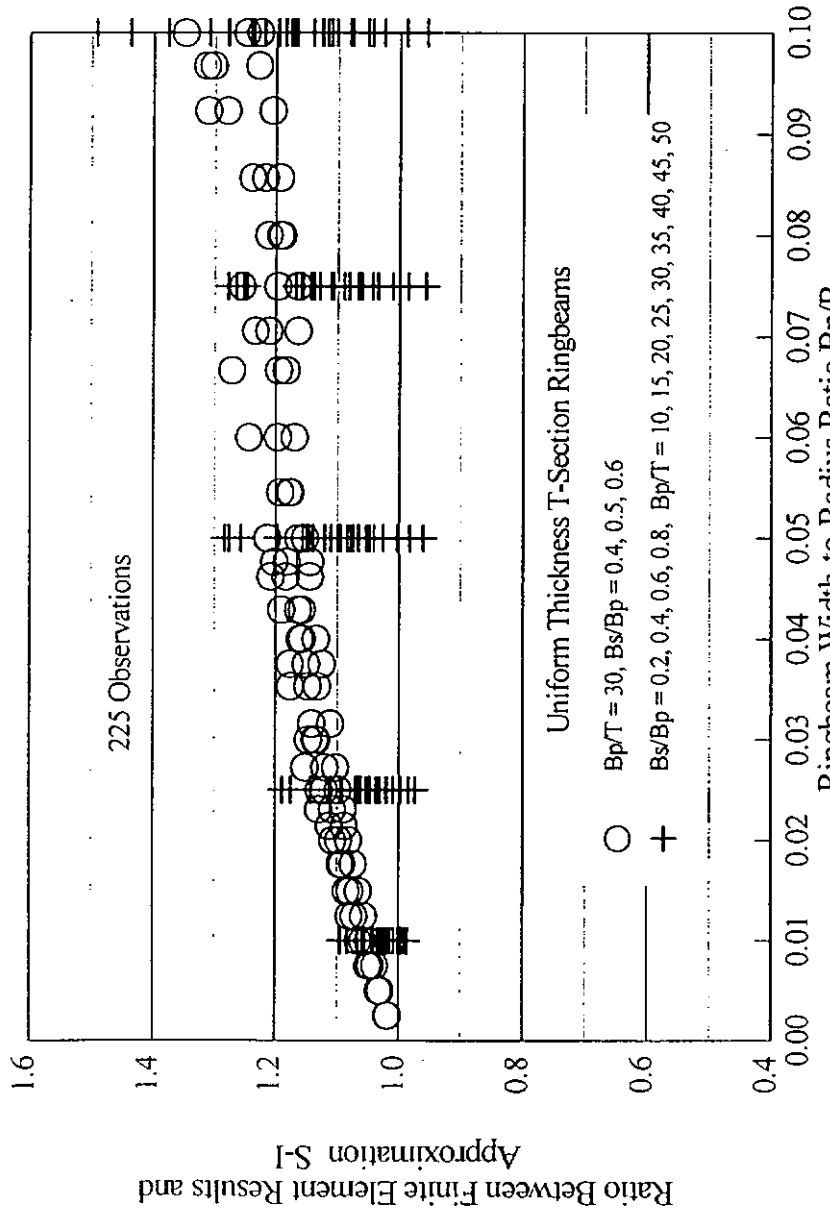

Fig. 4-6 Accuracy of Approximation S-I

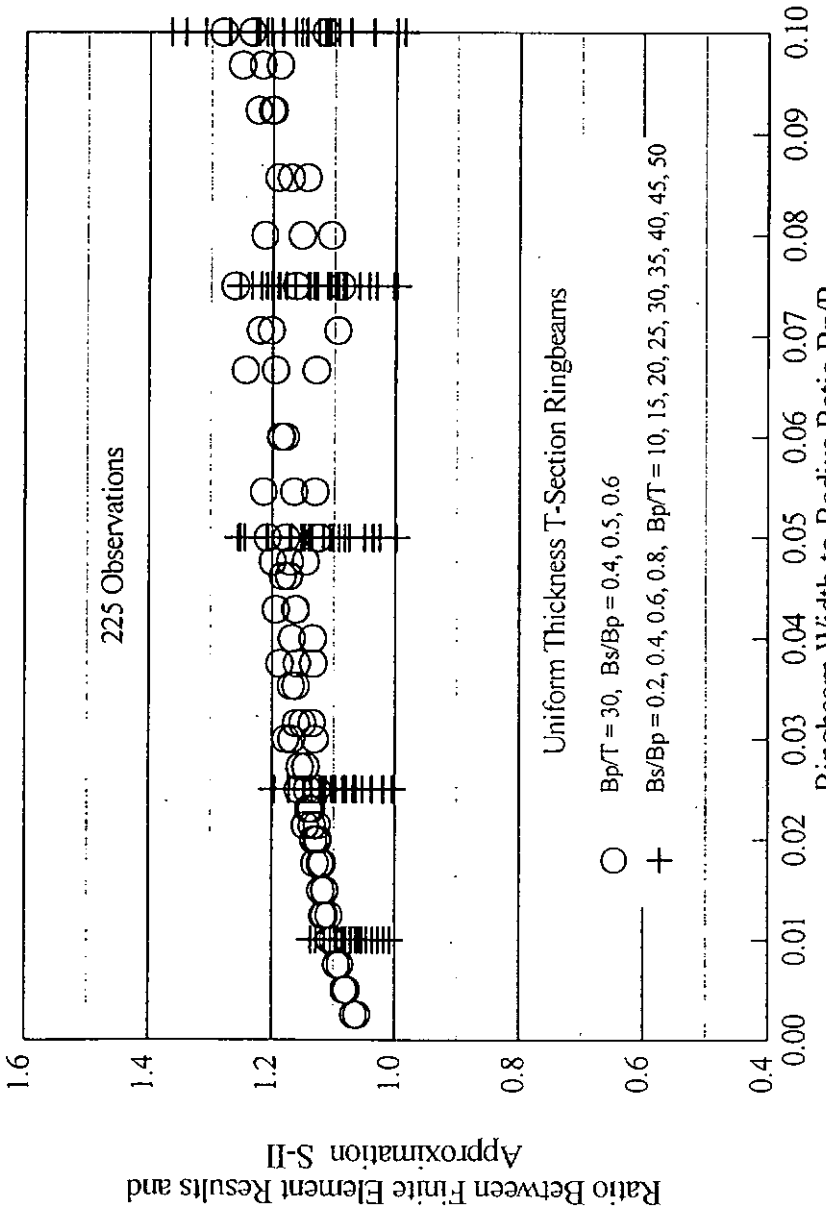

Fig. 4-7 Accuracy of Approximation S-II

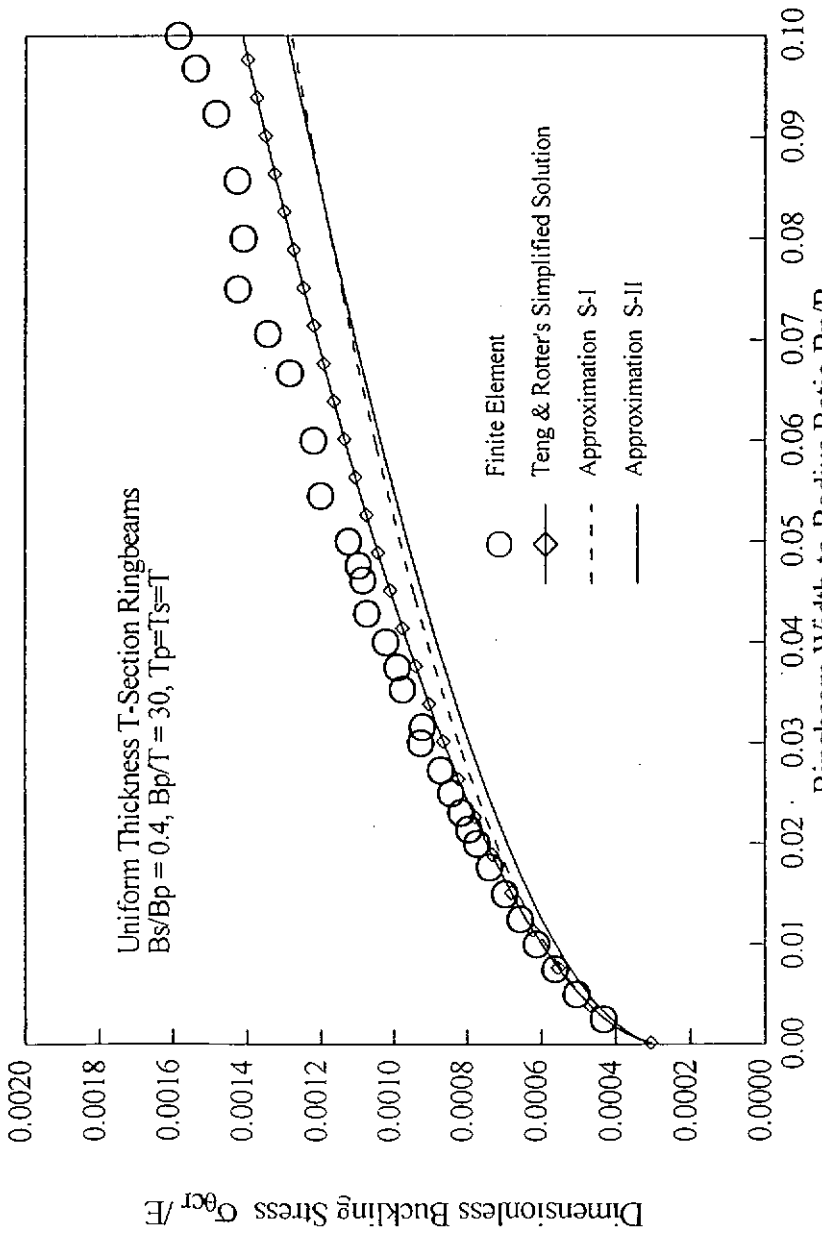

Fig. 4-8 Comprison between Approximations and Teng and Rotter's Simplified Solution

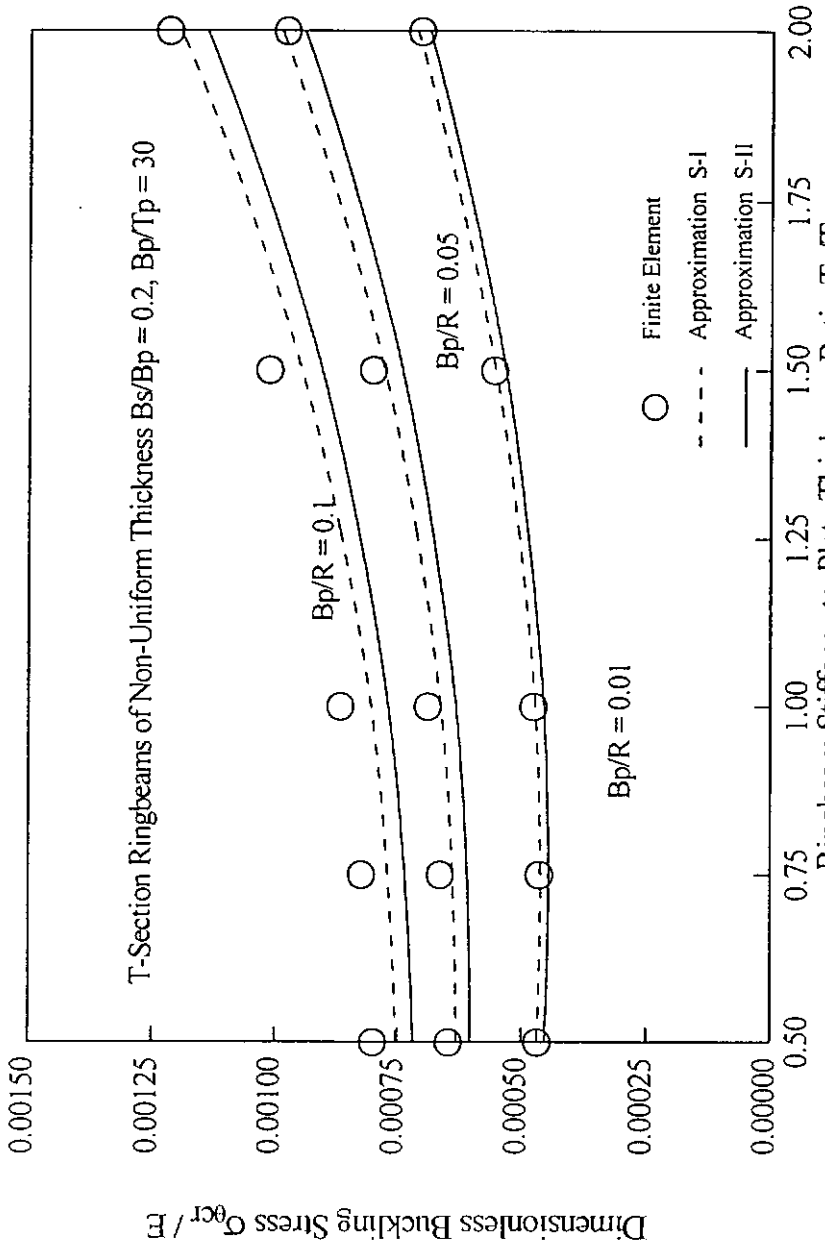

(a) Bs/Bp = 0.2

Fig. 4-9 Comparison between Approximations and Finite Element Results for Non-Uniform Thickness T-Section Ringbeams

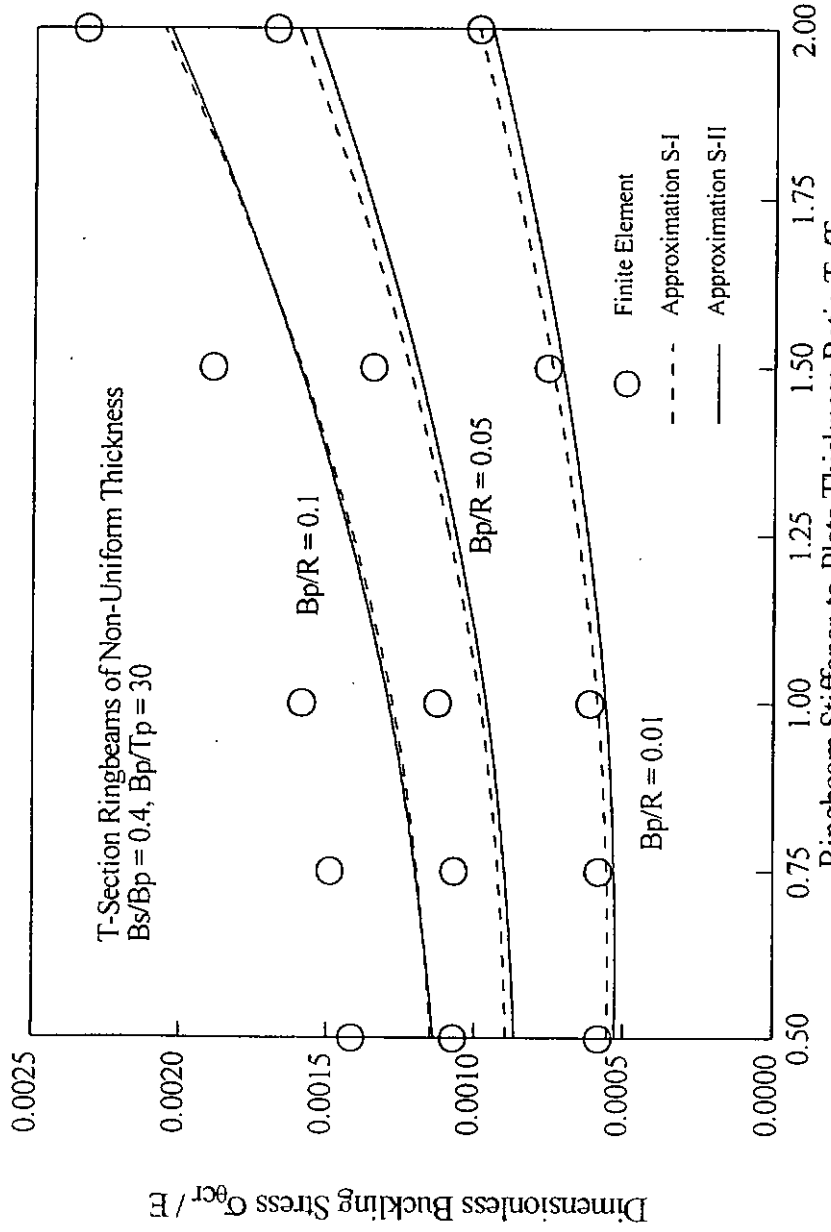

(b) Bs/Bp = 0.4

Fig. 4-9 Comparison between Approximations and Finite Element Results for Non-Uniform Thickness T-Section Ringbeams

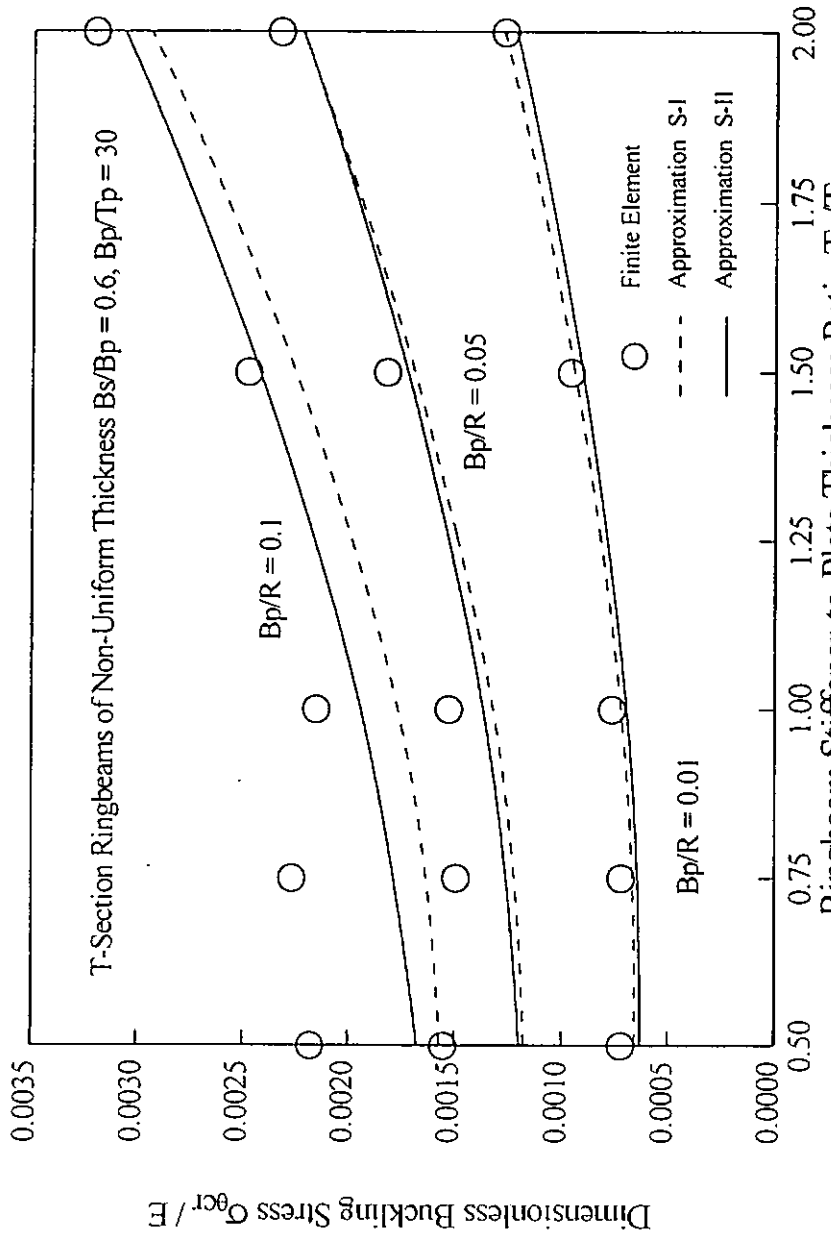

(c) Bs/Bp = 0.6

Fig. 4-9c Comparison between Approximations and Finite Element Results for Non-Uniform Thickness T-Section Ringbeams

CHAPTER 5 ELASTIC BUCKLING OF T-SECTION TRANSITION RINGBEAMS

5.1 Introduction

The aim of this chapter is to develop a simple elastic buckling strength approximation for T-section transition ringbeams in steel silos and tanks (Fig. 5-1) following the approach adopted by Jumikis and Rotter (1983). Previous efforts in this direction (Chapter 3 and 4) have led to simple approximations for the buckling strengths of inner edge clamped (Fig. 5-1d) and inner edge simply-supported (Fig. 5-1c) T-section ringbeams in terms of the maximum circumferential compressive stress which occurs at the inner edge of the T-section ringbeam. The task here is therefore to establish the necessary interpolation relationship so that the buckling strength in terms of the circumferential compressive stress at the inner edge can be established for a ringbeam with a semi-rigid rotational restraint. Furthermore, the issue of relating this buckling stress to the actual loading on the silo wall is also discussed.

5.2 Circumferential Compression at the Junction

A steel silo transition junction is generally subjected to non-uniform internal pressures and corresponding downward frictional tractions (Fig. 5-2). For the development of strength rules for the transition junction, some simple way of characterising this complex loading has to be used. As far as junction failures are concerned, the controlling force is the circumferential compressive force at the transition junction

derived chiefly from the radial component of the meridional tension at the top of the hopper. Denoting the meridional tensile force at the top of hopper as $N_{\phi t}$ (Fig. 5-2), the circumferential compressive force F_o due to the hopper meridional tension is given by

$$F_o = N_{\phi t} R \sin\alpha \tag{5-1}$$

in which R is the radius of the cylinder and α is the cone apex half angle. This value is only approximate because the effect of the local internal pressures on the cylindrical and conical shell walls adjacent to the transition has been conservatively ignored (Fig. 5-2).

The concept of an effective section of the transition junction in resisting circumferential compression is used in elastic stress analysis (Rotter, 1983; 1985) and in plastic collapse analysis (Rotter, 1987; Teng and Rotter, 1991a, 1991b; Teng, 1998). It is assumed that a short segment of each shell wall connected to the transition junction acts together with the ringbeam to form an effective ringbeam in resisting the circumferential compressive force at the junction (Fig. 5-2). Once the effective section is defined, a more accurate assessment of the circumferential compression F taking into account the effect of pressures on the effective ringbeam is given by (Rotter, 1985):

$$F = N_{\phi t} R \sin\alpha - 0.5(p_{c1} + p_{c2}) l_c R - 0.5(p_{h1} + p_{h2})(\cos\alpha - \mu \sin\alpha) l_h R \tag{5-2}$$

in which l_c and l_h are the effective lengths of the cylinder and the hopper respectively, and the pressure values p_{c1}, p_{c2}, p_{h1} and p_{h2} are as defined in Fig. 5-2. Although the variation of pressure p is generally non-linear, a linear approximation over the effective lengths can be used without much loss of accuracy as the effective lengths

are generally small compared to the total lengths of the shell walls. The circumferential compressive force F is an important parameter, as for a given geometry, the failure strength in terms of F is largely independent of the specific load distributions on the silo walls (Rotter, 1987; Greiner, 1991; Teng and Rotter, 1991a, 1991b). As pointed out by Teng (1997), the effective lengths l_c and l_h are different for elastic analysis and plastic collapse analysis, which leads to two values of the circumferential compressive force F which differ from each other very slightly. To avoid confusion and inconvenience, Teng (1997) recommended that in finding the circumferential compressive force F from Eq. 5-2, if the local pressure effects are considered for a more accurate assessment, the effective lengths under elastic conditions should always be used, regardless of whether elastic buckling and plastic collapse are being investigated. This recommendation is also adopted here.

5.3 Structural Modelling and Analysis

Two simplified structural models of transition junctions with T-section ringbeams were used in this study (Fig. 5-3). Both models include the complete conical hopper so that the loading on the hopper and the tension at the top of the hopper is properly related. The length modelled for both the cylinder and the skirt is 2 times its linear elastic meridional bending half wave length which is long enough in all cases considered for their end boundary conditions to have little influence on the ringbeam buckling behaviour. The structures are subject to a uniform internal pressure p with a friction drag of μp. The frictional coefficient μ of the stored material was assumed to be 0.5 except when the effect of this parameter was studied. This simple loading condition is sufficient as justified above since the buckling failure of the junction

depends chiefly on the circumferential compressive force rather than details of the loading. The cylinder, the conical hopper and the skirt may have different thicknesses (denoted by t_c, t_h and t_s respectively), with the T-section ringbeam having an annular plate of B_p x T_p and a stiffener of B_s x T_s (Fig. 5-1).

The model shown in Fig. 5-3a includes a skirt, representing a silo with a long skirt which is either supported on a number of columns or on the ground directly. The bottom end of the skirt is supported vertically in both prebuckling and buckling analysis.

The model shown in Fig. 5-3b does not include a skirt. Such a model represents closely a silo which sits directly on closely spaced discrete supports. Most of the numerical results to be presented later relate to this simpler model, which already captures the essential features of a T-section ringbeam with an elastic rotational restraint from the adjacent shell walls. For this model, a vertical support was provided at the point of intersection both in prebuckling and buckling analysis.

Junctions with a skirt (Fig. 5-3a) will first be examined, for which the finite element buckling loads presented here were obtained using both the linear elastic buckling option and the non-linear elastic bifurcation buckling analysis option of the NEPAS program for shells of revolution (Teng and Rotter, 1989b). A linear elastic buckling analysis ignores the effect of geometric changes due to prebuckling deflections while a non-linear elastic buckling analysis takes this effect into account. As will be shown later, the effect of prebuckling deflections is small and strengthening, so only linear

elastic buckling loads will be presented for junctions without a skirt. The finite element analysis, being based on a thin shell theory, does not suffer from the limitations of the thin-walled member theory. That is, all possible buckling modes of the ringbeam, including flexural-torsional, distortional and local buckling modes, are considered in the finite element model.

All results presented here were obtained with an elastic modulus E of 2 x 10^5 MPa and a Poisson's ratio of 0.3, which are typical values for steel. The results are all presented in a dimensionless manner so that they may also be used for other materials with a similar Poisson's ratio such as aluminium.

5.4 Prebuckling Stress Distributions and Characterisation of Buckling Strength

5.4.1 Prebuckling Stress Distribution

Figure 5-4 shows the distribution of prebuckling circumferential compressive membrane stress in a typical transition junction with a T-section ringbeam for two cases: one with a skirt (Fig. 5-4a) and the other without a skirt (Fig. 5-4b). Figure 5-4b shows that the T-section ringbeam is under nearly uniform circumferential compression, with maximum compressive stress at the inner edge of the ringbeam. Figure 5-4a shows a somewhat different situation: while the annular plate of the ringbeam is under nearly uniform compression with its maximum circumferential membrane stress at the inner edge, the maximum circumferential membrane stress for the entire ringbeam cross-section occurs at the top of the edge stiffener (flange). The

reason for this difference lies in the unbalanced meridional bending stiffnesses of the shell walls above and below the ringbeam. For the case of Fig. 5-4b, the cylinder and the hopper have the same thickness, so the meridional bending stiffness of the cylinder is similar to that of the hopper, requiring the T-section to carry little torsional load. For the case of Fig. 5-4a, since the combined bending stiffness of the hopper and the skirt exceeds that of the cylinder significantly, the junction has to accommodate this lack of balance by anti-clockwise rotation during radial deformations. As a result, the ringbeam is loaded by an anti-clockwise axisymmetric torque, leading to bending actions of the ringbeam about the radial axis. These bending actions are responsible for the linear variation of the circumferential membrane stress along the height of the stiffener. As the annular plate lies on the centroidal axis of the T-section ringbeam, the membrane stresses in the annular plate ringbeam are not affected by this torsional loading on the ringbeam.

5.4.2 Effective Section Analysis for the Inner Edge Compressive Stress in the Ringbeam

In an annular plate ringbeam, the circumferential compressive stress varies over the annular plate and reaches the maximum value at its inner edge. This maximum stress was used in Jumikis and Rotter (1983) and Sharma et al. (1987) to characterise the elastic buckling strength of annular plate ringbeams. The value of this maximum stress under elastic conditions may be determined accurately using the simple hand calculation method of Rotter (1983; 1985), which employs the concept of an effective cross-section for circumferential compression as mentioned earlier.

The studies presented in Chapters 3 and 4 on isolated T-section ringbeams have also used the circumferential compressive stress at the ringbeam inner edge as the key parameter in describing the buckling strength. This is also the maximum stress for the entire section for isolated T-section ringbeams. For T-section ringbeams connected to adjacent shell walls considered here, the buckling strength of the ringbeam is again described by the inner edge circumferential compressive stress although this may not be the maximum circumferential compressive stress for the entire section. For a junction under a general pattern of loading, the buckling strength will be defined using the equivalent circumferential compressive force given by Eq. 5-2. A link between the inner edge circumferential stress in a T-section ringbeam and this equivalent force can be established using a modified version of the effective section method proposed by Rotter (1983; 1985) for annular plate ringbeams. The modifications involve the omission of terms of the order of B_p/R which are judged to be small in comparison to 1. With such modifications, the inner edge circumferential compressive stress in a T-section ringbeam in a steel silo may be found as:

$$\sigma_\theta = \frac{F}{A_e} \tag{5-3}$$

where the total effective area A_e for elastic stress analysis is defined by:

$$A_e = A_r + \sum_{i=1}^{NS} l_{ei} t_i \tag{5-4}$$

where NS = number of shell segments present at the junction, A_r is the cross-sectional area of the T-section ringbeam (= $B_pT_p + B_sT_s$), and l_{ei} and t_i are the elastic effective length and thickness of the ith shell segment. To determine the effective length l_{ei} for each shell segment, it is necessary to first separate the shell segments into two groups,

those above and those below the annular plate. For each group with n shell segments, the equivalent thickness of the group is defined as:

$$t_{eq} = \sqrt{\sum_{i=1}^{n} t_i^2} \tag{5-5}$$

Denoting the thinner group as group A (the group with a smaller equivalent thickness) and the thicker one group B, the equivalent thickness ratio ζ is then found as:

$$\zeta = t_{eqA} / t_{eqB} \tag{5-6}$$

The effective length of each shell segment is given by:

$$l_{ei} = 0.778 \gamma_{ei} \sqrt{R t_i / \cos\phi} \tag{5-7}$$

where $\phi = 0$ for a cylindrical component and $\phi = \alpha$ for the hopper, the appropriate value of γ_{ei} for the ith shell segment is:

$$\gamma_{ei} = 1 \qquad \text{for the thinner group} \tag{5-8}$$

$$\gamma_{ei} = \gamma_e = 0.5(1 + 3\zeta^2 - 2\zeta^3) \qquad \text{for the thicker group} \tag{5-9}$$

The definition of the shell effective lengths as given above is based on the assumption that the ringbeam resists little torsion in the deformation process (Rotter, 1983), an assumption which is valid for the case of an annular plate ringbeam. A T-section ringbeam has significant resistance to axisymmetric torsion through bending about the radial axis, so the above definition is in some error. A recently developed method by Chen and Rotter (1997) could be adapted to give more accurate results for the problem. Their method can be particularly useful if a stiffener of unsymmetric section is used, but for the case of a T-section ringbeam, the complexity involved in their method does not seem to be justified for practical design application. On the

other hand, the simple method described above is sufficiently accurate as will be demonstrated later through numerical comparisons.

5.5 Buckling Strength Approximation for Ringbeams with Semi-Rigid Inner Edge Restraint

5.5.1 General Remarks

The buckling behaviour and strength of ringbeams with the two idealised inner edge conditions have been studied in Chapters 3 and 4. Chapter 3 also presented a chart defining the geometric limits of a T-section ringbeam to avoid local buckling in inner edge clamped T-section ringbeams. As local buckling is most likely in a inner edge clamped ringbeam due to its high flexural-torsional/distortional buckling strength, these limits are also sufficient for ringbeams with a simply-supported or semi-rigid inner edge.

5.5.2 Buckling Strength Approximation for a T-section Ringbeam in a Silo

Following the approach of Jumikis and Rotter (1983), the buckling stress of a T-section ringbeam attached to a silo transition junction may be approximated through

$$\sigma_{\theta cr} = \frac{\eta_s \sigma_s + \eta_c \sigma_c}{\eta_s + \eta_c} \tag{5-10}$$

where η_s and η_c are interpolation parameters which may be functions of the following eight dimensionless geometric parameters: t_c/T_p, t_h/T_p, t_s/T_p, B_p/R, B_p/T_p, B_s/B_p, T_s/T_p

and α for a T-section consisting of an annular plate of B_p x T_p and a stiffener of B_s x T_s (Fig. 5-1) on a silo with a hopper apex half angle of α.

Although it was expected that the expressions for η_s and η_c would turn out to have a form resembling that of Eq. 3-5 and 3-6 in Chapter 3, it was not expected that they would be the same. A number of attempts were made at developing appropriate expressions for η_s and η_c. It was eventually concluded that the expressions used by Jumikis and Rotter (1983) for annular plate ringbeams are also the best choices for T-section ringbeams.

5.5.3 Four Possible Approximations

Given the two possible approximations for each of the two idealised inner edge conditions developed in Chapters 3 and 4, four possible buckling strength approximations can be constructed using a single set of approximations for the coefficients η_s and η_c. The four possible approximations are given below:

Approximation E-I:

$$\sigma_{\theta cr\,E1} = \frac{\eta_s \sigma_{s1} + \eta_c \sigma_{c1}}{\eta_s + \eta_c} \tag{5-11}$$

Approximation E-II:

$$\sigma_{\theta cr\,E2} = \frac{\eta_s \sigma_{s1} + \eta_c \sigma_{c2}}{\eta_s + \eta_c} \tag{5-12}$$

Approximation E-III:

$$\sigma_{\theta cr\,E3} = \frac{\eta_s \sigma_{s2} + \eta_c \sigma_{c1}}{\eta_s + \eta_c} \tag{5-13}$$

Approximation E-IV:

$$\sigma_{\theta cr\,E4} = \frac{\eta_s \sigma_{s2} + \eta_c \sigma_{c2}}{\eta_s + \eta_c} \tag{5-14}$$

where σ_{s1} and σ_{s2} refer to buckling stresses predicted using Approximations S-I and S-II of Chapter 4, and σ_{c1} and σ_{c2} refer to buckling stresses of Approximations C-I and C-II of Chapter 3 respectively. The accuracy of the approximations are next checked through a parametric study which examines the effect of varying t_c/T_p, t_h/T_p, t_s/T_p, T_s/T_p, B_p/T_p, B_s/B_p, B_p/R and the apex half angle α.

5.6 Junctions with a Skirt and Effect of Prebuckling Deflections

5.6.1 General Remarks

The first set of comparisons here relates to junctions with a skirt (Fig. 5-3a), a case more general than junctions without a skirt as shown in Fig. 5-3b. The elastic buckling loads were obtained using both the linear elastic bifurcation buckling analysis option and the non-linear elastic bifurcation buckling analysis option of the NEPAS program (Teng and Rotter, 1989b) so that the effect of prebuckling deflections (geometric changes) can be clarified.

5.6.2 Effect of Skirt Thickness

The junctions considered have a skirt-to-annular plate thickness ratio t_s/T_p varying from 1 to 5, with the case of no skirt ($t_s/T_p = 0$) also included for comparison. The values of the other geometric parameters are: $t_c = t_h = T_p = T_s$, $B_p/R = 0.06$, $\alpha = 45^\circ$,

B_p/T_p = 30, B_s/B_p = 0.5. The predictions from the four approximations match the finite element linear elastic buckling stresses closely and are conservative (Fig. 5-5a). Approximations E-II and E-IV are the closer approximations. The accuracy ratios (ratios between finite element results and approximate results) for the linear elastic buckling stresses vary form 1.04 to 1.16 (Fig. 5-5b). In Fig. 5-5a, the finite element results at t_s/T_p = 0 and = 1 are connected by a smooth line to illustrate the general trend of the effect of skirt thickness. An actual structure or a finite element model with a very thin skirt cannot be expected to deliver a buckling stress close to this line, as a thin skirt can buckle with very low stress levels in the ringbeam.

Previous studies on transition junctions with an annular plate ringbeam (Jumikis, 1987; Teng, 1997) have demonstrated that in general, prebuckling large deflections have only a small effect on the buckling stress. Figure 5-5a shows that for the geometries considered in this figure, the effect of large deflections leads to small reductions in the buckling stress. It is however incorrect to conclude that the effect of prebuckling deflections is detrimental, because the buckling pressures are in fact increased as a result of the prebuckling deflections (Fig. 5-6a). This is because the prebuckling deflections affect both the restraining effect from the shells on the ringbeam (slightly weakening) and the relationship between the pressure and the stress in the T-section ringbeam (slightly lower stress at the same pressure as the cone is deformed into one with a steeper meridional slope), with the latter effect being a little stronger. While the significance of the overall effect of prebuckling deflections depends on many parameters, it is generally small for practical structures and can be safely ignored for simplicity.

5.6.3 Effect of Frictional Coefficient

Figure 5-7a shows the effect of varying the frictional coefficient from 0 to 0.8 on the elastic buckling strength of a transition junction with a skirt thickness $t_s = 2T_p$, and this effect is seen to be small. This supports the claim that details of the loading pattern are not important, and the equivalent circumferential compression or the circumferential stress in the ringbeam is the controlling parameter. Again the effect of prebuckling deflections leads to small reductions in the buckling stress but small increases in the buckling pressure (Fig. 5-6b). The finite element results are closely and conservatively predicted by the four approximations, with the accuracy ratios for the linear finite element buckling stresses ranging from 1.25 to 1.35 (Fig. 5-7b). Approximations E-II and E-IV are again the better approximations.

5.7 Junctions without a Skirt

5.7.1 General Remarks and Reference Geometry

The above section has shown that the buckling strength of junctions with a skirt can be closely predicted by the four approximations (Eqs 5-11 to 5-14). In the following parametric study, the skirt is thus omitted and the simpler structural model of Fig. 5-3b is used. This structural model, representative of real silos on a large number of discrete vertical supports, still retains the essential feature of shell wall restraint to the ringbeam during buckling, the key feature to be quantified in this study. The model has the further advantage that possible instability effects in the skirt are avoided. In practical design, adverse interaction between the axial compression in the skirt and

the circumferential compression at the junction should be avoided by proper proportioning so that only one of them is predominant, or interaction effects are appropriately accounted for. Only linear elastic buckling stresses will be discussed as the effect has been shown to be small and strengthening, and its omission is conservative. The frictional coefficient is taken to be 0.5 as it does not influence the buckling stress significantly.

Before describing the results of the following parametric study, it is useful to define a reference geometry. This reference geometry is given by: $t_c = t_h = T_p = T_s$, $t_s/T_p = 0$, $B_p/R = 0.06$, $\alpha = 45^\circ$, $B_p/T_p = 30$, $B_s/B_p = 0.5$. In the following parametric study, only one of the parameters will be varied at any one time while all the other parameters will be kept constant to study the effect of that particular parameter on the buckling strength and to assess the accuracy of the four buckling strength approximations.

5.7.2 Effect of Cylinder-to-Annular Plate Thickness Ratio

Figure 5-8a shows that as the cylinder-to-annular plate thickness ratio t_c/T_p increases from 0.25 to 4, a range wider than may be expected in practice, the buckling strengths from all four approximations (Eqs 5-11 to 5-14) and finite element analysis increase. All four approximations are seen to be conservative, with the accuracy ratios falling between 1.04 and 1.21 (Fig. 5-8b). The predictions of the four approximations are quite similar and are all satisfactory. Approximations E-II and E-IV provide better predictions than the other two approximations.

5.7.3 Effect of Hopper-to-Annular Plate Thickness Ratio

The effect of varying the hopper-to-annular plate thickness ratio t_h/T_p on the dimensionless elastic buckling strength of T-section ringbeams on a transition junction is shown in Fig. 5-9a. As expected, the effect of increasing hopper thickness is similar to that of increasing cylinder thickness shown in Fig. 5-8a. This indicates that the elastic buckling strength of the T-section ringbeam can be raised by making either the cylinder or the hopper thicker. The four approximations provide satisfactory predictions with accuracy ratios between 1.04 to 1.21 (Fig. 5-9b). Again Approximations E-II and E-IV show a closer agreement with the finite element results than the other two approximations.

5.7.4 Effect of Ringbeam Width-to-Radius Ratio

The buckling strength of junctions with varying ringbeam width-to-radius ratio B_p/R is examined here. The four approximations provide conservative predictions of the finite element results (Fig. 5-10a), with accuracy ratios ranging from 1.11 to 1.31 (Fig. 5-10b). The buckling stress is found to increase rapidly with increases in the B_p/R ratio initially, and then grow more slowly as this parameter increases further. Once again, Approximations E-II and E-IV provide closer predictions.

5.7.5 Effect of Cone Apex Half Angle

The interpolation coefficients do not include the cone apex half angle α. Figure 5-11a confirms that the effect on the buckling strength of varying cone apex half angle α is

rather small over a wide range of values (wider than may be expected in practical silo structures). The accuracy of the approximations is again satisfactory with accuracy ratios being between 1.10 to 1.21 (Fig. 5-11b). Approximation E-II and E-IV continue to give closer predictions of the finite element results.

5.7.6 Effect of Annular Plate Width-to-Thickness Ratio of the Ringbeam

The effect of the ringbeam annular plate width-to-thickness ratio B_p/T_p is a very influential parameter on the buckling strength. Its effect is shown in Fig. 5-12a. The buckling strength drops rapidly with increases in the B_p/T_p ratio. The four approximations all produce close and conservative predictions of the finite element results. Approximations E-II and E-IV are slightly more accurate than the other two approximations. The accuracy ratios fall between 1.05 and 1.16 (Fig. 5-12b), which is very good indeed.

5.7.7 Effect of Stiffener Height-to-Annular Plate Width Ratio of the Ringbeam

Figure 5-13a shows the effect of increasing the stiffener height-to-annular plate width ratio B_s/B_p. Initially, an increase in this parameter leads to an almost linear increase in the buckling stress, which then drops slightly once the B_s/B_p ratio exceeds 0.6. Before the B_s/B_p ratio reaches 0.6, the predictions of all four approximations are similar, with Approximations E-II and E-IV being the more accurate. Beyond the range, the predictions of Approximations E-I and E-III are significantly unconservative and

unsatisfactory. Approximations E-II and E-IV become unconservative when B_s/B_p exceeds 0.8, but the predictions are still close to the finite element results. The decrease in buckling stress at higher values of B_s/B_p is due to local buckling effects. The inaccuracy of the approximations is not of concern as the sections are already out of the range of geometries defined by the chart Fig. 3-3 in Chapter 3. For sections which satisfy the limits of Fig. 3-3, the accuracy ratios vary from 1.09 to 1.19 (Fig. 5-13b).

5.7.8 Effect of Stiffener-to-Annular Plate Thickness Ratio of the Ringbeam

So far, the ringbeams studied all have uniform plate thickness, that is $T_p = T_s$. The effect of stiffener-to-annular plate thickness ratio T_s/T_p is shown in Fig. 5-14a where it is seen that when the stiffener is twice as thick as the annular plate, the approximate equations become rather conservative. This conservativeness stems from the conservativeness in the approximations for ringbeams with a clamped inner edge where the torsional stiffness of the stiffener is not considered. Generally, ringbeams have similar thickness in the annular plate and the stiffener and for such ringbeams the accuracy ratio is about 1.15. For the less common cases of ringbeams with a thick stiffener, a bit more conservativeness is thus present in the approximations. The accuracy ratios vary from 1.09 to 1.39 (Fig. 5-14b).

5.8 Accuracy of the Effective Section Method

The effective section method described earlier is an adaptation of that developed by Rotter (1983; 1985) for junctions with an annular plate ringbeam. As was pointed out earlier, an assessment of the accuracy of the adapted method is necessary. Using the buckling pressure, the expression for the equivalent circumferential compression (Eq. 5-2) and the effective section analysis (Eqs 5-3 to 5-9), a prediction of the circumferential stress σ_{ef} at the inner edge of the ringbeam can be made. The ratio of this stress (σ_{ef})predicted using the effective section method and that directly taken from a finite element analysis, denoted by σ_{fe}, is expected to be close to 1 if the effective section method is accurate. A ratio greater than 1 means that the effective section analysis overestimates the stress and is conservative for structural design. The values of this ratio for all geometries analysed above are plotted in Fig. 5-15. This ratio is seen to be between 0.97 and 1.13 and is close to 1 for most cases. The effective section method thus provides a simple and accurate approach for the prediction of the inner edge circumferential compressive stress in a T-section ringbeam at a steel silo transition junction.

5.9 Design Recommendation

Based on the investigation presented above, a simple design proposal for assessing the elastic buckling strength of a transition junction with a T-section ringbeam under general non-uniform internal pressure and meridional frictional traction can be established. The elastic buckling strength of the ringbeam in terms of its inner edge circumferential stress may be found using one of the four possible approximations

(Eqs 5-11 to 5-14). The parametric study above has shown that Approximation E-II and Approximation E-IV provide closer predictions of finite elements results and the two have similar accuracy. The only difference between Approximation E-II and Approximation E-IV lies in the choice of the buckling strength approximation for an inner edge simply supported ringbeam. Approximation E-II makes use of Approximation S-I (Eq. 4 - 21), while Approximation IV adopts Approximation S-II (Eq. 4 - 22). Since Approximation S-II (Eq. 4 - 22) is slightly more complex in form than Approximation S-I (Eq. 4 - 21), Approximation E-II is therefore recommended for use in design.

Once the critical buckling stress $\sigma_{\theta cr}$ is determined, the elastic buckling strength in terms of the equivalent circumferential compressive force F can be found by

$$F_e = \sigma_{\theta cr} A_e \qquad (5\text{-}15)$$

where A_e is the effective section area calculated by Eq 5-4. The value of the equivalent circumferential compressive force obtained from Eq. 5-15 should then be compared to that predicted by Eq 5-2 for a given loading condition to assess the safety margin against an elastic buckling failure.

5.10 Conclusion

This chapter has presented a comprehensive investigation into the elastic buckling strength of T-section ringbeams at steel silo transition junctions. A simple approximation has been found for the elastic buckling strength of the ringbeam in terms of its inner edge circumferential compressive stress. This has been achieved by interpolating the buckling strengths of the two idealised cases of inner edge simply

supported and inner edge clamped ringbeams, for which simple elastic buckling strength approximations were developed in Chapters 3 and 4. The interpolation relationship adopted by Rotter and Jumikis for annular plate ringbeams has been found to be satisfactory also for T-section ringbeams.

Although the junction has been studied under a uniform internal pressure with accompanying meridional frictional traction, the results have been interpreted for use with junctions under general non-uniform loading by characterising the buckling strength using the equivalent circumferential compressive force. The final recommended elastic buckling strength approximation is the first ever rigorously based strength proposal for this problem and may be used directly in design. The effect of material yielding on the buckling strength is investigated in Chapter 6.

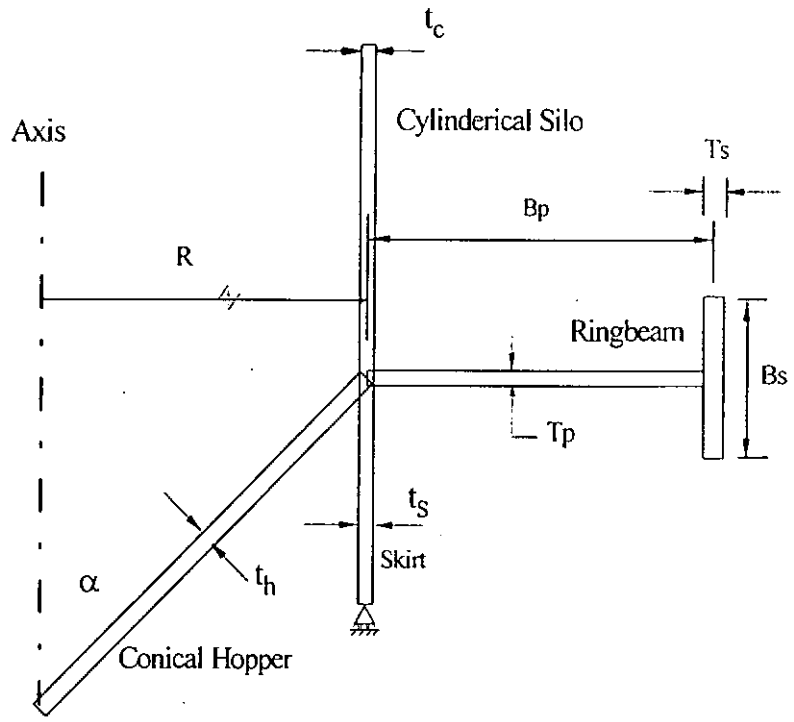

(a) Typical Transition Junction with a T-Section Ringbeam

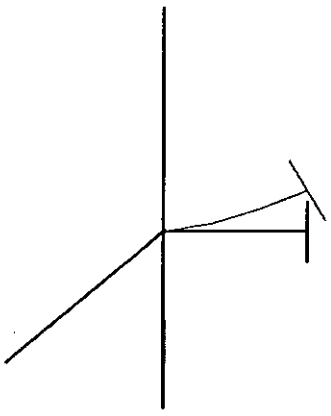

(b) Buckling Mode of a T-Section Transition Ringbeam

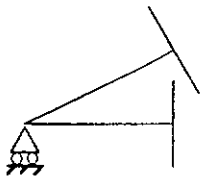

(c) Buckling Mode of an Inner Edge Simply-Supported Ringbeam

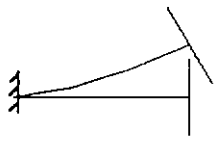

(d) Buckling Mode of an Inner Edge Clamped Ringbeam

Fig. 5-1 T-Section Transition Ringbeam in a Steel Silo and Buckling Mode

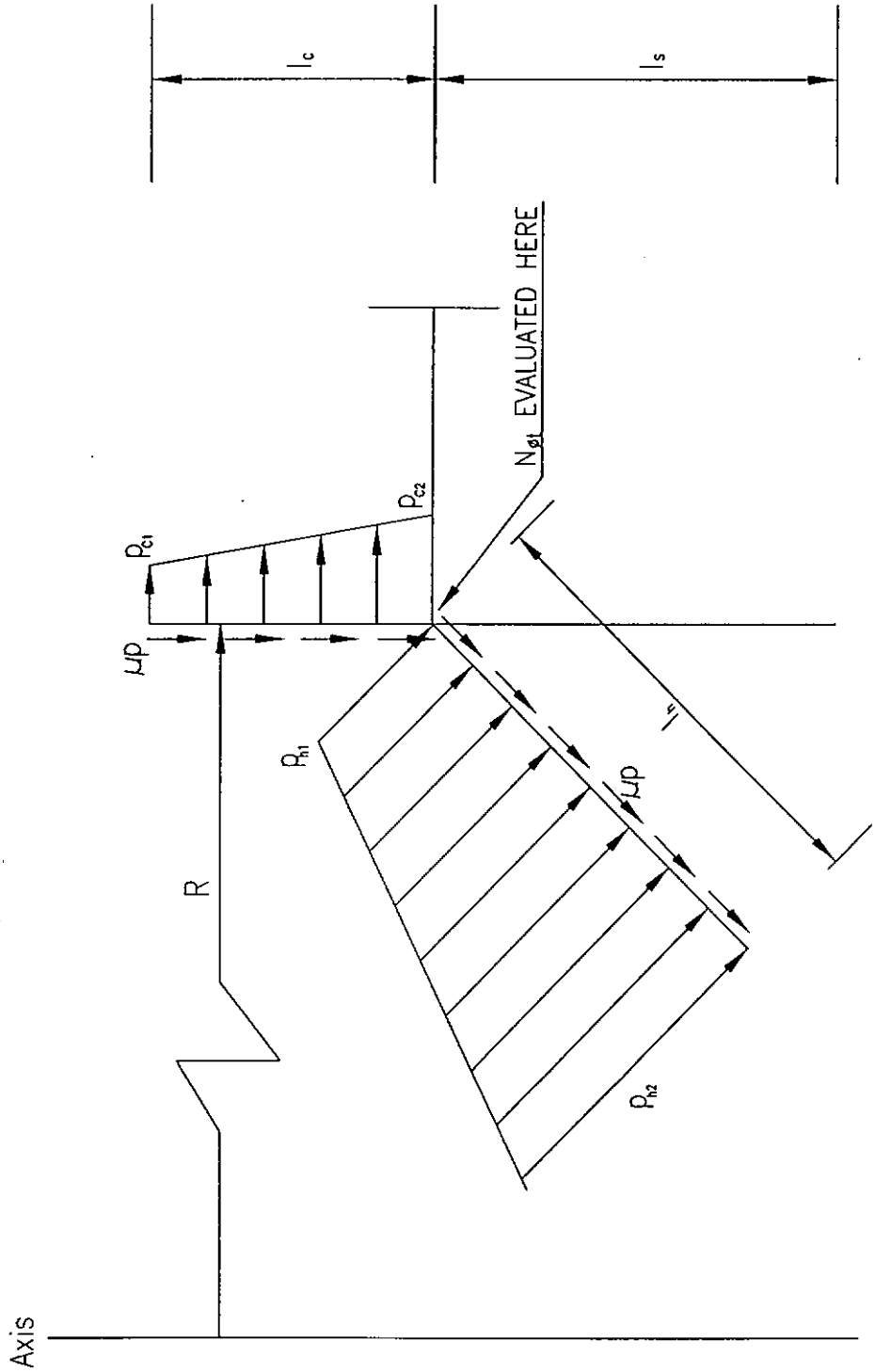

FIG. 5-2. EFFECTIVE SECTION AND LOCAL PRESSURE

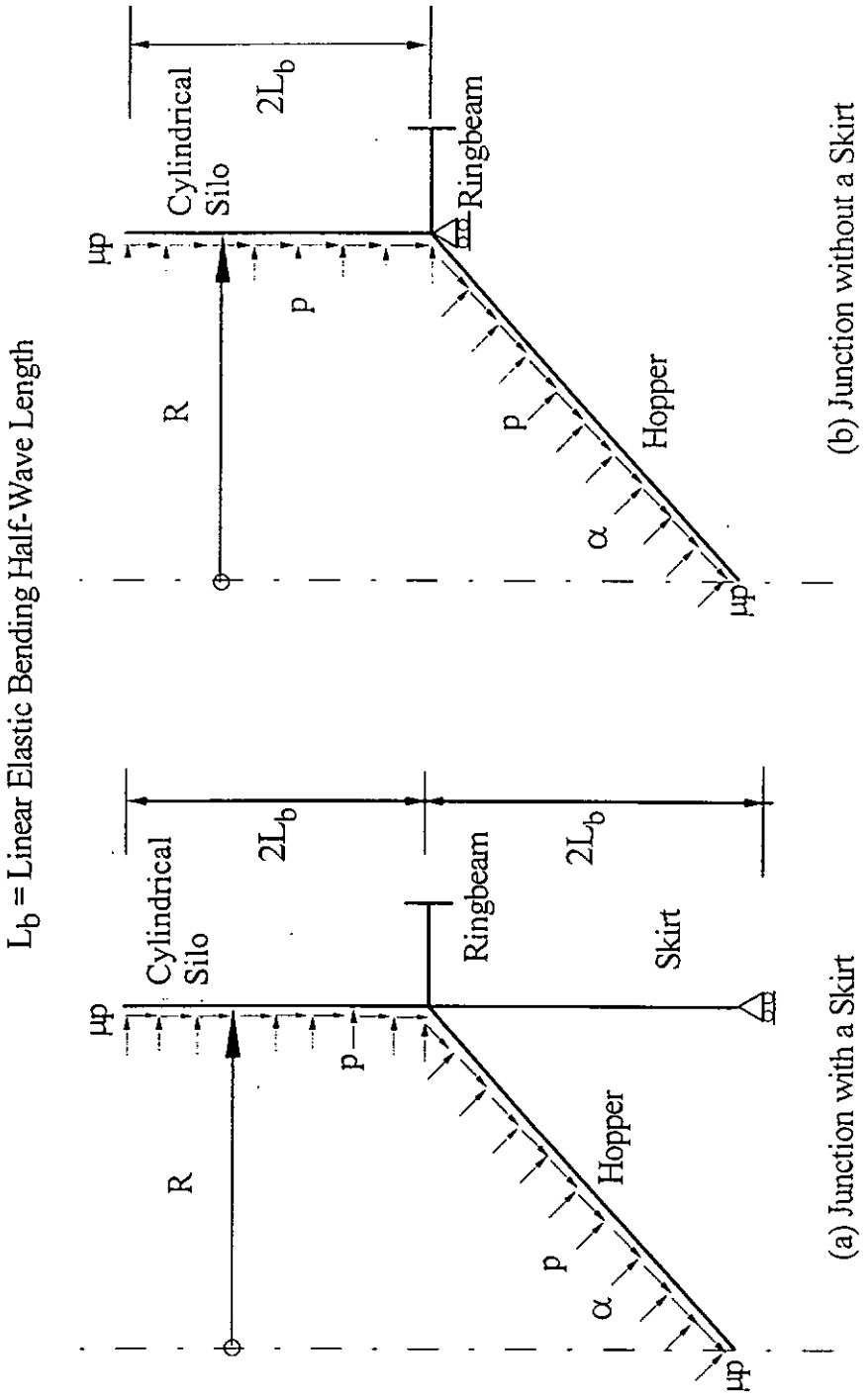

Fig. 5-3 Simplified Structural Models

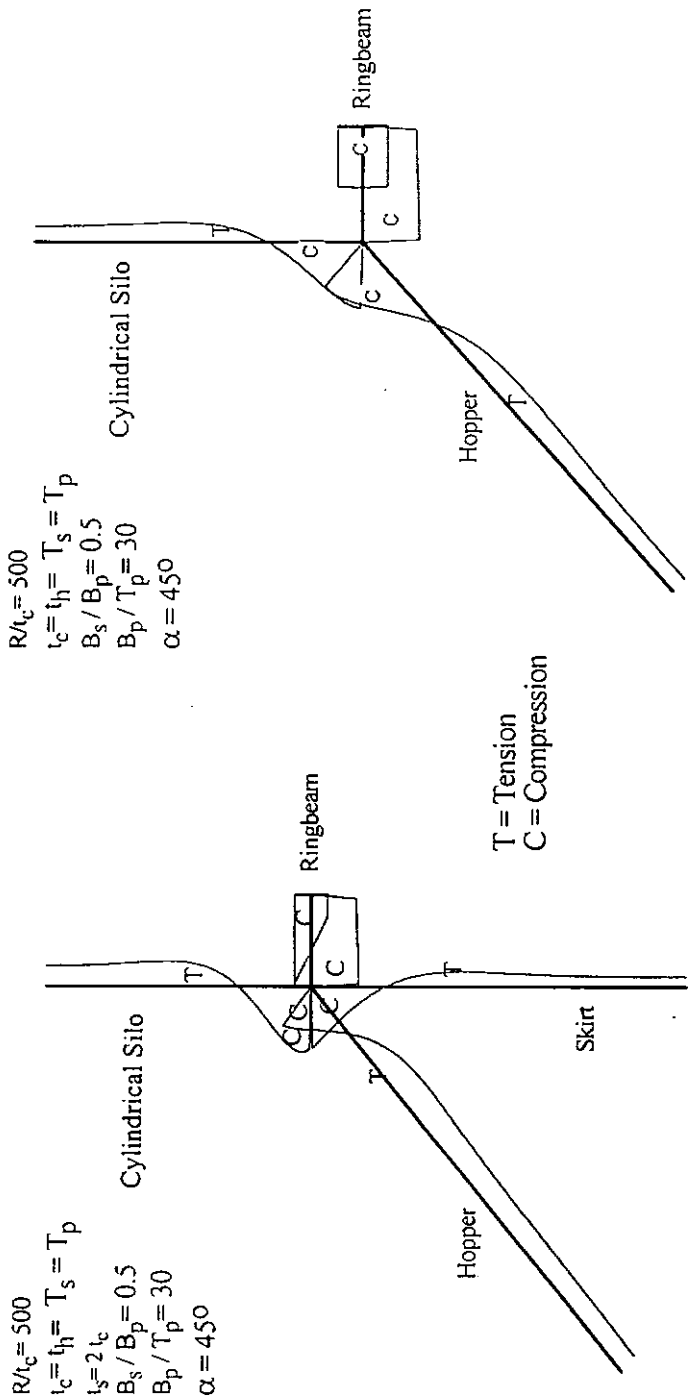

Fig. 5-4 Typical Distributions of Prebuckling Circumferential Compressive Stress

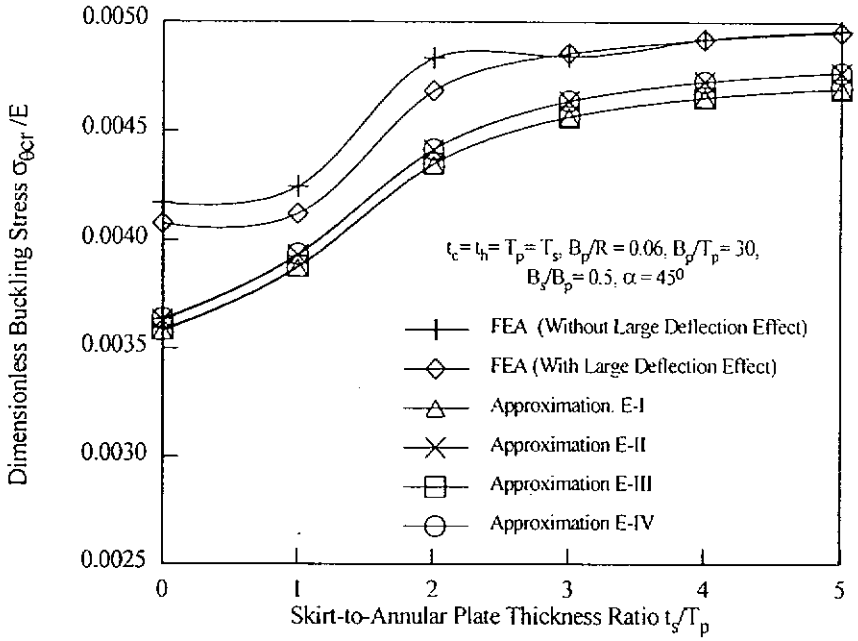

(a) Comparison of Buckling Stresses

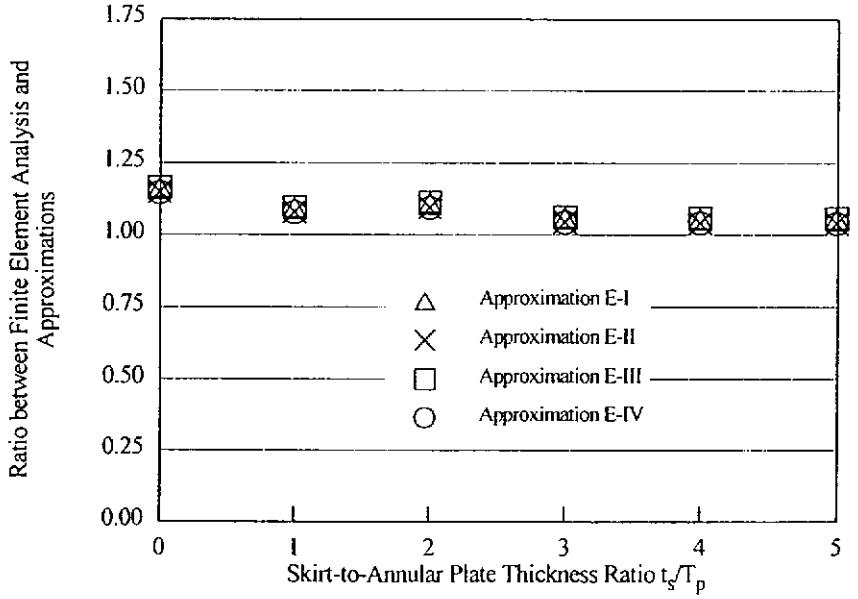

(b) Accuracy of Approximations

Fig. 5-5 Effect of Skirt-to-Annular Plate Thickness Ratio

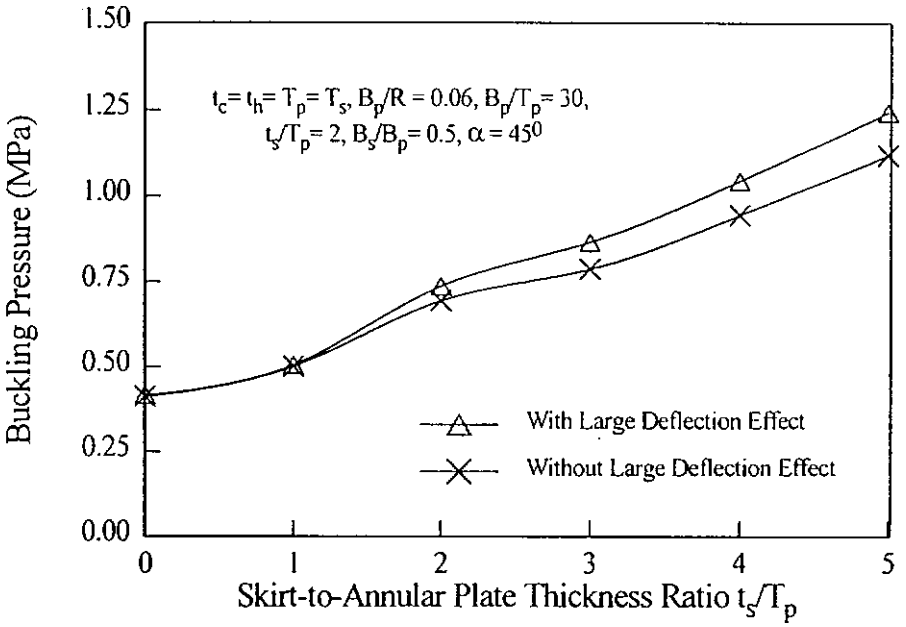

(a) Junction with Varying Skirt-to-Annular Plate Thickness Ratio

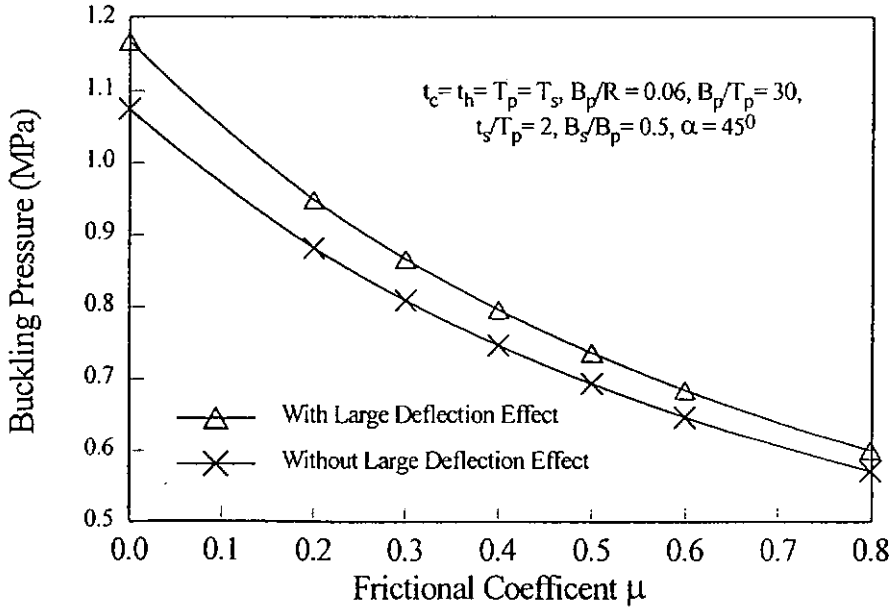

(b) Junction with Varying Frictional Coefficent

Fig. 5-6 Effect of Prebuckling Large Deflections on Buckling Pressure

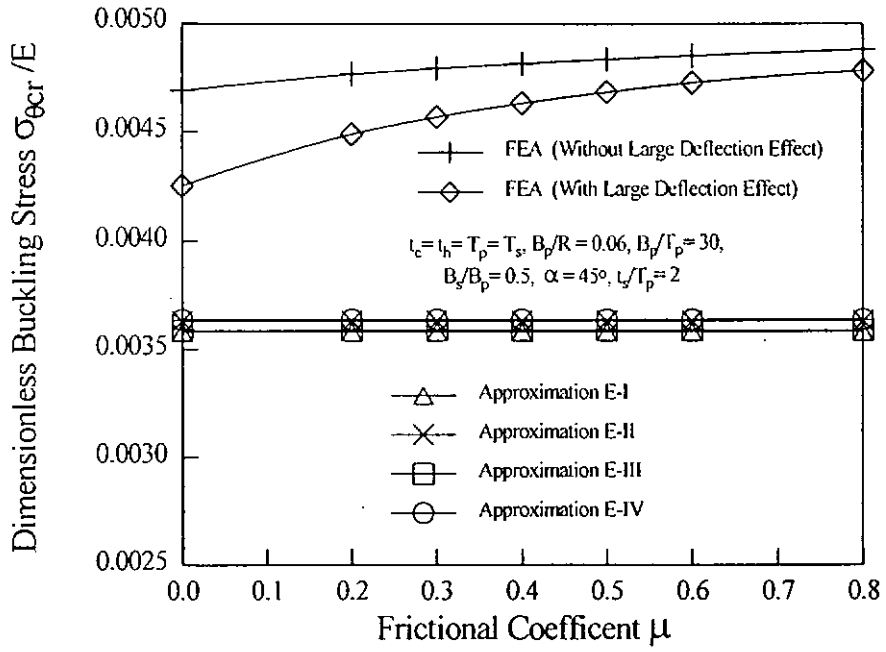

(a) Comparison of Buckling Stresses

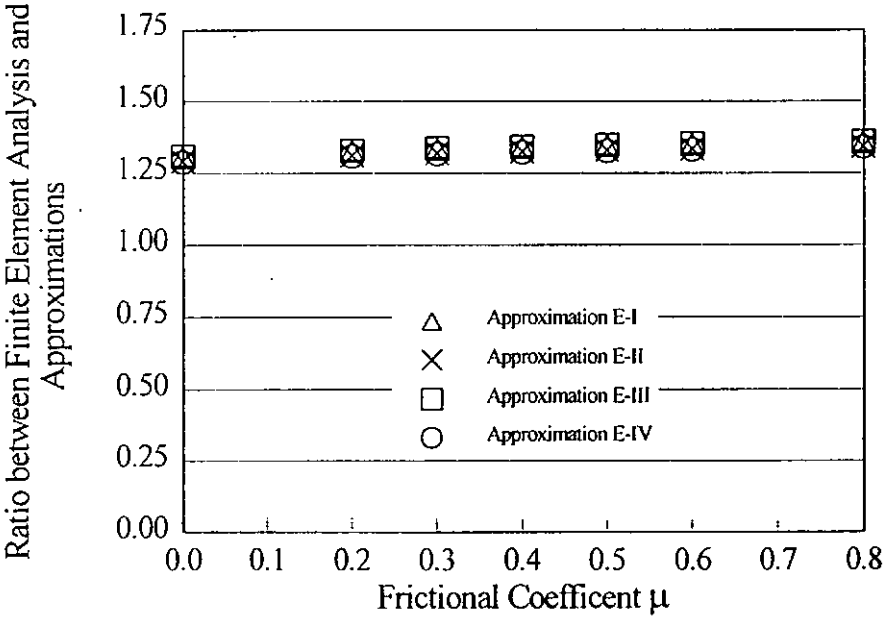

(b) Accuracy of Approximations

Fig. 5-7 Effect of Frictional Coefficent

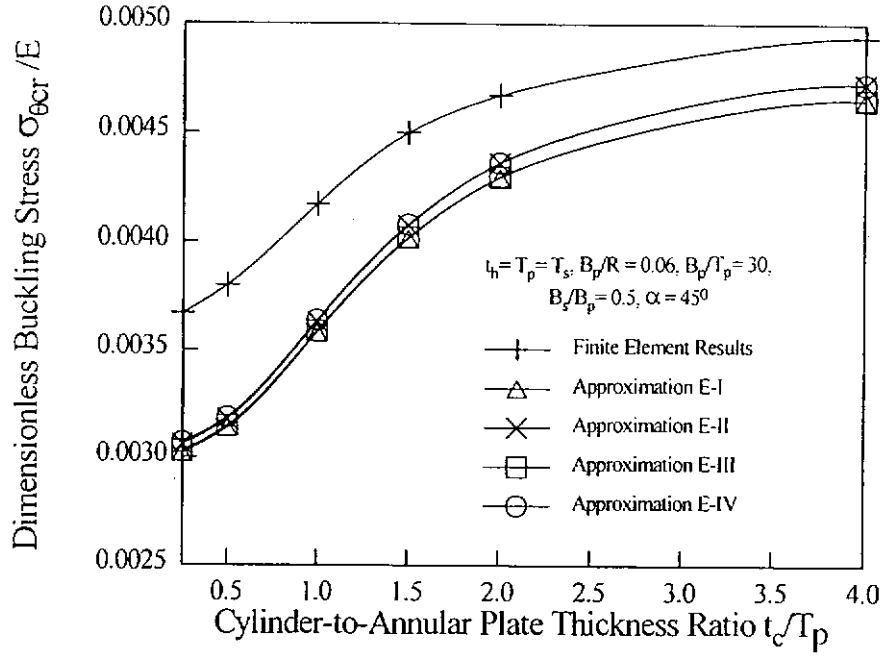

(a) Comparison of Buckling Stresses

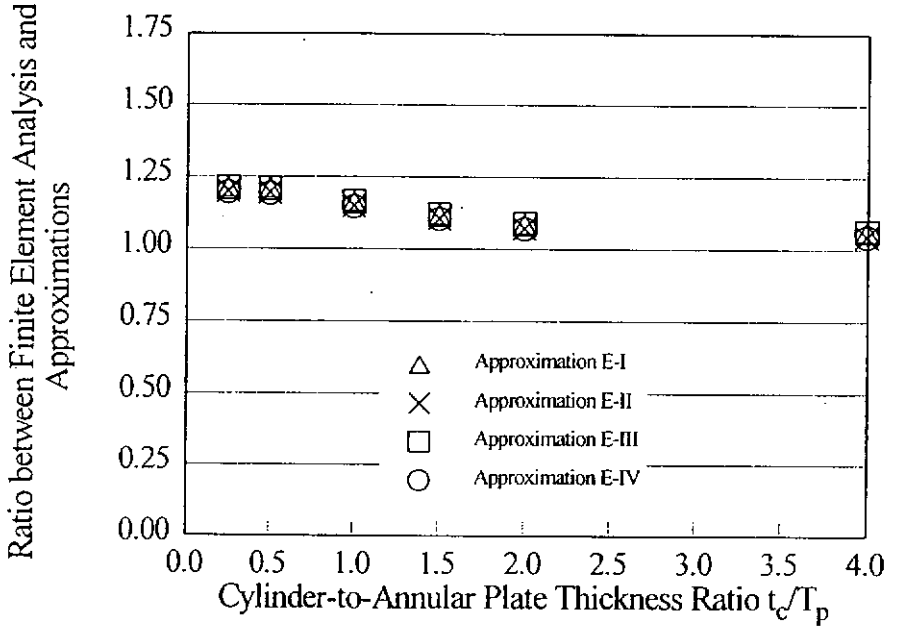

(b) Accuracy of Approximations

Fig. 5-8 Effect of Cylinder-to-Annular Plate Thickness Ratio

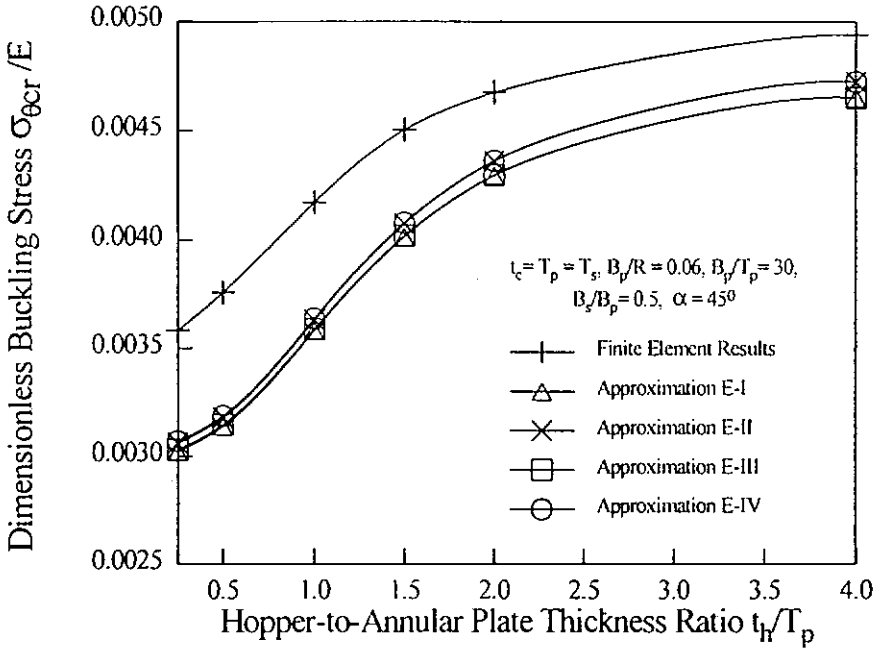

(a) Comparison of Buckling Stresses

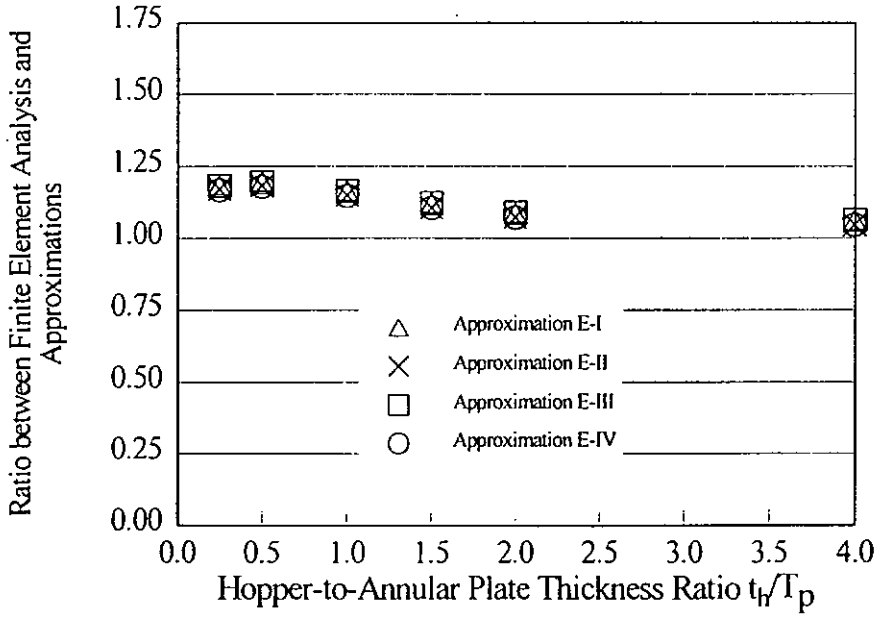

(b) Accuracy of Approximations

Fig. 5-9 Effect of Hopper-to-Annular Plate Thickness Ratio

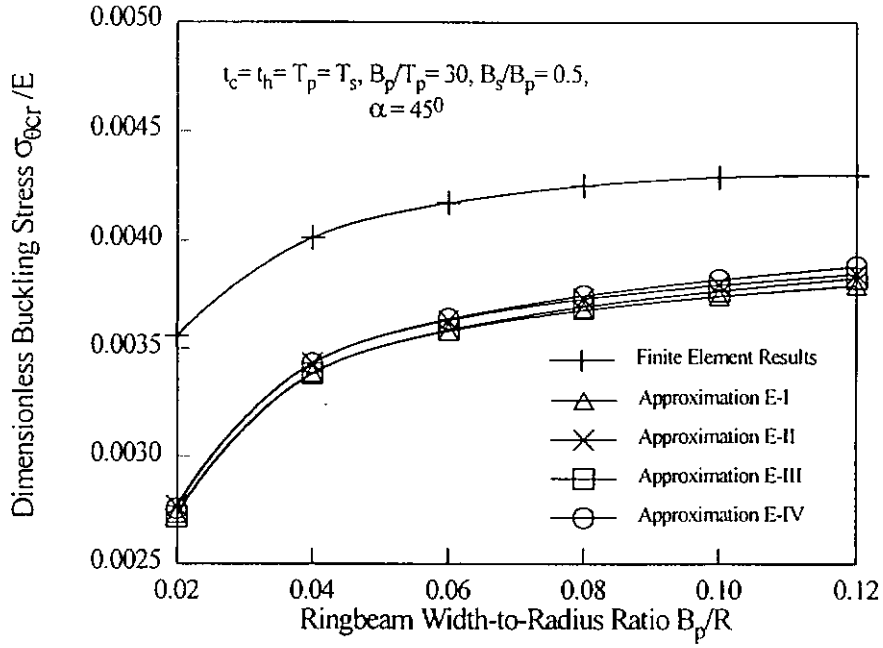

(a) Comparison of Buckling Stresses

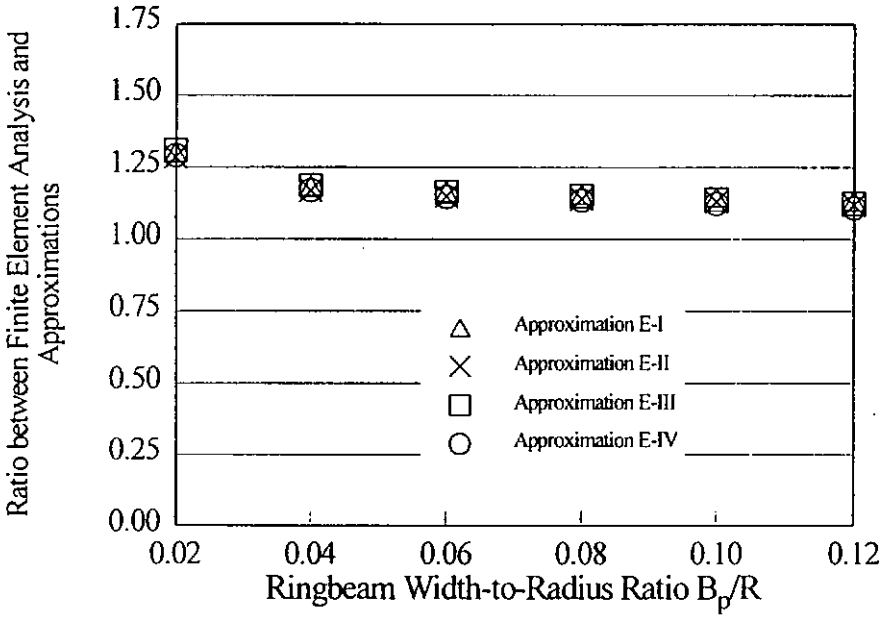

(b) Accuracy of Approximations

Fig. 5-10 Effect of Ringbeam Width-to-Radius Ratio

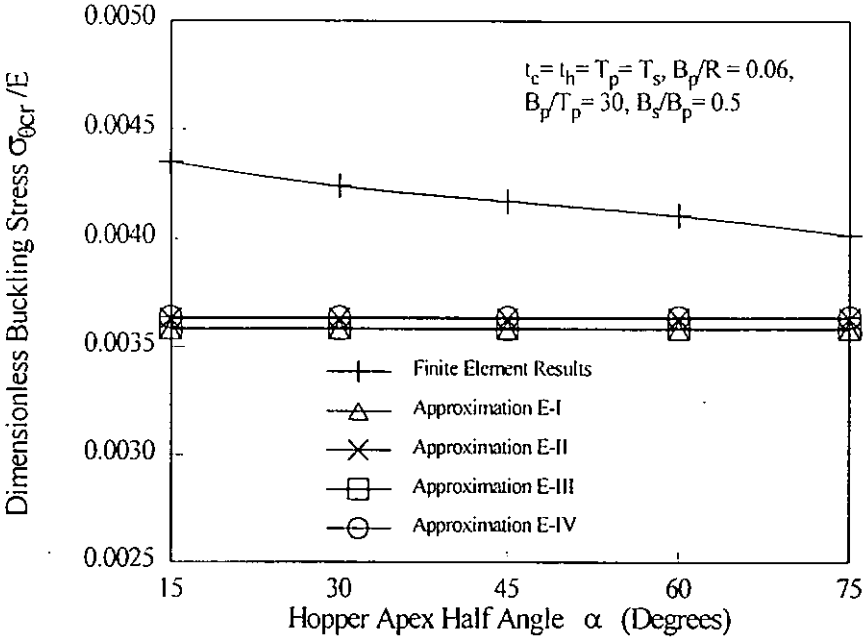

(a) Comparison of Buckling Stresses

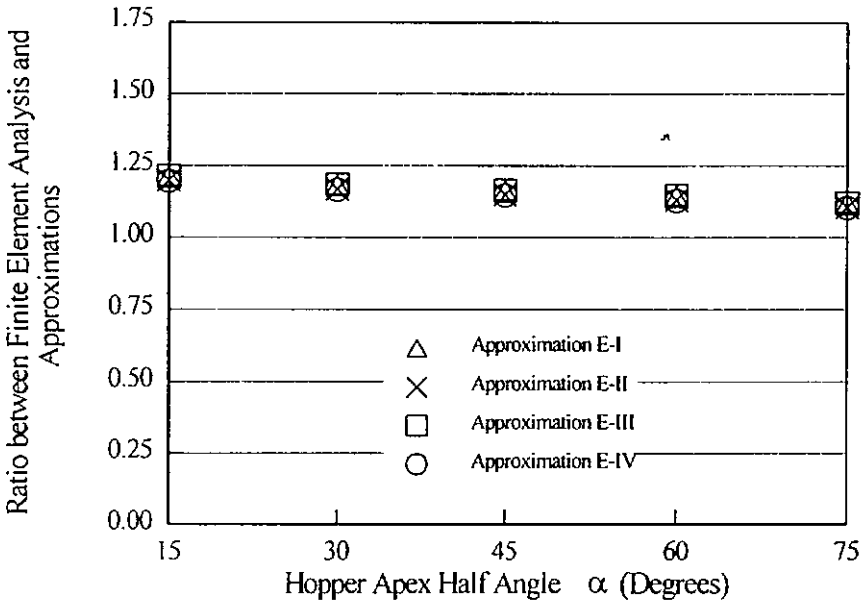

(b) Accuracy of Approximations

Fig. 5-11 Effect of Cone Apex Half Angle

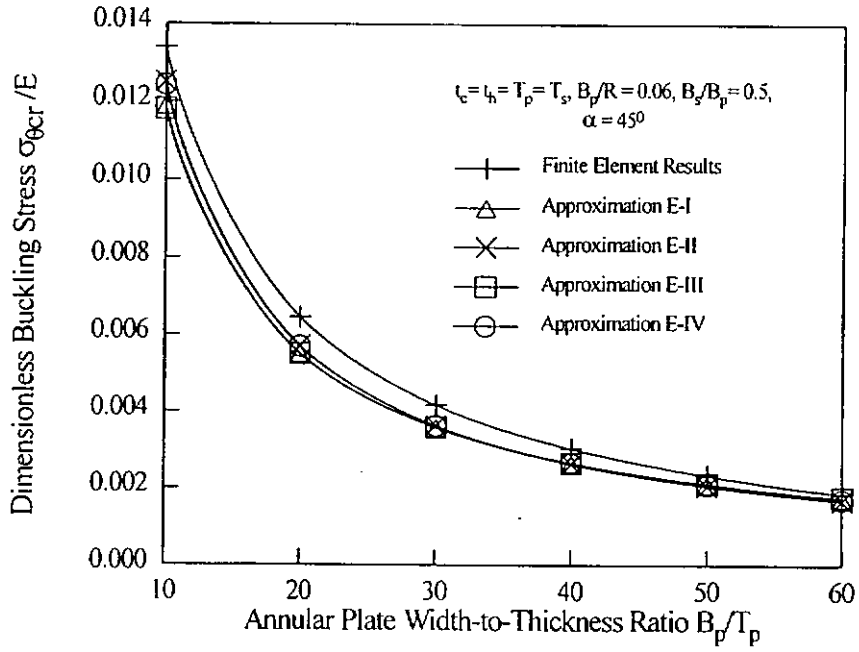

(a) Comparison of Buckling Stresses

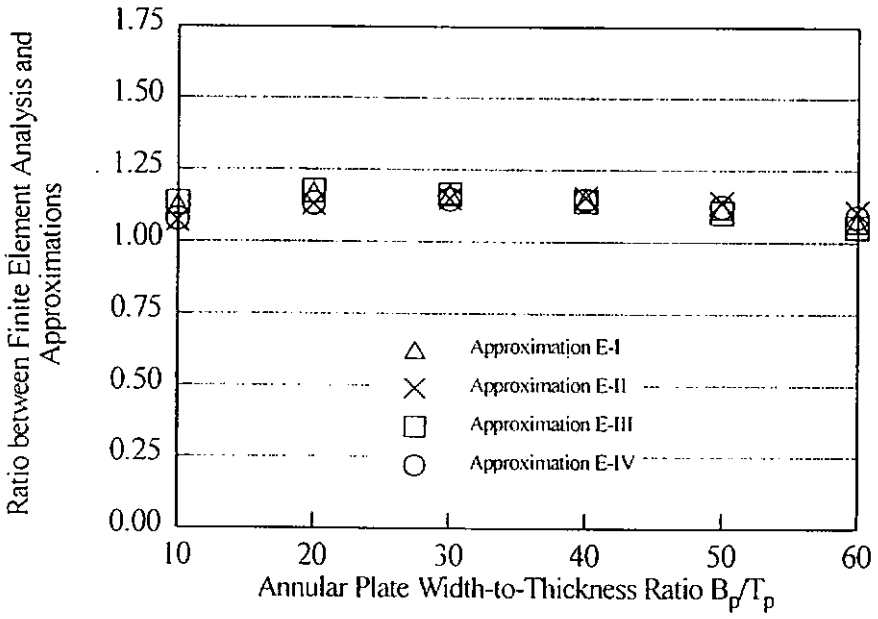

(b) Accuracy of Approximations

Fig. 5-12 Effect of Annular Plate Width-to-Thickness Ratio of the Ringbeam

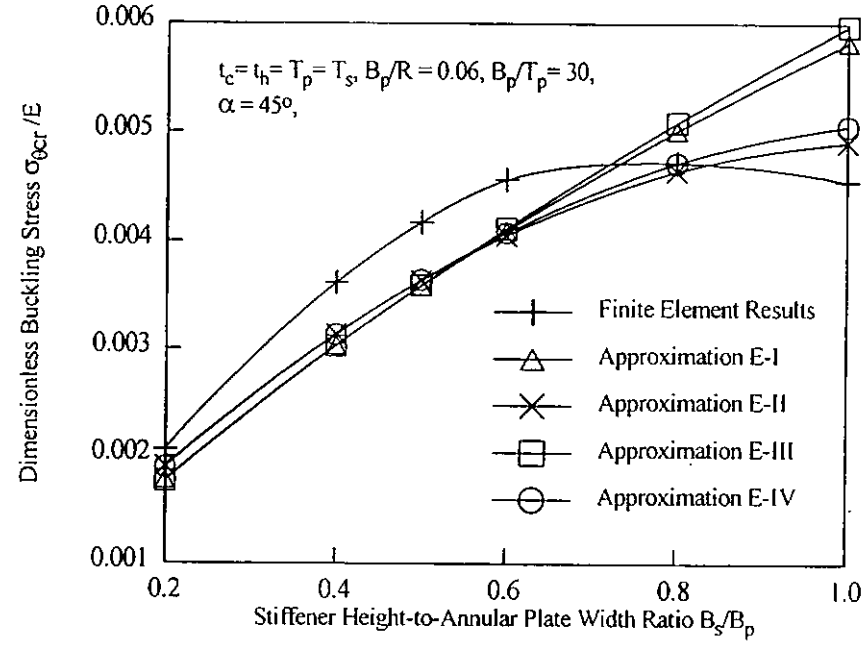

(a) Comprison of Buckling Stresses

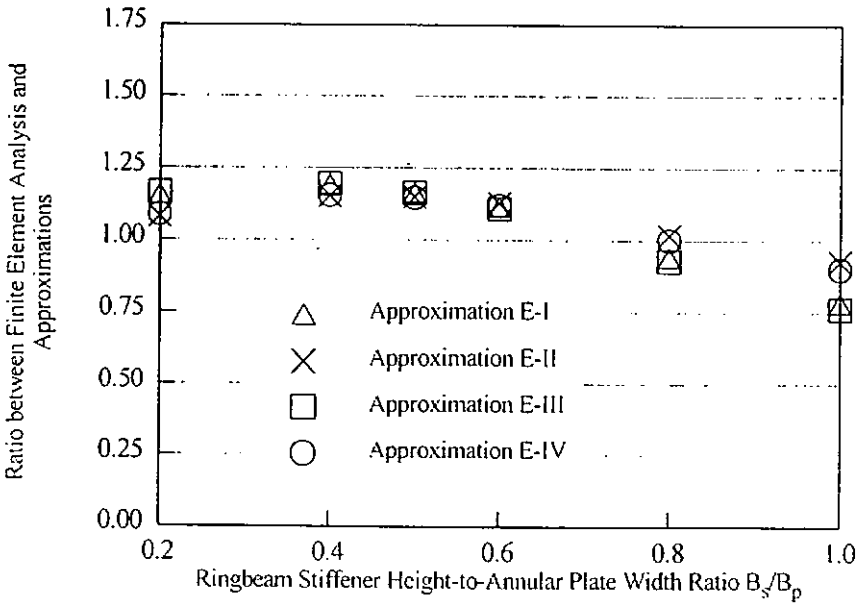

(b) Accuracy of Approximations

Fig. 5-13 Effect of Stiffener Height-to-Annular Plate Width Ratio of Ringbeam

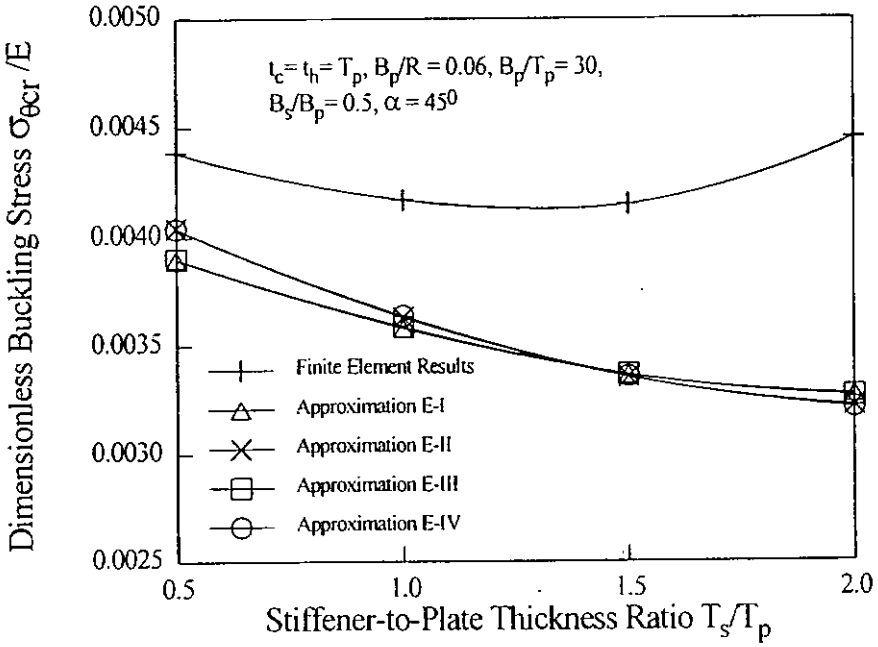

(a) Comprison of Buckling Stresses

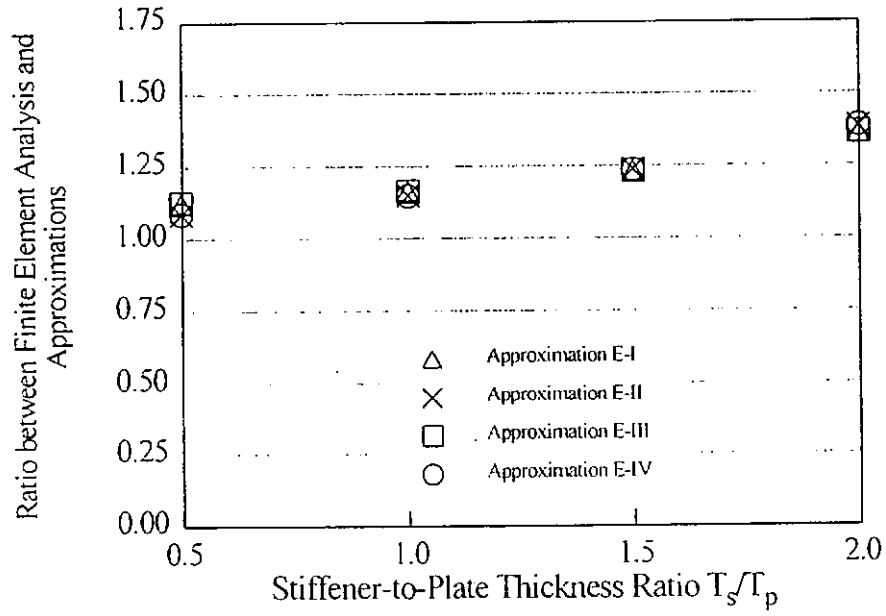

(b) Accuracy of Approximations

Fig. 5-14 Effect of Stiffener-to-Plate Thickness Ratio of the Ringbeam

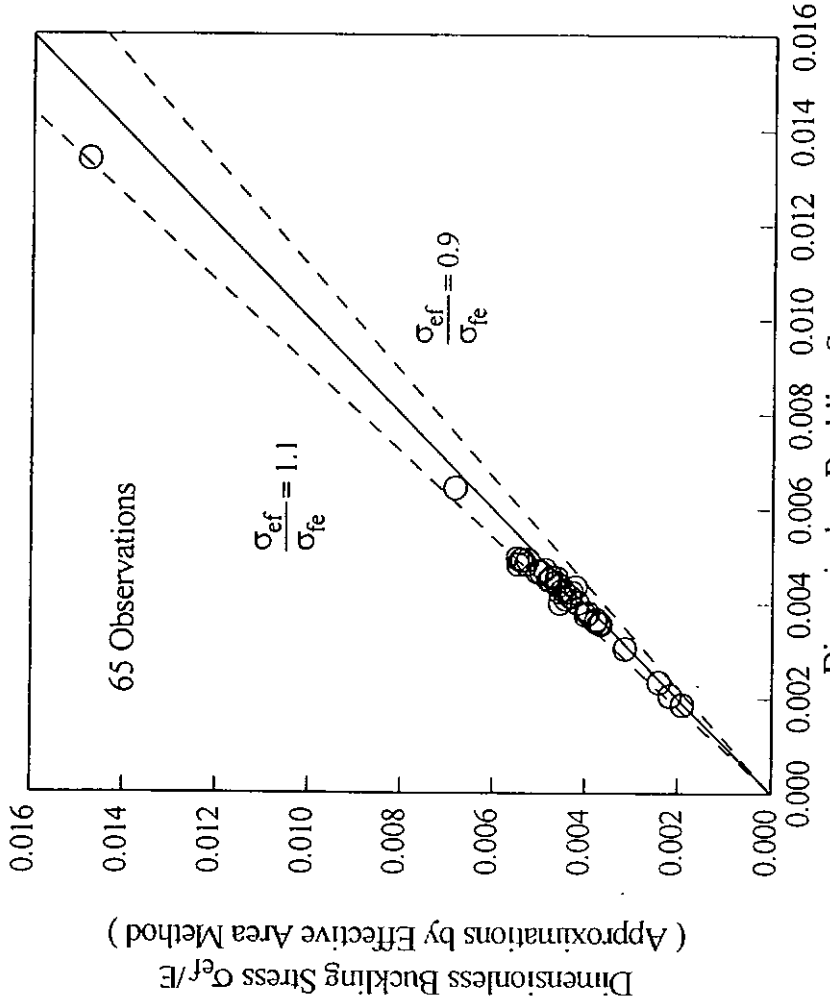

Fig. 5-15 Accuracy of the Effective Section Method

CHAPTER 6 PLASTIC BUCKLING OF T-SECTION TRANSITION RINGBEAMS

6.1 Introduction

The ringbeam provided at the transition junction of a uniformly-supported steel silos is subject to a large circumferential compressive force derived from the radial component of the meridional tension in the conical hopper. Under this compressive force, the ringbeam may fail in one of several possible modes, including out-of-plane buckling. When the ringbeam is slender or the yield stress of the material is high, buckling occurs in the elastic range. The elastic buckling strength has been thoroughly studied in the previous Chapters leading to the simple strength approximation described in Chapter 5. When the ringbeam is stocky, it may fail by axisymmetric plastic collapse. Plastic collapse of transition junctions has been studied by Rotter (1987) and Teng and Rotter (1991a; 1991b). A simple design equation has been developed. Although these studies all assumed an annular plate ringbeam instead of a T-section ringbeam at the junction, the design equation can be applied to junctions with T-section ringbeams with no difficulty. For ringbeams of intermediate slenderness, plastic buckling is the likely failure mode. Only one previous study (Teng and Rotter, 1991c) considered plastic buckling of T-section ringbeams together with the plastic buckling of annular plate ringbeams, but no simple design method was proposed and the scope of that study was limited. Plastic buckling of annular plate ringbeams has been examined in a number of studies

(Rotter, 1987; Greiner, 1991; Teng, 1997). Teng (1997) recently presented a comprehensive study on the plastic buckling strength of annular plate ringbeams and developed a simple strength approximation.

This chapter thus presents an investigation into the plastic out-of-plane buckling behaviour and strength of T-section transition ringbeams. Based on a thorough study of the effects of various factors, a simple plastic buckling strength approximation for design use is developed. Application of the proposed method is demonstrated through an example.

6.2 Elastic Buckling Strength and Plastic Collapse Strength

6.2.1 Strength Characterisation

As explained in Chapter 5 and in Teng (1997), the strength of the transition junction is best characterised by the equivalent circumferential compressive force at the junction. For any given loading pattern, this equivalent circumferential force can be evaluated without difficulty using Eq. 5-2 in Chapter 5.

Plastic buckling failures result from interaction between elastic buckling and yielding or plastic collapse. Plastic buckling strengths are thus often formulated in terms of the elastic buckling strength and the plastic yielding/collapse failure strength. For this reason, existing information on the plastic collapse strength of transition junctions is briefly summarised below for ease of reference later. The elastic buckling strength of

a transition junction with a T-section ringbeam in terms of this equivalent circumferential compressive force is given by Eq. 5-15 in Chapter 5.

6.2.2 Plastic Collapse Strength

The plastic collapse strength is given in terms of the equivalent circumferential compressive force as:

$$F_p = \sigma_y A_p = \sigma_y (A_r + A_{ps}) = \sigma_y (B_p T_p + B_s T_s + \sum_{i=1}^{NS} l_{pi} t_i) \qquad (6\text{-}1)$$

where A_r is the cross-sectional area of the T-section ringbeam and A_{ps} is the effective area of the shell segments in resisting the circumferential compression at an equivalent stress of the yield stress σ_y at plastic collapse and NS is the number of shell segments forming the transition junction. The plastic effective length l_{pi} for the ith shell segment is given by :

$$l_{pi} = 0.975 \gamma_{pi} \sqrt{R t_i} \qquad (6\text{-}2)$$

where γ_{pi} assumes different values for the two groups of segments above and below the annular plate of the ringbeam, respectively, and is given by

$$\gamma_{pi} = 1 \qquad \text{for the thinner group} \qquad (6\text{-}3)$$

$$\gamma_{pi} = \gamma_p = 0.7 + 0.6\zeta^2 - 0.3\zeta^3 \qquad \text{for the thicker group} \qquad (6\text{-}4)$$

with equivalent thickness ratio ζ being the same as that defined in Eq. 5-6 in Chapter 5. Equation 6-1 was initially developed for transition junctions with an annular plate ringbeam (Teng and Rotter, 1991a; 1991b), but it will be shown later that its predictions for transition junctions with a T-section ringbeam are also accurate.

6.3 Structural Modelling and Analysis

The numerical results to be described here were all obtained using the simplified structural model shown in Fig. 5-3b of Chapter 5. The use of this structural model ensures that the results obtained only relate to junction collapse and buckling without losing the generality of the results. Application of the developed design approximation to junctions with a skirt will be demonstrated in the design example. In addition, this model also represents real cases where a skirt is not present and the junction sits instead directly on a large number of closely-spaced discrete vertical supports.

The structure is subject to a uniform internal pressure p with a frictional drag of μp. The frictional coefficient μ of the stored material was assumed to be 0.5. Under this loading condition, the membrane theory of shells predicts that the meridional tension at the top of the hopper as:

$$N_{\phi} = \frac{pR}{2}\sec\alpha\left(1+\mu\cot\alpha\right) \tag{6-5}$$

and according to Eq. 5-2, the circumferential compressive force is given by :

$$F = \frac{pR^2}{2}\left(\tan\alpha+\mu\right) - pl_{ec}R - p\left(\cos\alpha-\mu\sin\alpha\right)l_{ch}R \tag{6-6}$$

or, if local pressure effects are ignored, by:

$$F = \frac{pR^2}{2}\left(\tan\alpha+\mu\right) \tag{6-7}$$

It is clear that a linear relationship exists between the pressure, the meridional tension at hopper top and the circumferential compression at the transition junction. Consequently, the following relations are valid:

$$\frac{F_p}{F_e} = \frac{p_p}{p_e}, \text{ and } \frac{F_f}{F_p} = \frac{p_f}{p_p} \tag{6-8}$$

where p_f, p_p, p_e are the pressures at failure (due to either elastic buckling, plastic buckling or plastic collapse), at plastic collapse and at elastic buckling respectively, and F_f, F_p and F_e are the corresponding values of the circumferential compressive force.

Finite element results presented in this chapter were again obtained using program NEPAS for the non-symmetric bifurcation buckling analysis of axisymmetric shells (Teng and Rotter, 1989b). For plastic buckling analysis, the program first carries out an axisymmetric elastic -plastic large deflection or small deflection analysis with the material modelled according to the J_2 flow theory of plasticity, and then performs a non-symmetric bifurcation buckling analysis based on one of the following three plasticity options: J_2 flow theory, J_2 deformation theory, and modified J_2 flow theory which is the J_2 flow theory with the shear modulus replaced by that predicted by the J_2 deformation theory. The accuracy of the program in predicting plastic buckling and collapse strengths of shells of revolution has been shown elsewhere (Teng and Rotter, 1989b). The program has also been applied widely to study plastic collapse and plastic buckling problems in shells of revolution (eg Teng and Rotter, 1991a; 1991b; 1991c; Teng, 1994; 1995; 1998). The material of the transition junction was

assumed to have properties typical of steel: a Young's modulus of 2 x 10^5 MPa, a Poisson's ratio of 0.3, and to exhibit an elastic-perfectly plastic behaviour.

6.4 Aspects of Plastic Buckling Behaviour

6.4.1 Effect of Prebuckling Large Deflections

The effect of prebuckling large deflections on the buckling strength of annular plate transition ringbeams in steel silos has been found to be small (Jumikis, 1987; Teng, 1997). Consequently, Teng (1997) developed his plastic buckling approximation ignoring this effect. For T-section ringbeams, the results presented in Chapter 5 indicate that the effect of prebuckling large deflections on the elastic buckling strength of T-section transition ringbeams is small and strengthening, so it can be safely ignored for simplicity. In Fig. 6-1, finite element results obtained using a small deflection prebuckling analysis and those using a large deflection prebuckling analysis are compared to examine the effect of prebuckling large deflections on the plastic buckling strength. The junctions examined in Fig. 6-1 are defined by the following geometric parameters: cone apex half angle $\alpha = 45^\circ$, uniform shell wall thickness for the cylinder and the hopper, that is $t_c = t_s$, a radius-to-thickness ratio R/t_c=500, a uniform thickness ringbeam ($T_s = T_p$) with the stiffener height-to-annular plate width ratio B_s/B_p,= 0.3, a dimensionless ringbeam cross-section area $A_r/t_c^2 = 45$ and a varying B_p/T_p ratio which is achieved by varying the thickness and the width of both the annular plate and the stiffener. The yield stress used is 450 MPa.

The effect of prebuckling large deflections is seen to increase the plastic buckling strength. This effect becomes more significant as the ringbeam becomes stockier and its buckling strength becomes higher. At a B_p/T_p value of 10, the increase in buckling strength due to this effect is 10.5%, which reduces to 0.04% when $B_p/T_p = 90$. This is as expected as at a higher buckling load, the prebuckling deformations are more significant for the same shell wall thicknesses. It should be noted that the high B_p/T_p ratios considered here are beyond those covered by Fig. 3-3 in Chapter 3. These high values are included here so that the full range of buckling behaviour including elastic buckling is covered. In the eventual application of the design proposal to be developed, the limits of Fig. 3-3 in Chapter 3 should still be observed, or necessary judgement is exercised so that local buckling does not become the critical mode.

Since the effect of prebuckling large deflections is strengthening, it is conservatively ignored in the parametric study presented below. As the plastic buckling load needs to be normalised by the plastic collapse load for a given junction geometry to establish a design approximation later, the plastic collapse strength was also determined using a small deflection elastic-plastic analysis. Such an analysis leads to a collapse load corresponding to the classical limit load. This leads to simplification in the following parametric study to develop a design proposal. Another justification for ignoring this effect is that it may not exist in the model with a skirt, due to the destabilising effect from the axial compression in the skirt.

6.4.2 Effect of Plasticity Modelling

Previous results of Rotter (1987), Teng and Rotter (1991c), and Greiner (1991) for plastic buckling analysis of ringbeams at steel silo transition junctions were based on the flow theory or modified flow theory. Although the flow theory is more rigorous, the bifurcation buckling loads it produces agree less closely with experimental results (Teng, 1996) and are higher than those from the deformation theory. Teng (1997) showed that for annular plate ringbeams, different plasticity models lead to slightly different results and the results from the deformation theory are again the most conservative among the three options allowed in NEPAS (Teng and Rotter, 1989b). The expectation that T-section ringbeams exhibit similar behaviour is confirmed in Fig. 6-2 where comparisons are shown between the three sets of results for the same junctions as examined in Fig. 6-1. The results from the flow theory are indistinguishable from those of the modified flow theory. For annular ringbeams, flow theory predicts a sudden jump in strength as the failure mode changes from axisymmetric collapse to plastic buckling (Teng, 1997). This behaviour is not observed for T-section ringbeams. As the results from the deformation theory are again found to be the most conservative among the three plasticity models, they are used to develop a strength approximation for the plastic buckling of T-section ringbeams at transition junctions. Consequently, only the results from the deformation theory based on a small deflection prebuckling analysis are discussed in the rest of this chapter.

6.4.3 Effect of Yield Stress

The effect of yield stress is examined next for the junctions previously examined in Figs. 6-1 and 6-2 by obtaining additional results for these junctions when the yield stress is 250 MPa or 350 MPa. The results are presented in a dimensionless manner, with the horizontal axis being the slenderness parameter of the ringbeam, defined as

$$\lambda = \left(\frac{F_p}{F_e} \right)^{0.5} \tag{6-9}$$

where F_p is the plastic collapse strength in terms of the circumferential compression at the junction, and F_e is the value of this force at elastic buckling. The vertical axis represents the failure load F_f of the ringbeam normalised by the axisymmetric plastic collapse strength F_p.

Figure 6-3 shows that there is little variation in this dimensionless strength with the yield stress for a given value of the slenderness parameter. For the same junction geometries, a higher yield stress leads to a wider range of values for the slenderness parameter λ. For a yield stress of 250 MPa, the lower and upper limits of λ are approximately 0.5 to 1.2. These limits are approximately 0.5 and 1.4 for a yield stress of 350 MPa , and 0.6 and 1.6 for a yield stress of 450 MPa.

The finite element results may be separated into three regions. In the first region where the slenderness parameter λ is below about 0.9, buckling occurs with extensive yielding in both the shell segments and the ringbeam (Fig. 6-4a), and since the area of the ringbeam is constant, there is little variation with λ in the buckling strength in this

region. When the slenderness parameter λ is between 0.9 and 1.4, buckling occurs with yielding being largely restricted to the shell segments (Fig. 6-4b). In the third zone with $\lambda > 1.4$, elastic buckling (or nearly elastic buckling with very limited yielding) occurs (Fig. 6-4c).

With a yield stress of 250 MPa, all junctions considered in Fig. 6-3 fall in the first region except two cases. Junctions with a yield stress of 350 MPa span over the first and second regions, while those with a yield stress of 450 MPa extends into the third region of elastic buckling. As a different yield stress does not alter the dimensionless strength and the results for a yield stress of 450 MPa cover the widest range of λ values among the three yield stresses considered, only results for junctions with a yield stress of 450 MPa are discussed below in the development of a design proposal. The developed proposal is also expected to be applicable to high strength steels with a yield stress greater than 450 MPa which are becoming increasingly common.

6.5 Development of Design Approximation

6.5.1 Dimensionless Ringbeam Size Parameter

As described earlier, the circumferential compressive force at the transition junction is resisted partly by the shell segments and partly by the ringbeam itself. As the load increases from zero, yielding is first attained in the shell segments and spreads in the shell segments until a certain load level at which the ringbeam cross section reaches membrane yielding (Teng and Rotter, 1991c). A parameter k, called the

dimensionless ringbeam size parameter, was first introduced and confirmed by Teng (1997) as the key parameter controlling the shape of the dimensionless strength curve for annular plate transition ringbeams. Teng (1997) defined the parameter as the ratio of the ringbeam area to the total effective area A_{ps} of the shell segments in resisting plastic collapse. That is:

$$k = A_r / A_{ps} \tag{6-10}$$

where A_{ps} can be found as the summation of the contribution to the plastic effective section from all shell segments. For junctions with a T-section ringbeam, the expression of k may be written as:

$$k = \frac{B_p T_p + B_s T_s}{A_{ps}} \tag{6-11}$$

To confirm that this is also the key parameter controlling the shape of dimensionless strength curves for T-section transition ringbeams, the plastic buckling strengths of a large number of junctions were obtained covering R/t_c = 250, 500 and 750; t_c/t_h = 0.5, 1, 2; and $\alpha = 20^0$, 45^0, and 60^0. Figure 6-5 confirms that, as long as k is kept constant, all finite element results fall approximately on a single curve. Therefore, the form of interaction between yielding and buckling is independent of all shell geometric parameters.

6.5.2 Effect of Ringbeam Geometric Parameters on Dimensionless Strength Curve

For annular plate ringbeams, Teng (1997) showed that the dimensionless ringbeam size parameter discussed above is the only parameter which affects the form of interaction between the buckling and yielding. For T-section ringbeams, there are two

other independent ringbeam geometric parameters: the stiffener-to-annular plate thickness ratio T_s/T_p, and the stiffener height-to-annular plate width ratio B_s/B_p.

Figure 6-6 shows that within the practical range of 0.5 to 2 for the ratio T_s/T_p, the variation of the dimensionless strength F_f/F_p is small. It may thus be assumed that this parameter does not affect the form of interaction between yielding and buckling.

The effect of varying the stiffener height-to-annular plate width ratio B_s/B_p is shown in Fig. 6-7. This effect is found to be stronger than the effect of varying T_s/T_p. Furthermore a change in B_s/B_p leads to different effects for different values of the slenderness parameter. When the ringbeams are stocky, a lower B_s/B_p ratio leads to some increase in the dimensionless failure strength, while for more slender ringbeams, this leads to a decrease in the dimensionless failure strength. The B_s/B_p ratio thus has a significant effect on the dimensionless strength curve.

6.5.3 Form of Failure Strength Approximation

Based on the discussion above, the ultimate failure strength F_f (due to either elastic buckling, plastic buckling or plastic collapse) is suggested to be formulated in the following manner:

$$F_f = f(k, B_s / B_p, \lambda) F_p \tag{6-12}$$

where $f(k, B_s/B_p, \lambda)$ is a function of the dimensionless ringbeam size parameter k, the stiffener height-to-annular plate width ratio B_s/B_p, and the slenderness parameter λ. For a given structure, all three parameters can be evaluated without difficulty, and the

plastic collapse failure strength is given by Eq. 6-1. Once the form of the function $f(k, B_s/B_p, \lambda)$ is determined, the ultimate failure strength of the junction can be assessed.

6.5.4 Design Approximation

It is difficult, if not impossible, to find a function which includes the effects of all three parameters k, B_s/B_p, λ accurately. Due to the present lack of information on the effect of geometric imperfections and residual stresses in steel silo transition junctions, a lower bound curve as a function of λ only is generated here. This is also the approach adopted by Teng (1997) for annular plate ringbeams.

To generate this lower bound curve, buckling strengths were obtained for transition junctions with the following geometric parameters: $R/t_c = 500$, $\alpha = 45^0$, $t_c = t_h = t$. The T-section ringbeam was assumed to have uniform thickness ($T_s = T_p$) but its other geometric parameters were varied to arrive at desired values of the dimensionless ringbeam size parameter k and the stiffener height-to-annular plate width ratio B_s/B_p.

Dimensionless failure strengths are plotted in Fig. 6-8 for three different k values (=0.3, 0.9428, and 4), and for each k value, three sets of results are shown corresponding to three different values of B_s/B_p (= 0.2, 0.45, and 0.6). Very small or very large ringbeams are not used in practice, so a k value of 0.3 may be viewed as a lower bound to practical k values while a value of 4 may be viewed as a practical upper bound. It is interesting to note that for stocky ringbeams (region 1), a small k value (ie., a small ringbeam) leads to lower dimensionless strength. However, for ringbeams falling in the second region, the largest ringbeam ($k = 4$) leads to the lowest

dimensionless strength. In addition, there is some variation with the parameter B_s/B_p. Two alternative lower bound approximations for use in design are proposed below.

6.5.5 Approximation P-I

Approximation P-I is proposed to provide almost a precise lower bound to all numerical results contained in Fig. 6-8. The entire strength approximation consists of two separate functions for the plastic buckling strength and is given by:

$$\frac{F_f}{F_p} = 0.78, \quad 0 < \lambda \leq 0.93 \quad \text{(Plastic buckling)} \tag{6-13}$$

$$\frac{F_f}{F_p} = \frac{0.71}{\lambda^{1.3}}, \quad 0.93 < \lambda \leq 1.62 \quad \text{(Plastic buckling)} \tag{6-14}$$

$$\frac{F_f}{F_p} = \frac{1}{\lambda^2}, \quad 1.62 < \lambda \quad \text{(Elastic Buckling)} \tag{6-15}$$

The division between elastic buckling and plastic buckling is based on the strength behaviour, so the elastic buckling region covers purely elastic buckling failures as well as nearly elastic buckling failures occurring after limited yielding which does not reduce the buckling strength appreciably. The above equations give the same value at the transition points of $\lambda = 0.93$ and $\lambda = 1.62$. The value for separating the elastic buckling region from the plastic region adopted here is the same as that used by Teng (1997) for junctions with an annular plate ringbeam. This consistency is certainly a desirable feature. Equation 6-13 to 6-15 are thus satisfactory as a design proposal.

6.5.6 Approximation P-II

Although Approximation P-I contains only simple expressions and provides a precise lower bound to the numerical results, the fact that three separate functions are required does present some awkwardness. An alternative simpler approximation (Approximation P-II) is thus proposed here as:

$$\frac{F_f}{F_p} = 1 - 0.383\lambda, \quad 0 < \lambda \leq 1.62, \text{ (Plastic Buckling)} \tag{6-16}$$

$$\frac{F_f}{F_p} = \frac{1}{\lambda^2}, \qquad 1.62 < \lambda, \qquad \text{(Elastic Buckling)} \tag{6-17}$$

Figure 6-8 shows that Approximation P-II is a conservative and satisfactory lower bound, and the conservativeness is at least tolerable if not a desirable feature to compensate for some uncertainty in the effect of imperfections and residual stresses.

6.5.7 Accuracy of the Effective Area Method for Plastic Collapse Strengths

In all dimensionless plots presented above, the finite element buckling load is normalised by the plastic collapse load from finite element analysis. In practical design, the value of F_p needs to be evaluated using Eq. 6-1. To clarify the accuracy of Eq. 6-1 for junctions with a T-section ringbeam, the ratios between finite element predictions using small deflection plastic analysis and those from the effective area method (Eq. 6-1) are plotted in Fig. 6-9. This comparison shows that Eq. 6-1 is accurate.

6.5.8 Comments

It is worth noting that the effects of imperfections and residual stresses have not been considered in this chapter. Little information is available on initial imperfections in these ringbeams, but their effect is expected to be mild, similar to that displayed by internally pressurized torispherical shells extensively studied by Galletly and his associates (Galletly, 1985; Galletly and Blachut, 1985). Current knowledge on the form and effect of residual stresses in thin metal shells is, in general, very limited. The few existing studies for cylindrical shells under axial compression suggest that they may be beneficial to the strength (Rotter, 1996), contrary to the role of residual stresses in steel beams and columns, although it is pre-mature to generalise this conclusion for all cases of metal shell buckling. The strength approximations proposed here are thus believed to be a good representation of real failure strengths suitable for use in design. Although both approximations are satisfactory as design proposals, it is recommended that the simpler and more conservative Approximation P-II be used considering the current uncertainty in the effect of imperfections and residual stresses. Appropriate load and resistance factors should be used with the design approximations in a limit state design formulation.

6.6 Application of Design Equations

6.6.1 Example Structure

A typical elevated steel silo supported on a skirt is considered (Fig. 6-10). The geometric and material parameters are R = 6000 mm; t_c = 10 mm; t_s = 20 mm; t_h=10mm; α = 30^0; B_p = 500 mm; T_p = 15 mm; B_s = 200 mm; T_s = 15 mm; E=2x10^5MPa; σ_y = 450 MPa, and a cylinder height H = 10,000 mm. The silo is filled with a bulk solid with the following properties: angle of repose ϕ_r = 30^0; internal angle of friction ϕ_i = 40^0; unit height = 15 KN/M^3; and wall frictional coefficient for both the cylinder the hopper μ = 0.4. The purpose here is to evaluate the load factor on the loads due to the stored bulk solid in a static state that will cause the junction to fail.

Under these conditions, the initial filling pressures on the cylindrical wall predicted by Janssen's (1985) theory and those on the hopper by Walker's (1966) theory, as described in Teng and Rotter (1991d), are shown in Fig. 6-11. The pressures are seen to be non-uniform in both the cylinder and hopper.

6.6.2 Application of Design Equations

6.6.2.1 Elastic and Plastic Effective Sections

$$t_{eqA} = t_c = 10\ mm$$

$$t_{eqB} = \sqrt{t_h^2 + t_s^2} = \sqrt{10^2 + 20^2} = 22.36\ mm$$

$$\zeta = \frac{t_{eqA}}{t_{eqB}} = \frac{10}{22.36} = 0.447$$

$$\sqrt{Rt_c} = \sqrt{6000 \times 10} = 244.95\ mm$$

$$\sqrt{\frac{Rt_h}{\cos\alpha}} = \sqrt{\frac{6000 \times 10}{\cos 30^0}} = 263.21\ mm$$

$$\sqrt{Rt_s} = \sqrt{6000 \times 20} = 346.41\ mm$$

$$\gamma_e = 0.5(1 + 3\zeta^2 - 2\zeta^3) = 0.5 \times (1 + 3 \times 0.447^2 - 2 \times 0.447^3) = 0.711$$

$$l_{ec} = 0.778\sqrt{Rt_c} = 0.778 \times 244.95 = 190.57\ mm$$

$$l_{eh} = 0.778\gamma_e\sqrt{\frac{Rt_h}{\cos\alpha}} = 0.778 \times 0.711 \times 263.21 = 145.51\ mm$$

$$l_{es} = 0.778\gamma_e\sqrt{Rt_s} = 0.778 \times 0.711 \times 346.41 = 191.50\ mm$$

$$A_r = B_p T_p + B_s T_s = 500 \times 15 + 200 \times 15 = 10{,}500\ mm^2$$

$$A_e = A_r + l_{ec}t_c + l_{eh}t_h + l_{es}t_s$$

$$= 10500 + 190.57 \times 10 + 145.51 \times 10 + 191.50 \times 20 = 17{,}688\ mm^2$$

$$\gamma_p = 0.7 + 0.6\zeta^2 - 0.3\zeta^3 = 0.7 + 0.6 \times 0.447^2 - 0.3 \times 0.447^3 = 0.7932$$

$$l_{pc} = 0.975\sqrt{Rt_c} = 0.975 \times 244.95 = 238.83\ mm$$

$$l_{ph} = 0.975\gamma_p\sqrt{\frac{Rt_h}{\cos\alpha}} = 0.975 \times 0.7931 \times 263.21 = 203.53\ mm$$

$$l_{ps} = 0.975\gamma_p\sqrt{Rt_s} = 0.975 \times 0.7931 \times 346.41 = 267.87mm$$

$$A_p = A_r + l_{pc}t_c + l_{ph}t_h + l_{ps}t_s$$

$$= 10500 + 238.83 \times 10 + 203.53 \times 10 + 267.87 \times 20 = 20{,}281mm^2$$

6.6.2.2 Elastic Buckling Strength of Simply-Support T-Section Ringbeam

$$I_x = \frac{1}{12}(B_p T_p^{\ 3} + B_s^{\ 3} T_s) = \frac{1}{12} \times (500 \times 15^3 + 200^3 \times 15) = 1.014 \times 10^7\ mm^4$$

$$A_r r_0^{\ 2} = I_x + \frac{1}{3} B_p^{\ 3} T_p + \frac{1}{12} B_s T_s^3 + B_p^{\ 2} B_s T_s$$

$$= 1..014 \times 10^7 + \frac{1}{3} \times 500^3 \times 15 + \frac{1}{12} \times 200 \times 15^3 + 500^2 \times 200 \times 15 = 1.385 \times 10^9 mm^2$$

$$c_1 = \frac{GJ}{EI_x} = \frac{B_p T_p^{\ 3} + B_s T_s^3}{6(1+\nu) I_x} = \frac{500 \times 15^3 + 200 \times 15^3}{6(1+0.3) \times 1.014 \times 10^7} = 0.0299$$

$$\beta = \frac{B_p}{R} = \frac{500}{6000} = 0.0833$$

$$\sigma_s = \frac{EI_x}{Ar_o^{\ 2}} [c_1 + 0.2\beta + 2\sqrt{c_1}\sqrt{\beta}]$$

$$= \frac{2 \times 10^5 \times 1.014 \times 10^7}{1.385 \times 10^9} \times [0.0299 + 0.2 \times 0.0833 + 2\sqrt{0.0299}\sqrt{0.0833}] = 214.33\ MPa$$

6.6.2.3 Elastic Buckling Strength of Clamped T-Section Ringbeam

$$\rho = 0.016 + 0.5\left(\frac{B_s}{B_p}\right) - 0.25\left(\frac{B_s}{B_p}\right)^2 = 0.016 + 0.5 \times \left(\frac{200}{500}\right) - 0.25 \times \left(\frac{200}{500}\right)^2 = 0.176$$

$$\sigma_c = E\rho\left(\frac{T_p}{B_p}\right)^{1.1} = 2 \times 10^5 \times 0.176 \times \left(\frac{15}{500}\right)^{1.1} = 743.66\ MPa$$

6.6.2.4 Elastic Buckling Strength

$$\eta_s = 0.43 + \frac{(R/B_p)^2}{4000} = 0.43 + \frac{(6000/500)^2}{4000} = 0.466$$

$$\eta_c = \frac{1}{2}\left[\left(\frac{t_c}{T_p}\right)^{2.5} + \left(\frac{t_h}{T_p}\right)^{2.5} + \left(\frac{t_s}{T_p}\right)^{2.5}\right] = \frac{1}{2}\times\left[\left(\frac{10}{15}\right)^{2.5} + \left(\frac{10}{15}\right)^{2.5} + \left(\frac{20}{15}\right)^{2.5}\right] = 1.389$$

$$\sigma_{\theta cr} = \frac{\eta_s\sigma_s + \eta_c\sigma_c}{\eta_s + \eta_c} = \frac{0.466\times 214.33 + 1.389\times 743.66}{0.466 + 1.389} = 610.69\ MPa$$

$$F_e = \sigma_{\theta cr} A_e = 610.69\times 17{,}688 = 10{,}801{,}885\ N = 10{,}802\ KN$$

6.6.2.5 Plastic Collapse Strength

$$F_p = \sigma_y A_p = 450\times 20{,}281 = 9{,}126{,}450 N = 9{,}126\ KN$$

6.6.2.6 Plastic Buckling Strength

Slenderness Parameter and Failure Strength

$$\lambda = \sqrt{F_p/F_e} = \sqrt{9{,}126/10{,}802} = 0.919 < 1.62$$

Plastic buckling controls,

$$F_f = (1 - 0.383\lambda)F_p = (1 - 0.383\times 0.919)\times 9{,}126 = 5{,}914\ KN$$

6.6.2.7 Circumferential Compressive Force due to Applied Load

According to the membrane theory of shells, for a hopper under a linearly varying pressure and accompanying frictional traction, the meridional membrane tension at the hopper top $N_{\phi i}$ is given by:

$$N_{\phi i} = \frac{1}{6}(p_a + 2p_t)R(1 + \mu\cot\alpha)\sec\alpha = 670.62\ N/mm,$$

where p_t = 0.0863 MPa, and p_α = 0.1758 MPa are the normal pressures in the hopper at the top and apex, respectively.

$$F = N_{\phi} R \sin\theta - 0.5(p_{c1} + p_{c2}) l_{ec} R - 0.5(p_{h1} + p_{h2})(\cos\theta - \mu \sin\theta) l_{eh} R$$

$$= 6000 \times [670.62 \times \sin 30^0 - 0.5 \times (0.0322 + 0.0326) \times 190.57 - 0.5$$

$$\times (0.0837 + 0.0848) \times (\cos 30^0 - 0.4 \times \sin 30^0) \times 145.51] = 1{,}925{,}848 N = 1{,}926\ KN$$

$$\text{Load factor at failure} = \frac{5{,}914}{1{,}926} = 3.07$$

6.6.3 Comparison with Finite Element Results

Finite element results were also obtained for this example structure. The finite element results were obtained using small deflection theory in prebuckling analysis and deformation theory of plasticity in prebuckling analysis and deformation theory of plasticity in bifurcation analysis. A comparison of the results from finite element analysis and the approximation design equations is given in Table 6-1.

Table 6-1 Comparison of Failure Load Factors of Example Structure

Mode of Failure	Elastic Buckling	Plastic Collapse	Plastic Buckling
Design Equation	5.61	4.74	3.07
FEA Results	6.30	4.57	3.82

It is found that the proposed design method provides a satisfactory prediction of the plastic buckling strength of this T-section transition ringbeam when compared with the finite element result. The fact that the plastic buckling load factor from the design

approximation is 20% lower (taking the finite element result as the reference value) is a direct consequence of the lower bound nature of the design approximation with intended conservatism.

6.7 Conclusion

This chapter has presented a comprehensive investigation into the effect of yielding on the buckling strength of T-section transition ringbeams in steel silos and tanks, leading to the first ever rigorous design proposal for their plastic buckling strength. The design approximations are based on results obtained using a small deflection prebuckling analysis as the effect of prebuckling large deflections is small, and the deformation theory of plasticity which is the most conservative among the three common plasticity models.

Similar to the case of annular plate ringbeams in steel silos (Teng, 1997), the interaction relationship between plastic yielding/collapse and elastic buckling, when cast in a suitable dimensionless form, is independent of yield stresses and various geometric ratios. It depends strongly on the dimensionless ringbeam size parameter. In addition, the stiffener height-to-annular plate width ratio of a T-section ringbeam also has a significant effect on this relationship. Two design approximations were devised as lower bound curves to finite element results covering a wide range of values of these two parameters. The first approximation, dividing ringbeams into three groups, is more complicated but provides a more accurate approximation to the finite element results, while the second approximation is simpler but more conservative. The second approximation has been proposed for use in design, with its

conservativeness acting as desirable precaution, before experimental results become available. Application of the second design approximation together with the elastic buckling strength approximation was demonstrated in an example.

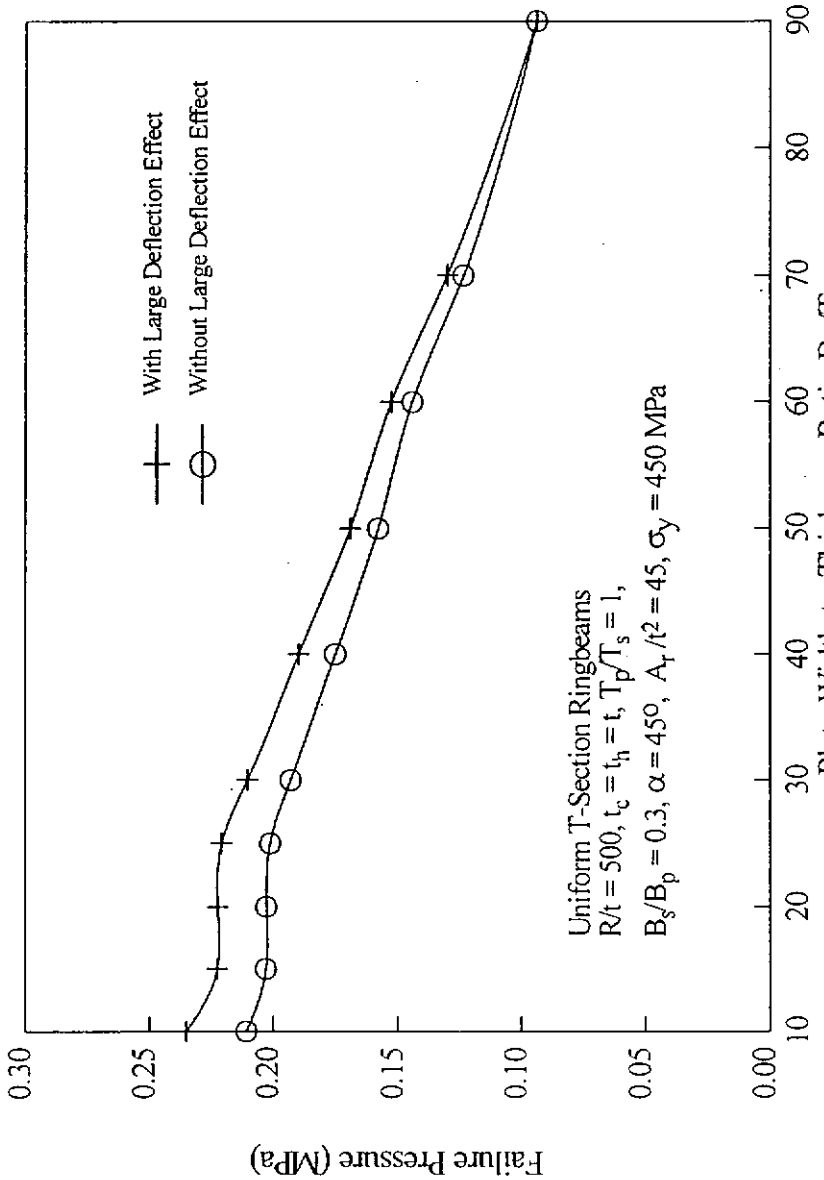

Fig. 6-1 Effect of Prebuckling Large Deflections on Plastic Buckling Strength

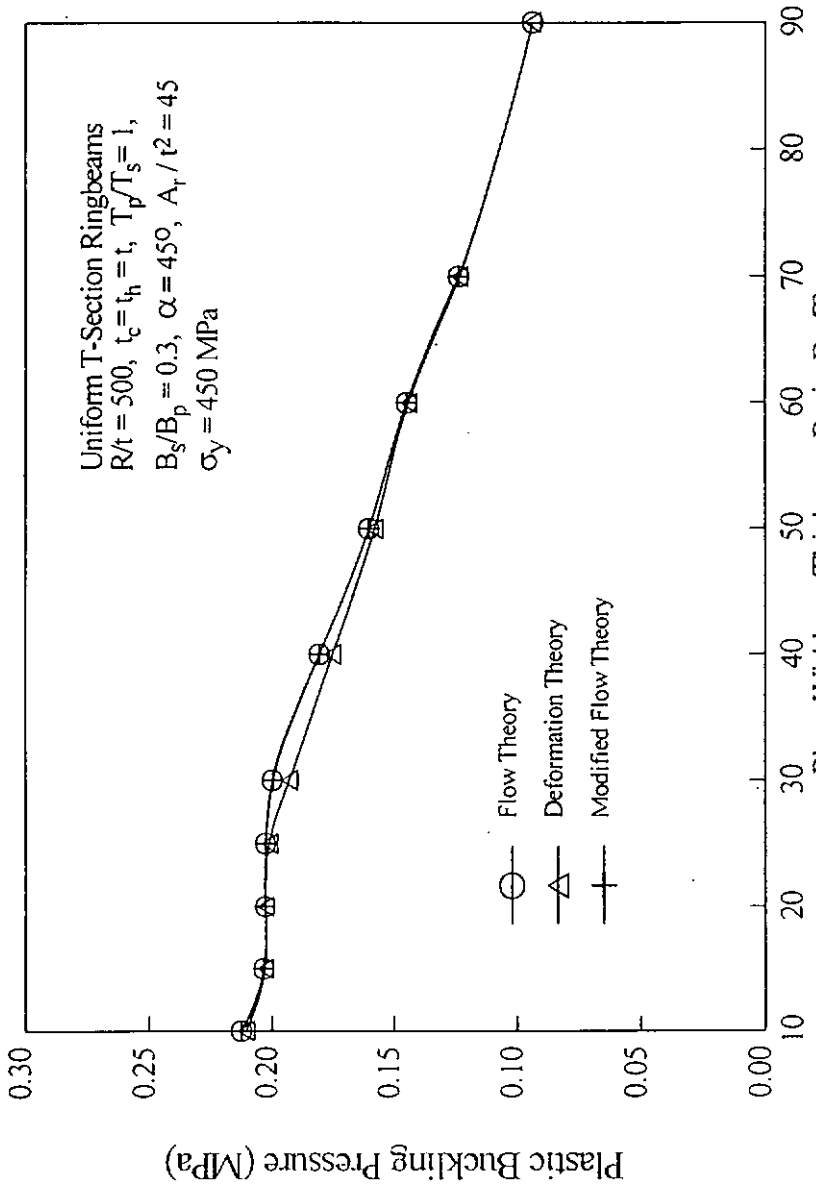

Fig. 6-2 Effect of Plasticity Modelling

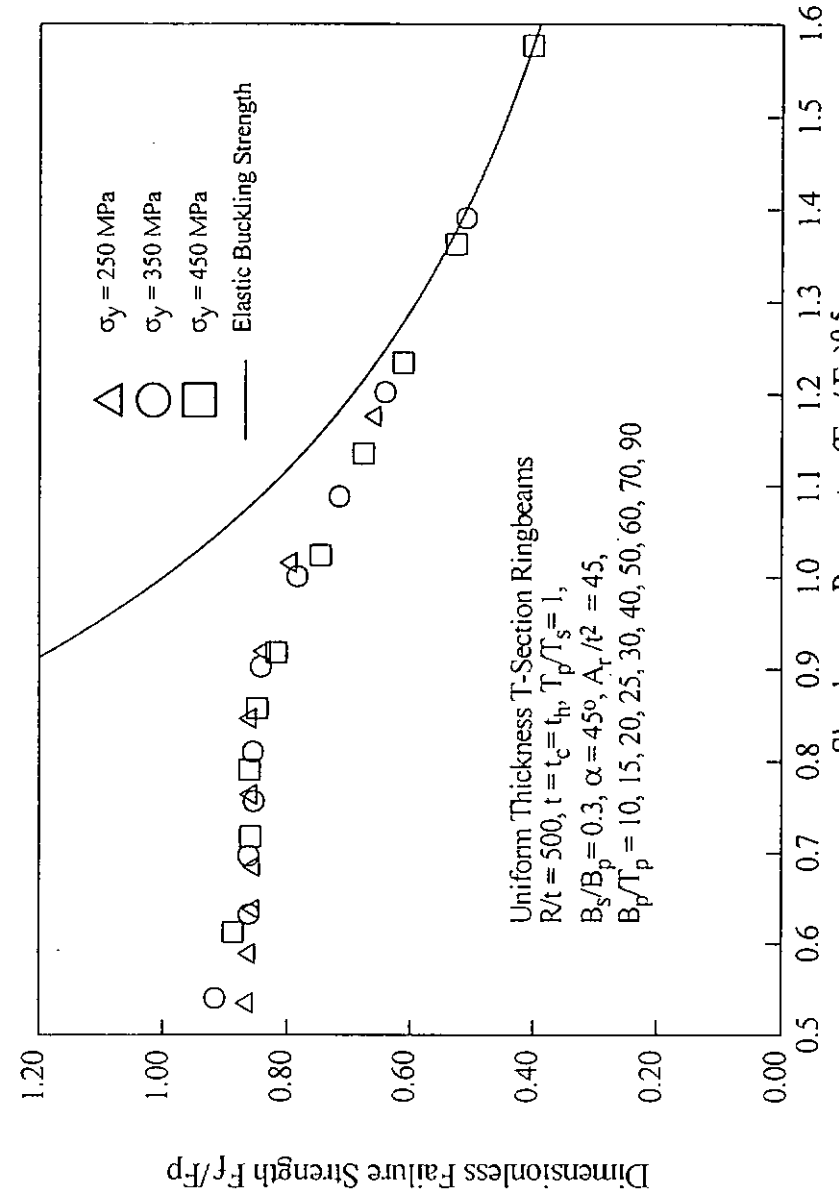

Fig. 6-3 Effect of Yield Stress

Uniform Thickness T-section Ringbeams

$R/t_c = 500$, $t_c = t_h = t$, $T_p/T_s = 1$, $B_s/B_p = 0.3$, $\alpha = 45°$, $A_r/t^2 = 45$, $\sigma_y = 450$Mpa

☐ Elastic ■ Yield

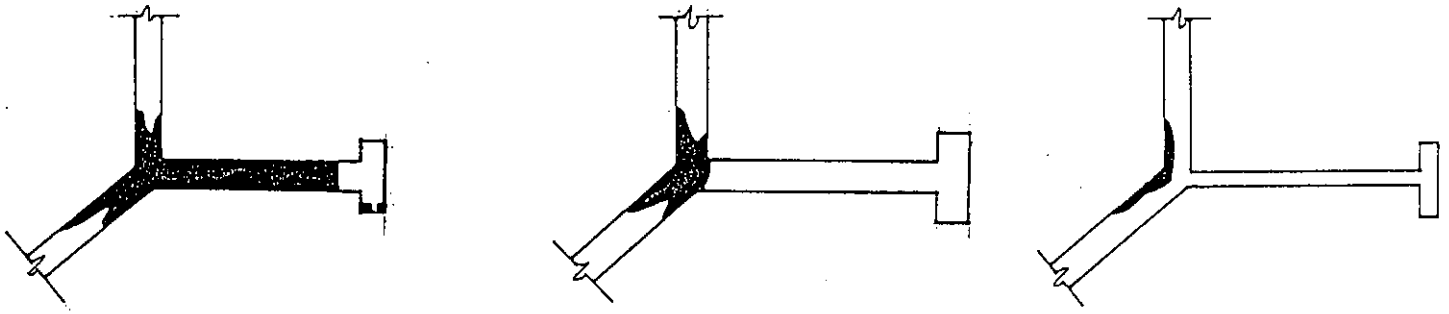

(a) $\lambda = 0.790$ (b) $\lambda = 1.024$ (c) $\lambda = 1.363$

Fig. 6-4 Yield Zones at Buckling

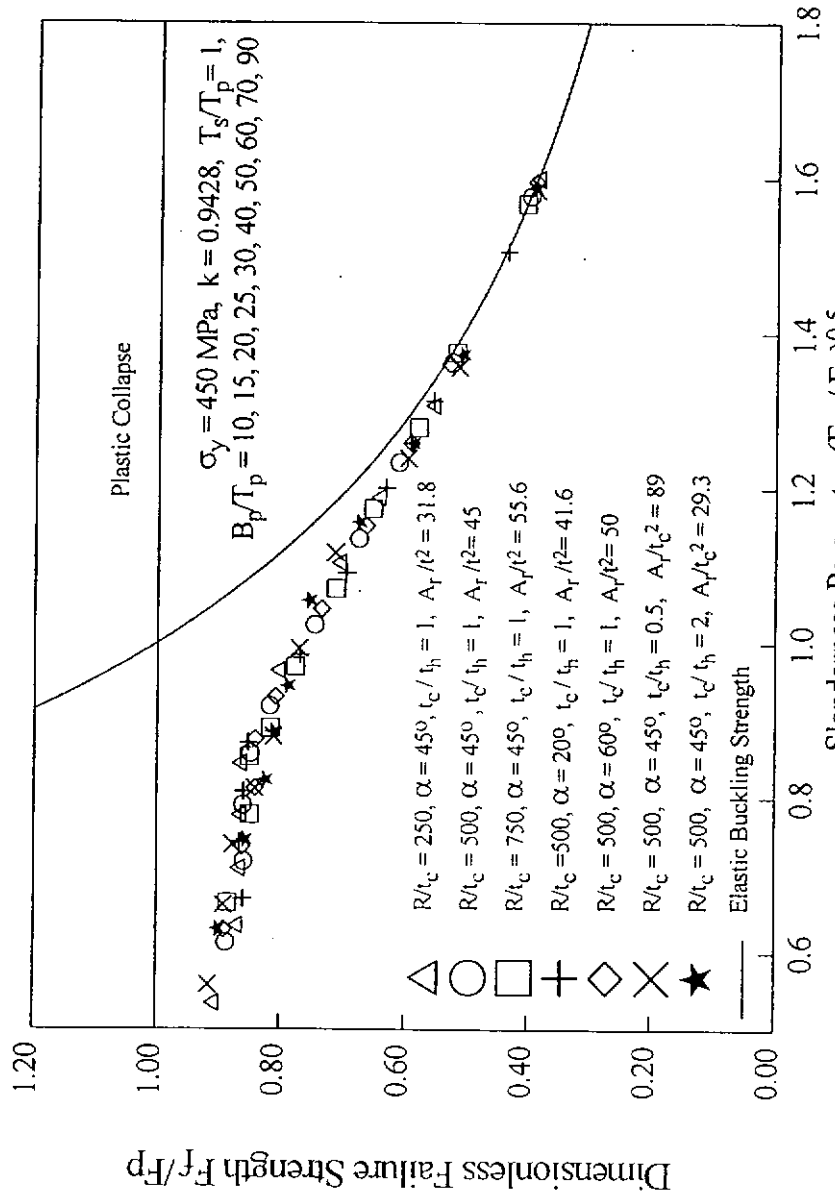

Fig. 6-5 Buckling Strengths of Ringbeams of Same Dimensionless Size

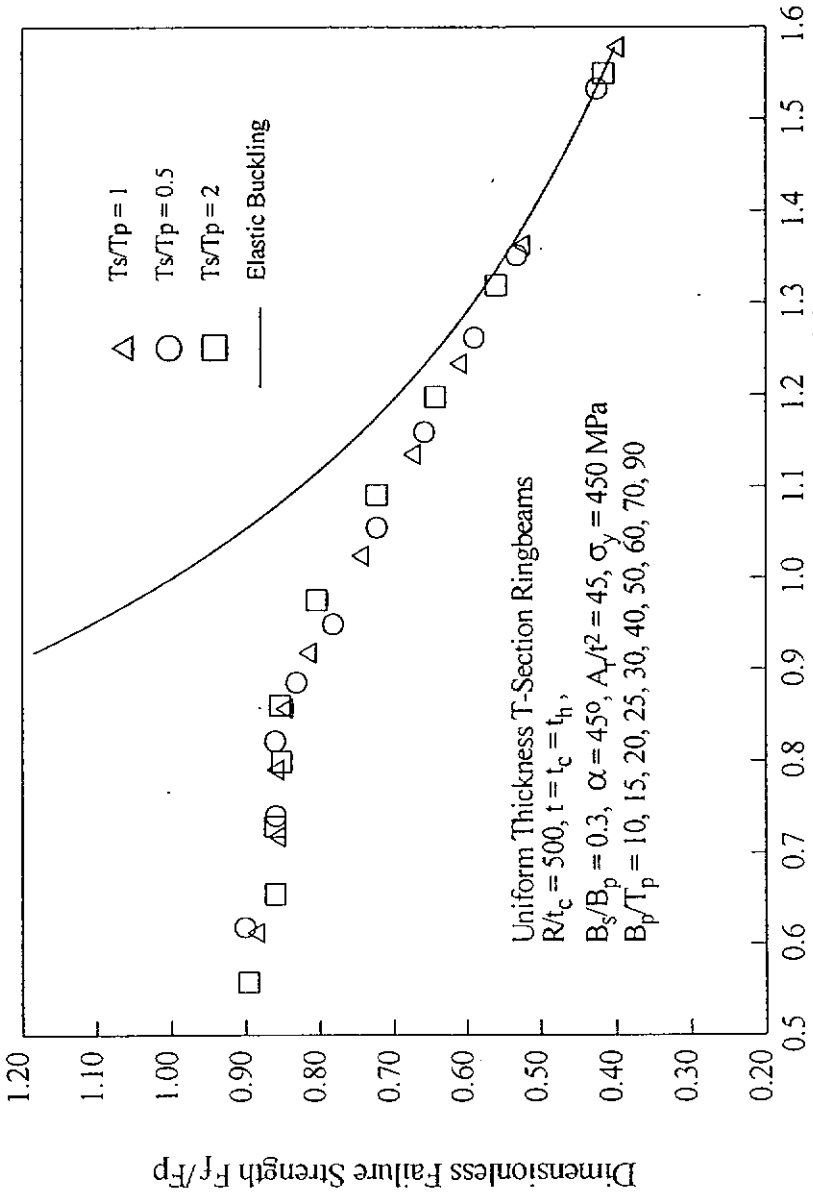

Fig. 6-6 Effect of Stiffner-to-Annular Plate Thickness Ratio of the Ringbeam

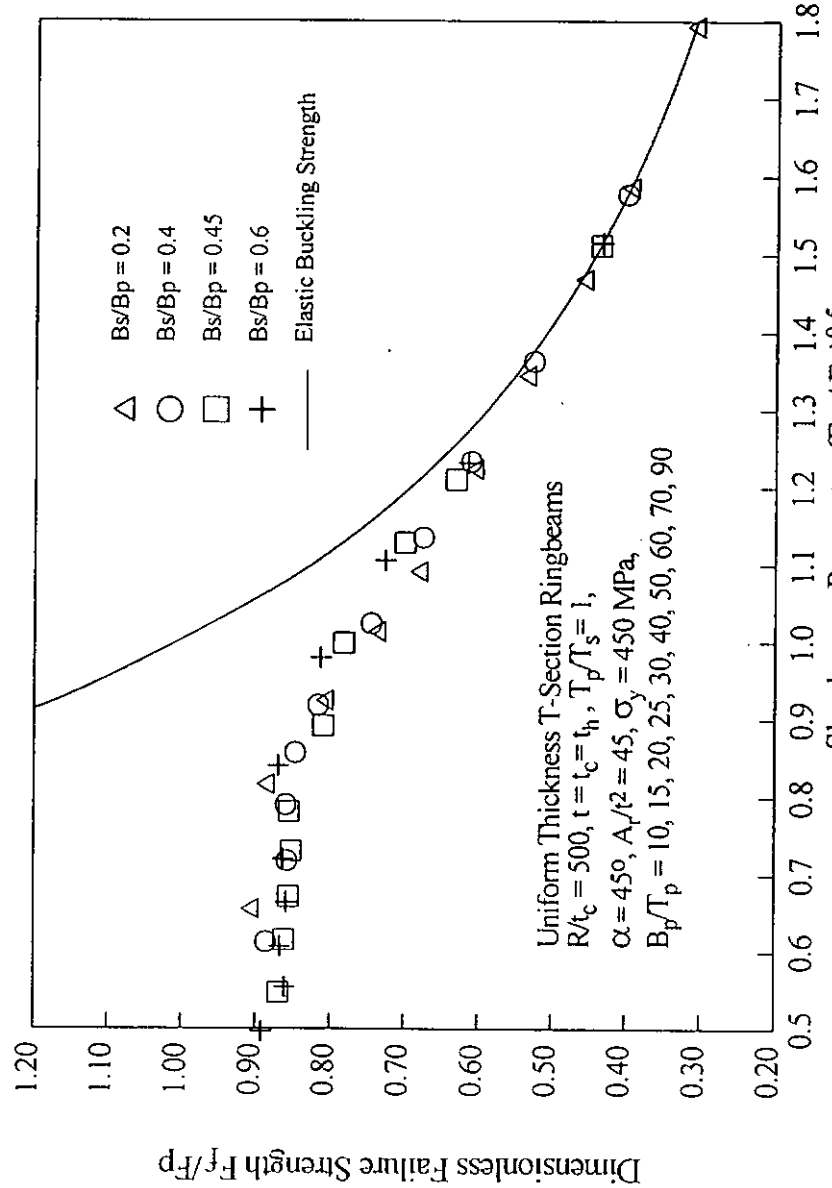

Fig. 6-7 Effect of Stiffner Height-to-Annular Plate Width Ratio of the Ringbeam

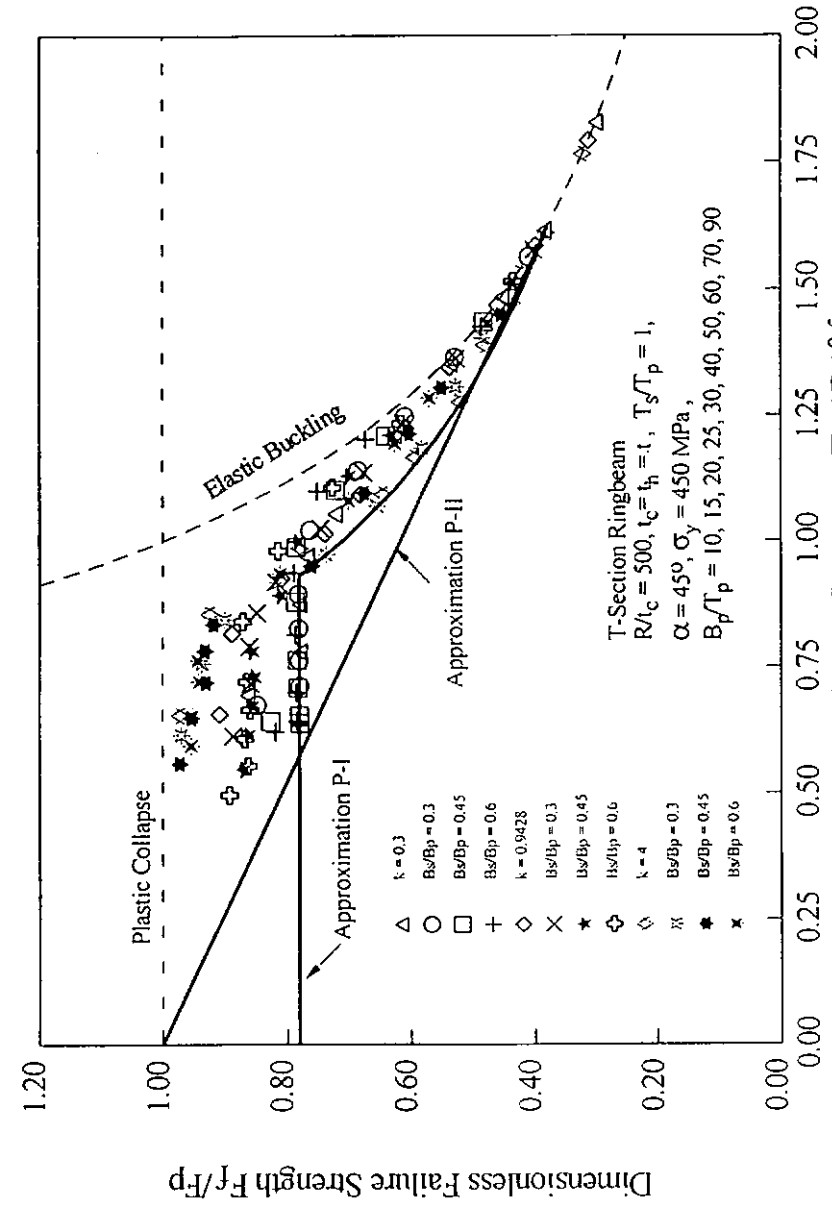

Fig. 6-8 Design Approximations

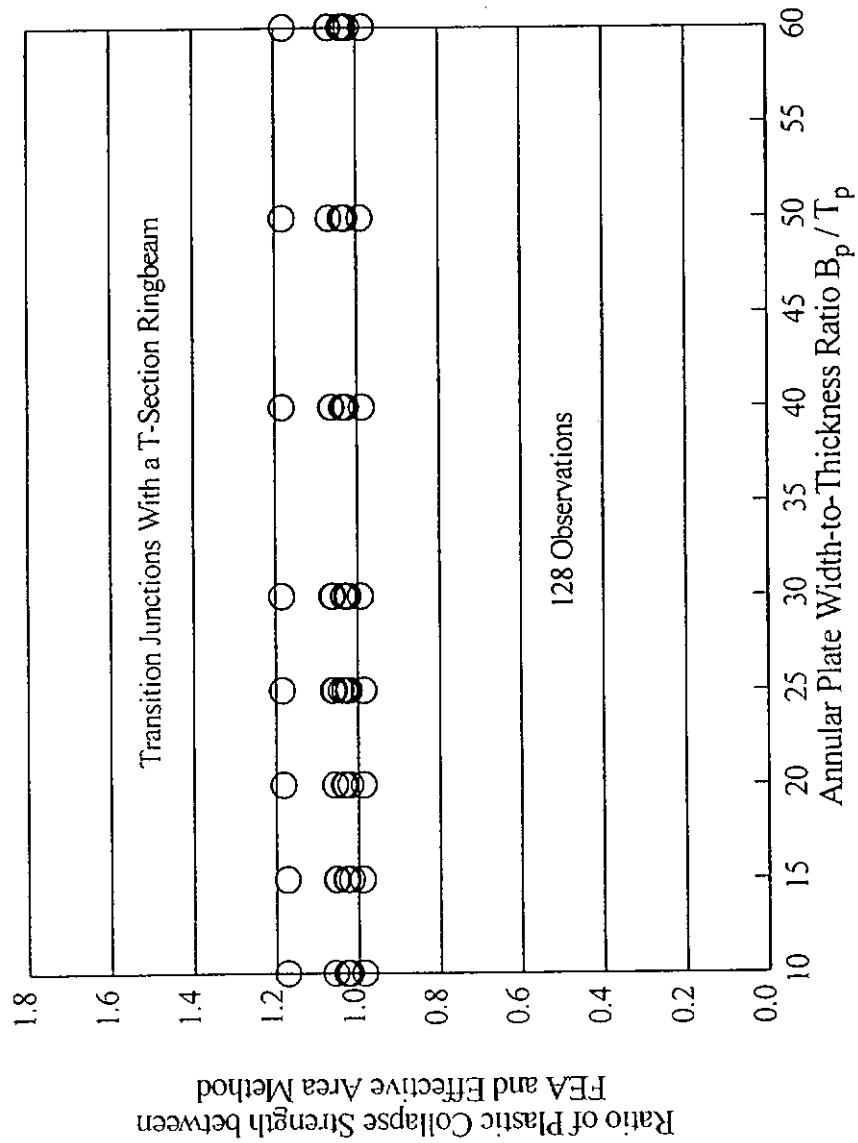

Fig. 6-9 Accuracy of the Effective Area Method for Plastic Collapse Strengths

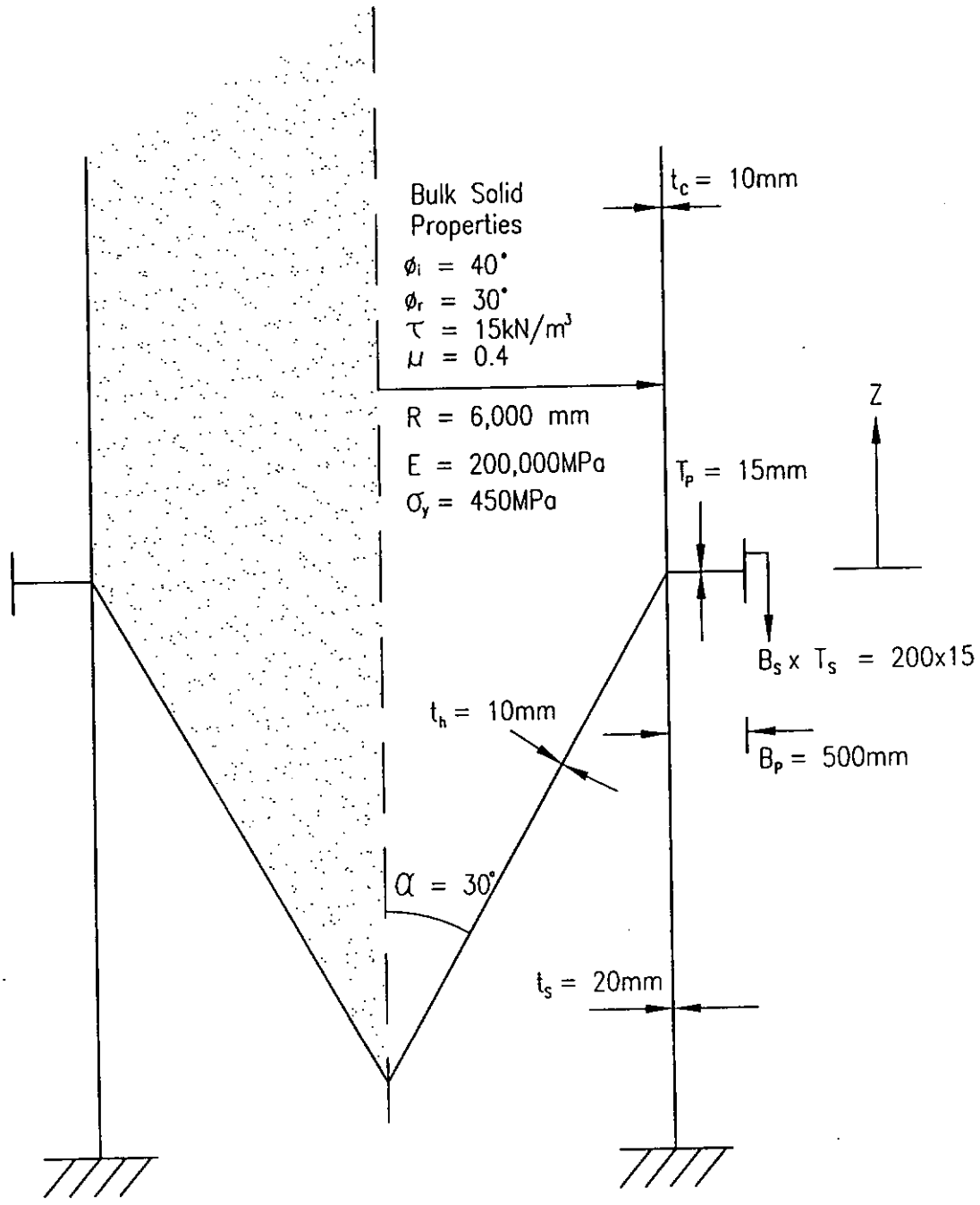

Fig. 6-10 Example Elevated Steel Silo

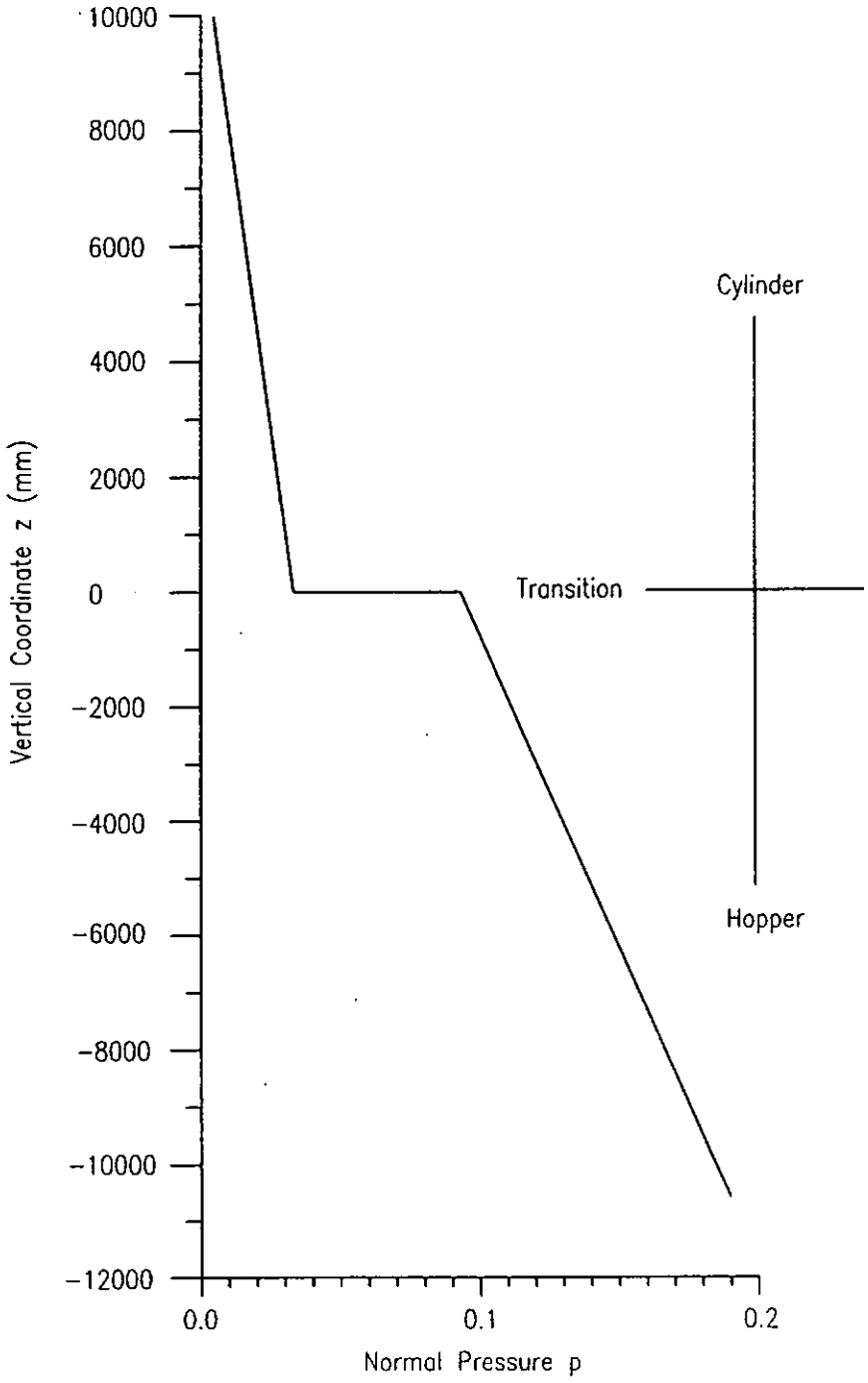

Fig. 6-11 Normal Pressure in Example Silo

CHAPTER 7 CONCLUSIONS

7.1 General

A T-section ringbeam is often provided at the transition junction of a uniformly-supported steel silo or tank. This ringbeam is subject to a large circumferential compressive force which is derived from the radial component of the meridional tension in the conical hopper. Under this compressive force, the ringbeam may fail in one of several possible modes, including out-of-plane buckling. This thesis has presented a comprehensive study on the buckling behaviour and strength of T-section ringbeams attached to the transition junction in a steel silo. Based on a thorough study of the effects of various factors, buckling strength approximations for design use have been developed. Application of the proposed method has been demonstrated through an example.

7.2 Elastic Buckling of T-section Ringbeams Clamped at Inner Edge

Chapter 3 has presented an investigation into the elastic buckling strength of T-section ringbeams clamped at inner edge. Such ringbeams can fail by either local buckling or distortional buckling. In practical design, local buckling should be avoided by proportioning the section properly following the limits set by the design chart proposed in this chapter. The distortional buckling strength of clamped T-section ringbeams has been shown to vary only slightly with the ringbeam radius and can be approximated by the existing solution of Bulson (1970) for an edge-stiffened rectangular plate clamped along the un-stiffened edge with a simple modification. An

alternative approximation for inner edge clamped T-section ringbeams has also been proposed. The alternative approximation is particularly simple for the common case of uniform thickness T-section ringbeams and may be used in place of the modified Bulson's solution to keep the design calculations to a minimum.

7.3 Elastic Buckling of T-section Ringbeams Simply-Supported at Inner Edge

The elastic buckling strength of T-section ringbeams simply-supported at inner edge was examined in Chapter 4. Teng and Rotter (1988) derived a solution for the out-of-plane buckling of mono-symmetric open section ringbeams radially loaded at any point in the plane of the symmetry using the thin-walled member theory. They also produced a simplified version of their more general solution for T-section ringbeams simply-supported at inner edge. In Chapter 4, Teng and Rotter's simplified solution was further simplified and modified, which led to two new approximations which are much simpler in form and have comparable accuracy.

7.4 Elastic Buckling of T-section Transition Ringbeams

The inner edge boundary conditions considered in Chapters 3 and 4 are idealised conditions. In a real structure, the ringbeam is usually provided with elastic (semi-rigid) rotational restraint by the adjacent shell walls. Chapter 5 described a comprehensive investigation into the elastic buckling strength of T-section ringbeams at steel silo transition junctions. A simple approximation was found for the elastic buckling strength of the ringbeam in terms of its inner edge circumferential

compressive stress. This was achieved by interpolating between the buckling strengths of the two idealised cases of inner edge simply supported and inner edge clamped ringbeams, for which simple elastic buckling strength approximations were developed in Chapters 3 and 4. The interpolation relationship adopted by Rotter and Jumikis for annular plate ringbeams has been found to be satisfactory also for T-section ringbeams.

Although the junction was studied under a uniform internal pressure with accompanying meridional frictional traction, the results were interpreted for use with junctions under general non-uniform loading by characterising the buckling strength using the equivalent circumferential compressive force. The final recommended elastic buckling strength approximation is the first ever rigorously based strength proposal for this problem.

7.5 Plastic Buckling of T-section Transition Ringbeams

The effect of yielding on the buckling strength of T-section transition ringbeams in steel silos and tanks was thoroughly investigated in Chapter 6, leading to the first ever rigorous design proposal for their plastic buckling strength. The design approximations were based on results obtained using a small deflection prebuckling analysis as the effect of prebuckling large deflections is small, and the deformation theory of plasticity which is the most conservative among the three common plasticity models.

Similar to the case of annular plate ringbeams in steel silos (Teng, 1997), the interaction relationship between plastic yielding/collapse and elastic buckling, when cast in a suitable dimensionless form, is independent of yield stresses and various geometric ratios. It depends strongly on the dimensionless ringbeam size parameter. In addition, the stiffener height-to-annular plate width ratio of a T-section ringbeam also has a significant effect on this relationship. Two design approximations were devised as lower bound curves to finite element results covering a wide range of values of these two parameters. The first approximation, dividing ringbeams into three groups, is more complicated but provides a more accurate approximation to the finite element results, while the second approximation is simpler but more conservative. The second approximation has been proposed for use in design with its conservatism acting as desirable precaution, before experimental results become available. Application of the second design approximation together with the elastic buckling strength approximation was demonstrated in an example.

7.6 Some Suggestions for Further Studies

The work presented in this thesis and the proposed design approximations have been theoretically-based. It would be very useful in the future to conduct experiments on model transition junctions with a T-section ringbeam to shed light on the effects of imperfections and residual stresses so that the safety margin of the proposed design approximations can be clarified and/or further improvements can be made to these design approximations.

Apart from annular plate ringbeams which have received extensive attention in the literature and T-section ringbeams studied in this thesis, angle section ringbeams are also often used at steel silo transition junctions. A study on the buckling strength of angle section transition ringbeams should be carried out in the future.

8. REFERENCE

1. Anad, S.C. and Griffith, A.R (1973) "Inelastic Buckling of Rings with Residual stresses". Journal of the Engineering Mechanics Division, ASCE, Vol. 99, No. EM5, pp. 927-942

2. AS 3774-1990, Loads on Bulk Solids Containers, Standards Australia.

3. AS 3774 Supp1-1990, Loads on Bulk Solid Containers - Commentary, Standards Australia.

4. Boresi, A. (1955) "A Refinement of the Theory of Buckling of Rings under Uniform Pressure", Journal of Applied Mechanics, ASME, Vol. 22, pp. 95-102

5. Bradford, M.A. (1992) "Lateral-Distortional Buckling of Steel I-Section Members", *Journal of Constructional Steel Research*, Vol. 23, pp 97-116

6. Bradford, M.A. (1996) "Lateral-Distortional Buckling of Continuously Restrained Columns", *UNICIV Report No. R-351*, School of Civil Engineering, The University of New South Wales.

7. Bresse (1866) *Cours de Mecanique Appliquee*, 2nd Edn, p 334.

8. Brush, D.O. and Almroth, B.O. (1975) *Buckling of Bars, Plates and Shells*, McGraw-Hill, New York, N.Y.

9. Bulson, P.S. (1970) *The Stability of Flat Plates*, London, Chatto & Windus

10. CEN (1997)Draft Eurocode 3: Design of Steel Structures, Part 4.1 Silos, CEN/TC 250/SC3/PT4.

11. Cheney, J.A. (1963a) "Deflection of Hinged Rings under Uniform Pressure", Journal of the Engineering Mechanics Division, ASCE, Vol. 89, No. EM6, pp161-176.

12. Cheney, J.A. (1963b) "Bending and Buckling of Thin-Walled Open Section Rings", Journal of the Engineering Mechanics Division, ASCE, Vol. 89, No. EM5, pp17-34.

13. Chen, J.F. and Rotter, J.M. (1997) "Stresses in Asymmetric Ring Stiffeners for Cylindrical Shells", *Proc., International Conference on Carrying Capacity of Steel Shell Structures*, 1-3 Oct., Brno, Czech Republic, pp 340-346.

14. Galletly, G.D. (1985) "Torispherical Shells", *Shell Structures: Stability and Strength*, R. Narayanan, ed., Elsevier Applied Science Publishers, London, UK.

15. Galletly, G.D. and Blachut, J. (1985) "Torispherical Shells under Internal Pressure-Failure due to Asymmetric Buckling or Axisymmetric Yielding", Proceedings, Institution of Mechanical Engineers, Vol. 199, No. C3, pp. 225-238

16. Gaylord, E.H. and Gaylord, C.N. (1984) Design of Steel Bins for Storage of Bulk Solids, Prentice-Hall, New Jersey.

17. Goldberg, J.E. and Bogdanoff, J.L. (1962) "Out-of-Plane Buckling of I-Section Rings"' Publications, International Association for Bridges and Structural Engineering, Vol. 22, pp. 73-92.

18. Greiner, R. (1991) "Elastic Plastic Buckling at Cone Cylinder Junctions of Silos", Buckling of Shell Structures on Land, in the Sea and in the Air, J.F Jullien, ed., Elsevier Applied Science, New York, N.Y.

19. Janssen, H.A. (1895) " Versuche uber Getreidedruck in Silozellen", Zeitschrift des vareines Deutscher Ingenieure, Vol. 29, No. 35, pp 1045-2049.

20. Jumikis, P.T. (1987) Stability Problems in Silo Structures, PhD Thesis, School of Civil and Mining Engineering, University of Sydney, N.S.W., Australia.

21. Jumikis, P.T. and Rotter, J.M. (1983) "Buckling of Simple Ringbeams for Bins and Tanks", Proc., International Conference on Bulk Materials Storage, Handling and Transportation, Institution of Engineers, Australia, Newcastle, Aug., pp 323-328.

22. Ketchum, M.S. (1909) Walls, Bins and Grain Elevators, McGraw-Hill, New York.

23. Lambert, F.W. (1968) The Theory and Practical Design of Bunkers, British Constructional Steelwork Association, Publication No.32, pp 67.

24. Rotter, J.M. (1983) "Effective Cross-Section of Ringbeams and Stiffeners for Bins", Proceedings, International Conference on Bulk Materials, Storage, Handling and Transportation, Institution of Engineers, Australia, Newcastle, NSW, August, pp. 329-334.

25. Rotter, J.M. (1985) "Buckling under Axial Compression", Design of Steel Bins for the Storage of Bulk Solids, School of Civil and Mining Engineering, University of Sydney, March, pp 122-137.

26. Rotter, J.M. (1987) "The Buckling and Plastic Collapse of Ring Stiffeners at Cone/Cylinder Junctions", Proceedings, International Colloquim on Stability of Plate and Shell Structures, Gent, Belgium, April, pp 449-456.

27. Rotter, J.M. (1996) "Shell Structures: Design Standards, Recent Progress and Unsolved Problems", Advances in Steel Structures, eds S.L. Chan and J.G. Teng, Elsevier Science, Oxford, 1996.

28. Rotter, J.M. and Jumikis, P.T. (1985) "Elastic Buckling of Stiffened Ringbeams for Large Elevated Bins", Proc., Metal Structures Conference, Institution of Engineers, Australia, Melbourne, May, pp 104-111.

29. Sharma, U.C., Rotter, J.M. and Jumikis, P.T. (1987) "Shell Restraint to Ringbeam Buckling in Elevated Steel Silos", Proceedings, First National Structural Engineering Conference, Institution of Engineers, Australia, August, 1987, pp 604-609.

30. Smith, C.V. and Simitses, G.J. (1969) "Effect of Shear and Load Behaviour on Ring Stability", Journal of the Engineering Mechanics Division, ASCE, Vol. 95, No. EM3, pp 559-569.

31. Teng, J.G. (1994) "Cone-Cylinder Intersection under Internal Pressure: Axisymmetric Failure", *Journal of Engineering Mechanics*, ASCE, Vol. 120, No. 9, pp 1896-1912.

32. Teng, J.G. (1995) "Cone-Cylinder Intersection under Internal Pressure: Non-Symmetric Buckling", Journal of Engineering Mechanics, ASCE, Vol. 121, No. 12, pp 1298-1305.

33. Teng, J.G. (1996) "Buckling of Thin Shells: Recent Advances and Trends", *Applied Mechanics Reviews*, ASME, Vol. 49, No. 4, pp 263-274.

34. Teng, J.G. (1997) "Plastic Buckling Approximation for Transition Ringbeams in Steel Silos", Journal of Structural Engineering, ASCE, Vol. 123, No. 12, December, pp 1622-1630.

35. Teng, J.G. (1998) "Collapse Strength of Complex Shell Intersections by the Effective Area Method", Journal of Pressure Vessel Technology, ASME, Accepted for Publication.

36. Teng, J.G. and Barbagallo, M.A., (1997) "Shell Restraint to Ring Buckling at Cone-Cylinder Intersections", *Engineering Structures*, Vol. 19, No. 6, pp. 425-431.

37. Teng, J.G. and Lucas, R.M. (1994) "Out-of-Plane Buckling of Restrained Rings of General Open Cross-Section", Journal of Engineering Mechnics, ASCE 120(5), pp. 929-948

38. Teng, J.G. and Rotter, J.M. (1987) "Unrestrained Out-of-Plane Buckling of Monosymmetric Rings", Journal Construction Steel Research 7, pp. 451-471

39. Teng, J.G. and Rotter, J.M. (1988) "Buckling of Restrained Monosymmetric Rings", Journal of Structural Engineering, ASCE, Vol. 114, No. 10, pp 1651-1671.

40. Teng, J.G and Rotter, J.M. (1989a) "Buckling of Rings in Column-Supported Bins and Tanks", Thin-Walled Structures, Vol., 7, Nos 3 & 4, pp. 251-280

41. Teng, J.G and Rotter, J.M. (1989b) "Non-Symmetric Bifurcation of Geometrically Non-Linear Elastic-Plastic Axisymmetric Shells subject to Combined Loads including Torsion", Computers and Structures, Vol., 32, No.2, pp.453-477.

42. Teng, J.G and Rotter, J.M. (1991a) "Collapse Behaviour and Strength of Steel Silo Transition Junctions-Part I: Collapse Mechanics", Journal of Structural Engineering, ASCE, Vol. 117, No. 12, pp. 3587-3604.

43. Teng, J.G. and Rotter, J.M. (1991b) "Collapse Behaviour and Strength of Steel Silo Transition Junctions-Part II: Parametric Study", Journal of Structural Engineering, ASCE, Vol. 117, No. 12, pp. 3605-3622.

44. Teng, J.G. and Rotter, J.M. (1991c) "Plastic Buckling of Rings at Steel Silo Transition Junctions", J. Constr. Steel Res., 19, 1-18.

45. Teng, J.G. and Rotter, J.M. (1991d) "Strength of Welded Steel Silo Hoppers under Filling and Flow Pressures", Journal of Structural Engineering, ASCE, Vol. 117, NO. 9, 2567-2583.

46. Teng, J.G and Rotter, J.M. (1992) "Recent Research on the Behaviour and Design of Steel Silo Hoppers and Transition Junctions", Journal Construct Steel Research 23, pp. 313-343

47. Timoshenko, S.P. and Gere, J.M. (1961) Theory of Elastic Stability, 2nd Edn, McGraw-Hill, New York

48. Trahair, N.S.; Abel, A.; Ansourin, P.; Irvine, H.M.; and Rotter, J.M. (1983) Structural Design of Steel Bins for Bulk Solids, Australian Institute of Steel Construction, November.

49. Trahair, N.S. and Papangells, J.P. (1987) "Flexural-Torsional Buckling of Monosymmetric Arches", Journal of Structural Engineering, ASCE, Vol. 113, No. 10, pp.2271-2288

50. Wah, T. (1967) "Buckling of Thin Circular Rings under Uniform Pressure", International Journal of Solids and Structures, Vol. 3, pp. 967-974

51. Walker, D.M. (1966) "An Approximate Theory for Pressure and Arching in Hopper", Chem. Engg Sci., Vol 21, pp 975-997.

52. Wasserman, E. (1961) "The Effect of the Behaviour of the Load on the Frequency of Free Vibration of a Ring", NASA TT F-52

53. Wempner, G.A. and Kesti, N. (1962) "On the Buckling of Circular Arches and Rings", Proceedings, 4th U.S. National Congress of Applied Mechanics, ASME, Vol. 2, pp.843-852

54. Wozniak, R.S. (1979) "Steel Tanks", in Structural Engineering Handbook, 2nd Edn, Section 23, edited by Gaylord and Gaylord, McGraw-Hill.

55. Yoo, C.H. (1982) "Flexural-Torsional Stability of Curved Beams", Journal of the Engineering Mechanics Division, ASCE, Vol. 108, No. EM6, December, pp. 1351-1369